University of Massachusetts Medical School

eScholarship@UMMS

2017-09-15

Ki-67 Regulates Cell Cycle Progression and Heterochromatin Organization

Xiaoming Sun
University of Massachusetts Medical School

Let us know how access to this document benefits you.

Follow this and additional works at: https://escholarship.umassmed.edu/gsbs_diss

Part of the Cell Biology Commons

Ki-67 REGULATES CELL CYCLE PROGRESSION AND

HETEROCHROMATIN ORGANIZATION

A Dissertation Presented

By

Xiaoming Sun

Submitted to the Faculty of the
University of Massachusetts Graduate School of Biomedical Sciences, Worcester
in partial fulfillment of the requirements for the degree of

DOCTOR OF PHILOSOPHY

September 15, 2017

Interdisciplinary Graduate Program

Ki-67 REGULATES CELL CYCLE PROGRESSION AND HETEROCHROMATIN ORGANIZATION

A Dissertation Presented
By

Xiaoming Sun

Dissertation Defense Committee Members

Paul Kaufman, Ph.D., Thesis Advisor

Job Dekker, Ph.D., Member of Committee

Thomas Fazzio, Ph.D., Member of Committee

Thoru Pederson, Ph.D., Member of Committee

Oliver Rando, M.D., Ph.D., Member of Committee

Richard Freiman, Ph.D., External Member of Committee

Craig Peterson, Ph.D., Chair of Committee

Interdisciplinary Graduate Program

September 15, 2017

Dedication

I dedicate this work to my great father who has supported me

all the time.

Acknowledgements

First and foremost I must thank my mentor Paul Kaufman. Over the past seven years Paul has been an exceptional PI and mentor. He has a deep knowledge of the field and continues to remain on the cutting edge of experimental techniques. His sharp mind and critical questioning has shaped the way I approach problems. He has continued to encourage me to grow as a scientist, but was also sympathetic to the humanity and understood that major life events will sometimes take precedence. He especially has made graduate school comfortable, as he has always been so understanding, supportive, responsive, and warmhearted. I am grateful for his knowledge, patience, motivation, and support throughout my graduate career.

I am indebted to my committee members and colleagues who supported me during the progression of my projects. I would like to express my gratitude to Job Dekker, Thomas Fazzio, Craig Peterson, Thoru Pederson and Oliver Rando who all served on my Thesis Research Advisory for all of their constructive feedback, recommendations, and advice. I also would like to thank current and past members of the Kaufman Lab: Dr. Eric Campeau, Dr. Jessica Lopes Da Rosa-Spiegler, Dr. Ahmed Fazly, Dr. Vineeta Bajaj, Dr. Dan Trombly, Dr. Timothy Matheson, Dr. Ana Vertii, Dr. Yuichi Ichikawa, and Aizhan Bizhanova. It has been an horror to work in such a collaborative environment.

Abstract

A subset of eukaryotic heterochromatin is located around the nucleoli, and this localization is correlated with gene silencing. Although there is some evidence for trans-acting factors organizing genomic loci around the nucleolus, the characterization of proteins and /or RNAs involved in perinculeolar heterochromatin organization is incomplete. Notably, the mammalian female inactive X chromosome, a well-studied model of facultative heterochromatin, frequently resides in the perinucleolar regions during S phase. The disruption of the Xi–nucleolus association results in the erosion of several features of heterochromatin and silencing, which renders it a good model to investigate the mechanism and biological relevance of perinucleolar heterochromatin organization. This dissertation will present evidence showing that Ki-67 regulates Xi association with nucleoli, maintains Xi heterochromatic structures, and regulates cell cycle progression in cell-type-specific manner dependent on checkpoint proficiency.

Upon Ki-67 depletion, the Xi from a subset of human female hTERT-RPE1 cells moved away from the nucleolus and displayed several features of compromised heterochromatin. These chromatin alterations were limited to Xi chromosomes localized away from the nuclear lamina and were not observed in 293T cells upon Ki-67 depletion. Furthermore, different Xi heterochromatin alteration responses result from cell-type-specific reduced proportion of cells in S

phase upon Ki-67 depletion. In human hTERT-RPE1, WI-38, IMR90 and hTERT-BJ cell lines, depletion of Ki-67 slowed entry into S phase and coordinately downregulated DNA replication genes. These cell lines are able to induce p21 expression upon Ki-67 depletion. On the contrary, alteration of transcription and cell cycle progression were not observed in tumor-derived HeLa, U2OS and 293T cell lines. These cell lines do not induce p21 expression either. Overall, our results indicate that Ki-67 integrates normal S phase progression and Xi heterochromatin maintenance in p21 checkpoint-proficient human cells.

TABLE OF CONTENTS

LISTS Of TABLES

LISTS OF FIGURES

List of copyrighted Materials

Portions of this dissertation have appeared in:

Xiaoming Sun, Aizhan Bizhanova, Timothy D. Matheson, Jun Yu, Julie L. Zhu and Paul D. Kaufman. " Ki-67 contributes to normal cell cycle progression and inactive X heterochromatin in p21 checkpoint-proficient human cells. " Molecular and Cellular Biology, 2017 Aug 11; 37 (17). pil: e00569-16.doi:10.1128/MCB.00569-16

List of Abbreviations Used Commonly in this Work

3C: Chromosome conformation capture

aa: Amino Acids

AC: Astrocytes

bp: base pairs

CAF-1: Chromatin Assembly Factor 1

CDK: Cyclin Dependent Kinase

ChIP: Chromatin immunoprecipitation

ChIP-seq: Chromatin immunoprecipitation coupled with high throughput deep sequencing

cLADs: Constitutive LADs

Co-IP-MS: Coimmunoprecipitation combined with mass spectrometry

CRISPR: Clustered regularly interspaced short palindromic repeats

DNA: Deoxyribonucleic acid

DSB: Double stranded break

EdU: 5-ethynyl-2-deoxyuridine

esiRNAs: Endoribonuclease-prepared siRNAs

FBL: Fibrillarin

fLADs: Facultative LADs

FHA: Forkhead associated domain

FISH: Fluorescence in-situ hybridization

H3K27me3: Histone H3, lysine 27 trimethylation

H3K9me3: Histone H3, lysine 9 trimethylation

H4K20me3: Histone H4, lysine 20 trimethylation

HDR: Homology directed repair

HFF: Human Foreskin Fibroblast

Hi-C: Chromosome conformation capture coupled with high-throughput deep sequencing

HP1: Heterochromatin Protein 1

HR: Homologous recombination

IF: Immunofluorescence

LADs: Lamina Associated Domains

LncRNAs: Long non-coding RNAs

Luc: Luciferase

NADs: Nucleolar Associated Domains

MEF: Mouse Embryonic Fibroblast

mESC: mouse embryonic stem cells

NCL: Nucleolin

NHEJ: Non-homologous end joining

NL: Nuclear Lamina

NOR: Nucleolus organizer region

NPC: Neural precursor cells

NPM: Nucleophosmin

p150C: C-terminal domain of CAF-1 subunit p150

p150N: N-terminal domain of CAF-1 subunit p150

PCH: pericentromeric heterochromatin

PCL: Perichromosomal Layer

PCR: Polymerase Chain Reaction

PH: Periphery heterochromatin

PN: Perinucleolar

PNH: Perinucleolar heterochromatin

PP1: Protein phosphatase 1

RNA: Ribonucleic acid

rRNA: ribosomal RNA

RT-qPCR: Reverse Transcription quantitative PCR

Scr: Scramble sequence

sgRNA: short guide RNA

shRNAs: Short hairpin RNAs

siRNAs: Small interfering RNAs

TADs: Topologically associating domains

XI: Inactive X chromosome

XIC: X inactivation center

CHAPTER I: INTRODUCTION

1.1 Abstract

This dissertation is focused how Ki-67 regulates perinucleolar heterochromatin organization in respond to cell cycle progression. Ki-67 has long been used as clinical marker of cell proliferation to grade tumors. Despite the strict correlation between Ki-67 expression and cell proliferation, differing results have been obtained in the test of requirement of Ki-67 in cell growth. Recent studies identified that Ki-67 acts as trans-acting factor to promote alpha satellite repeats to perinucleolar regions. But the mechanisms by which Ki-67 coordinates cell cycle progression with perinucleolar heterochromatin organization remain incomplete. Inactive X chromosome (Xi) is a well-studied example of facultative heterochromatin that associates with the nucleoli of female mouse and human cells in mid-to-late S phase. Trans-acting proteins and the RNAs are required to target Xi to perinucleolar regions. This chapter will summarize the dynamics, mechanisms and functional implications of perinucleolar localization of Xi and other genomic loci.

1.2: Ki-67

Ki-67 was first identified as an antigen in Hodgkin lymphoma cell nuclei (Gerdes *et al.*, 1983) that is highly expressed in cycling cells but strongly down-regulated in resting G0 cells (Gerdes *et al.*, 1984). This characteristic has made Ki-67 a clinically important proliferation marker for grading multiple types of

cancers (Gerdes *et al.*, 1987; Dowsett *et al.*, 2011), with well-established prognostic value in large studies(Luo *et al.*, 2015; Pyo *et al.*, 2015; Richards-Taylor *et al.*, 2015; Pezzilli *et al.*, 2016). Despite this broad medical utility, surprisingly little is known about the molecular functions of Ki-67. Here, I review recent studies that have uncovered roles for Ki-67 in cell cycle regulation, heterochromatin maintenance, and assembly of the perichromosomal layer on mitotic chromosomes.(Booth *et al.*, 2014; Sobecki *et al.*, 2016; Cuylen *et al.*, 2016)

1.2.1: Ki-67 structure

Ki-67 protein is highly conserved in vertebrates (Booth and Earnshaw, 2017). In humans, Ki-67 is encoded by the gene *MKI67* located on chromosome 10q. Alternative splicing of the Ki-67 mRNA generates two isoforms with molecular weight of 320kDa and 359kDa. Functional differences between these isoforms have not been described, however, this huge nuclear protein does contain several characterized functional regions.

The N-terminus of Ki-67 contains a forkhead associated domain (FHA)(Takagi *et al.*, 2001), a motif that preferentially recognizes phosphorylated protein epitopes (Durocher *et al.*, 1999; Durocher and Jackson, 2002). Via this FHA domain, Ki-67 interacts with two proteins during mitosis: phosphorylated kinesin-like motor protein Hklp2/Kif15 and phosphorylated nucleolar RNA-binding protein NIFK (Takagi *et al.*, 2001; Sueishi *et al.*, 2000; Durocher and Jackson, 2002). The interaction between Ki-67 and Hklp2 contributes to mitotic spindle stability (Vanneste *et al.*, 2009). Hklp2 is a plus-end-directed spindle

motor(Vanneste *et al.*, 2009). In mitotic cells, Hklp2 distributes between microtubules and chromosomes. Upon Ki-67 depletion, Hklp2 fails to localize to the chromosome and concentrates in microtubules. More microtubule associated Hklp2 generates more pushing forces on spindles and metaphase spindles become longer than the control cells(Vanneste *et al.*, 2009). NIFK promotes cell proliferation and cancer metastasis (Pan *et al.*, 2015; Lin *et al.*, 2016). Downregulation of NIFK in H661 and H1299 cells reduced cancer cell growth(Lin *et al.*, 2016). Conversely, in both A549 and PC13 lung cancer cell lines, overexpression of wild type NIFK but not mutants lacking the Ki-67 binding motif increase cell proliferation (Lin *et al.*, 2016). NIFK enhances the metastatic ability of lung cancer cells via destabilizing transcription factor RUNX1, which in turn promotes a pro-metastatic Wnt/β-catenin signaling pathway (Hernandez *et al.*, 2012; Li *et al.*, 2012). Notably, repression of RUNX1 is largely attenuated when NIFK is incapable of Ki-67 binding (Lin *et al.*, 2016). Therefore, the pro-proliferative activities of NIFK are exerted in complex with the Ki-67 FHA domain.

An additional activity has been mapped to the Ki-67 FHA domain. In the tumor-derived DLD-1 cell line, the Ki-67 FHA domain maintains expression of cancer stem cell markers CD133 and CD44 (Cidado *et al.*, 2016). It would therefore be of interest to know whether FHA-mediated cancer stem cell maintenance is also dependent on the NIFK protein.

All homologues of Ki-67 contain a canonical Protein Phosphatase 1 (PP1) binding motif (RVxF)(Booth *et al.*, 2014). The PP1 family contains three isoforms, PP1 α, PP1β, and PP1γ and is predicted to catalyze approximately one third of

all eukaryotic protein dephosphorylation events, spanning a wide variety of cellular functions (Rebelo *et al.*, 2015). The versatility of PP1 functions is largely determined by the binding of its catalytic subunits to different regulatory proteins that define when and where the phosphatase acts (Rebelo *et al.*, 2015). In a ~40 residue region containing the PP1 binding motif, Ki-67 displays high similarity to the PP1-interacting protein, RepoMan(Booth *et al.*, 2014), which contributes to targeting PP1γ to anaphase chromosomes (Trinkle-Mulcahy *et al.*, 2006). In vivo, both Ki-67 and RepoMan bind specifically to PP1β and PP1γ isoforms, but not to PP1α (Booth *et al.*, 2014)(Kumar *et al.*, 2016). Crystal structures of Ki-67:PP1γ and RepoMan:PP1γ holoenzyme complexes identified a supplementary, novel PP1 interaction motif termed KiR-SLiM (Ki-67-RepoMan small linear motif), which is just C-terminal to the canonical RVxF motif (Kumar *et al.*, 2016). Ki-67 and RepoMan are the only known PP1 interactors that require this additional motif for binding (Kumar *et al.*, 2016). Because PP1 has 200 interacting/regulator proteins, KiR-SLiM:PP1 interaction surface could be a candidate drug target that inhibit only 2 PP1 holoenzymes in the cell(Rebelo *et al.*, 2015). Ki-67 /PP1 holoenzyme is a functional phosphatase complex in vivo. It dephosphorylates S125 on nucleophosmin/B23. Following Ki-67 depletion, phosphorylation on S125 of nucleophosmin/B23 is significantly increased(Booth *et al.*, 2014).

The central region of Ki-67 is comprised of multiple tandem repeats that are phosphorylated by CDK1 during mitosis (Schluter *et al.*, 1993; MacCallum and Hall, 1999; Endl and Gerdes, 2000; Takagi *et al.*, 2014). Ki-67 localization and dynamics are controlled by phosphorylation. In interphase,

dephosphorylated Ki-67 tightly associates with chromatin and localizes to the nucleolus in human cell lines (Saiwaki *et al.*, 2005). During mitosis, hyperphosphorylated Ki-67 binds less avidly to DNA and is highly mobile on the chromosome periphery (MacCallum and Hall, 1999; Endl and Gerdes, 2000; Saiwaki *et al.*, 2005). Dephosphorylation of mitotic Ki-67 delocates it away from the perichromosomal layer (MacCallum and Hall, 1999). On the mitotic chromosome surface, the highly positive electrostatic charge of Ki-67 serves as an electrostatic barrier important for prevention of hyperaggregation of chromosome arms. This will be discussed in more detail in 1.2.3 (Cuylen *et al.*, 2016).

Ki-67 has a weakly conserved leucine/arginine-rich C-terminal domain (LR domain) which can bind to DNA in vitro (Takagi *et al.*, 1999; Scholzen *et al.*, 2002) and is required for association with chromosomes in living cells (Saiwaki *et al.*, 2005; Cuylen *et al.*, 2016). This C-terminal domain of human Ki-67 binds all three isoforms of heterochromatin protein 1 (HP1) in vitro and in vivo (Kametaka *et al.*, 2002; Scholzen *et al.*, 2002). Via its methyllysine-binding chromodomain, HP1 binds to the hallmark of constitutive heterochromatin, di- and tri-methylated histone H3K9 residues(Jacobs and Sepideh, 2002; Nielsen *et al.*, 2002). By reading H3K9 methyl marks and recruiting histone methyltransferase and chromatin assembly factor 1 complex (CAF-1), HP1 facilitates assembly and maintenance of constitutive heterochromatin that contains centromeres and telomeres and remains compact in every cell type(Quivy *et al.*, 2004; Hiragami-Hamada *et al.*, 2016). Therefore, the interaction with HP1 suggests

heterochromatic roles for Ki-67. Indeed, overexpression of the human, chmadrin or Xenopus Ki-67 produces accumulation of HP1 and H3K9me3 and induces ectopic heterochromatin formation. (Takagi *et al.*, 1999; Scholzen *et al.*, 2002) Other examples will be discussed in Section 1.2.5.

Figure 1.1   A schematic diagram of human Ki-67 structure

FHA: forkhead-associated domain

PP1: PP1 binding domain

CD: conserved domain with unknown function
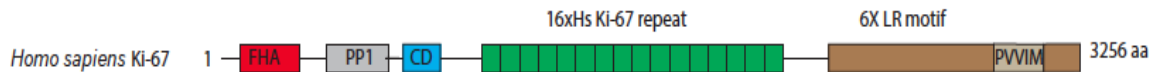
1.2.2: Ki-67 expression during the cell cycle

The initial characterization of Ki-67 localization detected a nuclear protein in proliferating human cells (Gerdes *et al.*, 1983). Additionally, studies of phytohemagglutinin (PHA)-stimulated peripheral mononuclear blood leukocytes (PBL) showed that unstimulated (G0 phase) cells were negative for the Ki-67 antigen (Gerdes *et al.*, 1984). We now know that the MKI67 gene promoter itself is cell cycle-regulated, containing binding sites for the canonical G1-regulatory E2F family of transcription factors (Ishida *et al.*, 2001), and that Ki-67 mRNA levels increase during G1 (Sobecki *et al.*, 2016; Sobecki *et al.*, 2017). Ki-67 protein degradation also occurs during G1 via ubiquitin proteasome complex APC/C-Cdh1 (Chierico *et al.*, 2017; Sobecki *et a.,2017)*. Therefore, Ki-67 protein concentrations in G1 are controlled by two opposing mechanisms. In addition, unlike deeply quiescent or senescent cells, cells in early stages of cell cycle arrest have low levels of Ki-67, which can carry over after re-entering the cell cycle (Sobecki *et al.*, 2017). Therefore, slight variation in the degree of

quiescence can result in variable Ki-67 levels in the first G1 phase after cell cycle re-entry, likely contributing to variable observations of in different experiments (Gerdes *et al.*, 1984; Lopez *et al.*, 1991; Sobecki *et al.*, 2017).

1.2.3: Ki-67 coats mitotic chromosomes

In the past few years, several studies have greatly increased our understanding of Ki-67's mitotic functions. As cells enter mitosis, chromosomes undergo a remarkable series of structural transformations known as chromosome condensation. A proteinaceous sheath termed the perichromosomal layer (PCL) exists at the outer surfaces of individual chromosomes (Hernandez-verdun and Gautier, 1994; Van Hooser *et al.*, 2005). Ki-67 is one of the earliest proteins associated with this structure and remains on it until telophase (Van Hooser *et al.*, 2005). Several studies have found that Ki-67 is required for the formation of the human PCL. Acute depletion of Ki-67 in human cells caused dispersal of all other non structure layer components tested, including nucleolin, nucleophosmin, NIFK, cPERP-B, cPERP-C, cPERP-D and cPERP-F. Conversely, depletion of these components did not alter perichromosomcal localization of Ki-67 (Booth *et al.*, 2014). The abnormal localization of nucleolar components during mitosis in turn leads to their asymmetric distribution in daughter cells(Booth *et al.*, 2014). A recent study shows that CAF-1 p150, the largest subunit of histone chaperone Chromatin Assembly Factor-1 (CAF-1) regulates normal levels of Ki-67 accumulation on the PCL. This activity was mapped to the sumoylation interacting motif (SIM) within p150, which was also required for the localization of

Ki-67 and nucleolus association domain to the nucleolus during interphase(Smith *et al.*, 2014).

While the function of Ki-67 on PCL is still being explored, one recent study suggests that Ki-67's large size and high density of positively charged amino acids causes it to act as a surfactant, keeping mitotic chromosomes from aggregating (Cuylen *et al.*, 2016). Upon Ki-67 depletion, adhesion between neighboring mitotic chromosomes impaired spindle assembly and metaphase plate formation. As a result, in HeLa cells, depletion of Ki-67 impaired access of spindle microtubules to chromosomes, and chromosome alignment during metaphase and caused a prolonged mitosis (Starborg *et al.*, 1996; Vanneste *et al.*, 2009)

1.2.4: Is Ki-67 required for proliferation

Although Ki-67 expression is tightly correlated with proliferation, differing results have been obtained in tests of the role of Ki-67 in cell growth. In early studies, microinjection of an anti-Ki-67 antibody inhibited proliferation of Swiss 3T3 cells (Starborg *et al.*, 1996). Likewise, human tumor cell lines, including human IM-9 multiple myeoloma, RT-4 bladder carcinoma, and 786-0 renal carcinoma cells reduced proliferation rate upon treatment of either Ki-67 targeted anti-sense oligonucleotides or si-RNA(Schluter *et al.*, 1993; Zheng *et al.*, 2006). Also, light-mediated inactivation of chromophore-marked Ki-67 inhibited ribosomal RNA synthesis in HEP-2 cells (Rahmanzadeh *et al.*, 2007). However, another study did not detect altered ribosomal RNA production upon Ki-67 depletion in several cancer cell lines tested, including HeLa, U2OS and HCT116

(Sobecki *et al.*, 2016). Additionally, the cell cycle distribution of HeLa and U2OS cells remains unaltered upon depletion of Ki-67 (Sobecki *et al.*, 2016). In human MCF-10A epithelial breast and DLD-1 colon cancer cells, loss of Ki-67 does not affect cell proliferation in bulk culture but clonogenic growth of highly diluted cell population is decreased(Cidado *et al.*, 2016). These data raise the possibility that Ki-67 function may have different consequences in different cell types.

1.2.5: Interphase Ki-67 organizes heterochromatin

The finding that Ki-67 colocalized with Hoechst 33258-stained chromocenters in mouse Swiss 3T3 fibroblasts during the S and the G2 phase indicated that it may play a more general role in heterochromatin organization (Starborg *et al.*, 1996). Ki-67 association with heterochromatic regions was also detected in early G1 phase cells. In this case, immuno-FISH experiments revealed that Ki-67 localizes to hundreds of distinct foci within two hours after mitotic exit (Lopez *et al.*, 1991; Isola *et al.*, 1990). These early G1 foci co-localize with several different classes of heterochromatic repetitive elements, including centromeric alpha satellite, telomeric repeats, and Satellite III (Bridger *et al.*, 1998). Notably, these repeats frequently localize to the nucleolar periphery during the rest of interphase.

These observations are underpinned by several recent studies showing that Ki-67 promotes association of multiple heterochromatic regions with the nucleolar periphery. Nucleoli are surrounded by a subset of the genome termed nucleolar-associated DNA sequences (NADs) (Norton *et al.*, 2009; Koningsbruggen *et al.*, 2010; Németh *et al.*, 2010; Dillinger *et al.*, 2016). Multiple

studies showed that Ki-67 depletion decreased the nucleolar assocation of NADs, including a LacO array proximal to the rDNA repeats on chromosome 13 (Booth *et al.*, 2014), or chromosome 17 alpha satellite repeats (Matheson and Kaufman, 2017b). Additionally, Ki-67 depletion delocalized centromeric histone variant CENP-A away from nucleoli, indicating reduced centromeric chromatin association with nucleoli (Sobecki *et al.*, 2016).

How does Ki-67 promote these interactions? There are several possibilities that are not mutually exclusive. These include recognition of primary sequences or chromatin features of NADs (Bridger *et al.*, 1998; Kreitz *et al.*, 2000), via direct interaction(Takagi *et al.*, 1999; Scholzen *et al.*, 2002), or via binding of other nucleolar–targeting proteins. Furthermore, RNAs are important for several higher order chromosome interactions (Hacisuleyman *et al.*, 2014; Yang *et al.*, 2015), including examples at nucleoli (Mondal *et al.*, 2008; Fedoriw *et al.*, 2012a) , and these have not been investigated in this regard. Ki-67 may also form a charged surface coating on nucleoli in analogy to its role on mitotic chromosomes (Cuylen *et al.*, 2016)and thereby attract heterochromatin(Strom and Alexander, 2017). It is possible that phase separation of heterochromatin could contribute to such a mechanism.

Besides mediating long-range chromosome interactions, Ki-67 also promotes short-range chromatin interactions. Upon Ki-67 depletion, HeLa cells displayed reduced forster resonance energy transfer (FRET) signals between H2B-eGFP and H2B-mCherry (Sobecki *et al.*, 2016), which reports on inter-nucleosomal interactions on the scale of ~1-10 nm (Llères *et al.*, 2009).

Elimination of condensed FRET signal foci occurring from heterochromatin suggests Ki-67 promotes heterochromatin compaction(Sobecki *et al.*, 2016). Heterochromatin compaction in most eukaryotes depends on core histone deacetylation and histone H3K9 di- and tri-methylation (Eissenberg and Elgin, 2014). In the absence of Ki-67, H3K9Me3 and H4K20Me3 become less focally clustered(Sobecki *et al.*, 2016). Methylation of H3K9 is recognized by HP1(Jacobs and Sepideh, 2002; Nielsen *et al.*, 2002). Ki-67 directly binds HP1 with high affinity(Kametaka *et al.*, 2002; Scholzen *et al.*, 2002). In HeLa cells, Ki-67 partly overlaps with HP1 and relocalizes to sites of high ectopic HP1 expression (Kametaka *et al.*, 2002; Scholzen *et al.*, 2002). The interaction between Ki-67 and HP1 may allow Ki-67 to link H3K9me2/3 enriched regions with its other interactors that are involved in histone methylation including UHRF1 that binds H3K9me3 and DNA methyltransferase DNMT1 and components of H3K27 methyltransferase complex and H3K4 demethylase complexes(Bostick *et al.*, 2007; Sobecki *et al.*, 2016). To further understand how interaction between HP1 and Ki-67 contributes to heterochromatin organization, it is improtant to examine phenotypes of cells in which Ki-67 can not bind HP1.

1.3: Heterochromatin compartments

Chromatin has historically been segregated into two categories, depending on how densely they are stained by DNA dyes. Euchromatin stains lightly with DAPI (4', 6-diamidino-2-phenylinodole), indicative of "open" structure and accessible to transcription factors. It includes mostly transcriptional active regions that are rich in genes and regulatory sequences(Grewal and Elgin, 2002).

On the contrast, inactive gene-poor regions are packaged into highly condensed heterochromatin that are stained more intense with DAPI than the euchromatic segments(Grewal and Elgin, 2002). Heterochromatin is further classified into two types: constitutive heterochromatin and facultative heterochromatin. Constitutive heterochromatin contains centromeres and telomeres. They are silent in all cell types(Saksouk *et al.*, 2015). Facultative heterochromatin is silenced in a cell-type specific manner(Johnson and Straight, 2017). Heterochromatin shows preferred clustering at the nuclear periphery, near the nucleoli or pericentromeric bodies (Politz *et al.*, 2013; Padeken and Heun, 2014; Politz *et al.*, 2016). The mechanisms which drive chromatin partition in the nucleus remain incomplete.

1.3.1: Lamina Associated Domains

In metazoans, the nucleoplasmic surface of the inner nuclear membrane is structurally supported by the nuclear lamina (NL), a filamentous meshwork consisting of filament proteins named lamins (Akhtar and Gasser, 2007). NL acts as a surface for anchoring specific DNA sequences(Taddei *et al.*, 2004). The regions contacting it are referred to as lamina associated domain (LADs). LADs have been identified by means of the DNA adenine methyltransferase identification followed by genome-wide sequencing (Dam ID)(Pickersgill *et al.*, 2006; Guelen *et al.*, 2008; Peric-Hupkes *et al.*, 2010). Briefly, fusion of nuclear lamina protein (typically Lamin B1) with bacteria DNA adenine methyltransferase (Dam) methylated genomic loci which are in close proximity to the fused nuclear lamina protein at nucleotide adenine(Steensel and Henikoff, 2000; van Steensel *et al.*, 2001). Because eukaryotes lack adenine methylation, genome-scale

mapping of this orthologous mark reveals genomic loci that contact nuclear lamina.

LADs are remarkably large genomic segments, ranging in size from 40 kilobases to over 30 megabases(Pickersgill *et al.*, 2006; Guelen *et al.*, 2008; Peric-Hupkes *et al.*, 2010).   In mouse and human cells, they covered ~40% of the genome. LADs are primarily heterochromatic AT rich regions(Pickersgill *et al.*, 2006; Guelen *et al.*, 2008; Peric-Hupkes *et al.*, 2010). Intuitively, LADs possess several molecular features typical of heterochromatin. For example, LADs have a low overall gene density and are enriched in repressive histone modifications H3K9me2 and H3K9me3 (Guelen *et al.*, 2008; Wen *et al.*, 2009). Although most genes in LADs are expressed at very low levels or transcriptional silent, LADs also contain some H3K4me3-marked chromatin that is presumably unrepressed(Guelen *et al.*, 2008; Peric-Hupkes *et al.*, 2010) , suggesting nuclear periphery position can function more than a repressive compartment.

Understanding the organization of genomes require the identification of mechanisms that mediate this targeting. Various molecular mechanisms have been proposed to explain how endogenous loci become targeted to the periphery.

First, repressive histone modifications have a prominent role in facilitating NL –LADs association(van Steensel and Belmont, 2017). In *C. elegans* and mammalian cells, disruption of methyltransferase mediated H3K9me3 deposition weaken the association between LADs and NL(Towbin *et al.*, 2012; Bian *et al.*, 2013; Kind *et al.*, 2013a; Chen *et al.*, 2014; Harr *et al.*, 2015). The repressive histone mark H3K27me3 is also linked to LADs.   Disruption of H3K27Me3

relocated a periphery located transgene array to the nuclear interior (Harr *et al.*, 2015).

Second, there are specific protein factors that contribute to promote LADs to the nuclear periphery. NL proteins and proteins interacting with both NL proteins and chromatin components are important for peripheral tethering of heterochromatin(van Steensel and Belmont, 2017). For example, the interaction between *Xist* and Lamin B receptor anchors Xi to nuclear periphery (Chun-Kan Chen *et al.*, 2016).

Several studies have reported a correlation between transcription and nuclear periphery sequestration. Artificial tethering experiments in which exogenous loci were fused with lamins showed reduction in expression upon peripheral relocalization(Reddy *et al.*, 2008; Finlan *et al.*, 2008). However, nuclear periphery reposition does not result in gene repression at every loci tested. Some active genes near the tethering sites were present on chromosomes repositioned to the nuclear periphery(Finlan *et al.*, 2008)indicating that transcription is compatible with nuclear periphery. Indeed, with a strong transcription activator, relocation of a reporter gene array to the nuclear lamina displays similar kinetics of reporter activation when it was positioned in the nuclear interior(Kumaran and Spector, 2008). NL harbors enzymatic activities such as histone deactylase HDAC3 that modify chromatin state(Somech *et al.*, 2005; Demmerle *et al.*, 2012). During the in vitro differentiation of mESC to NPC, many genes with neural functions were released from the lamina. They were activated immediately or become "unlocked" from silent states that are more

likely to be activated later(Peric-Hupkes *et al.*, 2010).Therefore, perinuclear localization appears to alter chromatin states rather than initiate transcriptional changes *per se*(Mattout *et al.*, 2015).

1.3.2: Nucleolus Associated Domain (NADs)

Nucleoli are the largest non-membrane bound organelles within the nucleus. It is where rDNA transcription, rRNA processing and ribosome biogenesis occur. In human cells, nucleoli form around genomic regions called nucleolar organizing regions (NORs) located on the short arms of five acrocentric human chromosomes 13,14,15,21 and 22 (Sirri *et al.*, 2008; Pederson, 2011).

Nucleoli are surrounded by a subset of highly structured genomic elements termed nucleolar associated DNA sequences(NADs) (Norton *et al.*, 2009; Koningsbruggen *et al.*, 2010; Németh *et al.*, 2010; Dillinger *et al.*, 2016). Similar to LADs, NADs are large genomic regions with low gene density and enriched with multiple repressive histone marks. Satellite repeats and gene families including 5S rRNA, immunoglobulins, defensin (DEF), olfactory receptor (OR), and tRNA are enriched in the NADs(Norton *et al.*, 2009; Koningsbruggen *et al.*, 2010; Németh *et al.*, 2010; Dillinger *et al.*, 2016). These gene families cluster as multigene arrays and are expressed in a tissue specific manner. In female IMR-90 cell line, almost the entire Xi appeared as NADs (Dillinger *et al.*, 2016). Therefore, nucleolus sequestration maybe one means of transcriptional regulation during development.

1.4: NAD dynamics

Repressive heterochromatin compartments change form and composition during development. So far, reorganization of NADs during differentiation has not been investigated in a genome-wide manner. One study compared NADs between human proliferating cells and senescent cells and revealed the extensive dissociation of centromeric and pericentromeric satellite repeats from nucleoli (Dillinger *et al.*, 2016). On the scale of each cell division, NADs must disassembly, replicate, undergo mitosis, and then reestablish in cycling cells.

Below I will summarize the current understandings of three individual NADs loci during the cell cycle progression from single-cell studies.

1.4.1: 1q12

Three decades ago, the association of a pericentromeric region of chromosome 1 with the nucleolus was described in MCF-7 human breast cancer cells(Leger *et al.*, 1994). It was unexpected at that time because chromosome 1 does not contain nucleolus organizer regions (NORs) (Sirri *et al.*, 2008; Pederson, 2011). Using Ki-67 staining patterns to distinguish stages of the cell cycle, cells display increased association from early G1 to mid S phase, where reaches the maximum and then decreases from mid S to G2. The number of nucleoli per cell, nor the fraction of the nuclear area occupied by nucleoli does not influence 1q12 localization(Leger *et al.*, 1994) .Notably, the nucleoli that associated with 1q12 enlarged much more from S to G2 phase (Leger *et al.*, 1994), indicating that it may provide a signal to promote nucleolar transcription activity. Sequencing

analysis of purified nucleoli from different cell lines reveals that 1q12 contain satellites repeats that are identified as NADs (Koningsbruggen *et al.*, 2010; Németh *et al.*, 2010).

1.4.2: Inactive X chromosome

In Eutheria, males have one X chromosome and females have two X chromosomes. In order to achieve gene dosage balance between two sexes, females randomly inactivate one X chromosome. This process is called random X chromosome inactivation. X-inactivation is a preeminent example of facultative heterochromatin formation as it culminates in the transcriptional silencing of thousands of X-linked genes(Anguera *et al.*, 2006).

X inactivation initiates when *XIST* RNA is transcribed exclusively from a randomly selected X chromosome. Both the human *XIST* and mouse *Xist* genes lack an open reading frame, and produce long noncoding RNAs (lncRNA)(Brown *et al.*, 1992; Brown *et al.*, 1992). During the initiation step of X chromosome inactivation, Lamin B Receptor (LBR) interacts with *Xist* to recruit Xi to the nuclear periphery and enable *Xist* to spread into actively transcribed genes along the chromosome (Chun-Kan Chen *et al.*, 2016). Another preferred location of Xi is the nucleolar periphery(Barr and Bertram, 1949; Zhang *et al.*, 2007; Dillinger *et al.*, 2016). In MEFs, during mid-to-late S phase, Xi frequently visited nucleoli. In the rest of cell cycle or G0 phase, Xi rarely localized to the perinucleolar regions. Loss of perinucleolar localization in cycling cells results in erosion of several features of heterochromatin and reactivation of Xi at the single gene level(Zhang *et al.*, 2007).

1.4.3: *Kcnq1*

Kcnq1 region from placental is another example that associates with the nucleoli specifically during mid-late S phase. The lnc RNA Kcnq1ot1 silences imprinted genes in the lineage-specific manner(Pandey *et al.*, 2008)(Mohammad *et al.*, 2010). In the liver, *Kcnq1ot1* silences ubiquitously imprinted genes next to the *Kcnq1* domain. In the placental, *Kcnq1ot1* can repress both nearby ubiquitously imprinted genes and distal placental-specific imprinted genes(Lewis *et al.*, 2004; Pandey *et al.*, 2008; Mohammad *et al.*, 2010). The imprinting of placental-specific imprinted genes is controlled by repressive histone modifications H3K27me3 and H3K9m3(Lewis *et al.*, 2004; Pandey *et al.*, 2008). In placenta cells, *Kcnq1ot1* targets *Kcnq* locus to the nucleolus twice as frequently as observed in fetal liver cells during S phase(Pandey *et al.*, 2008; Matheson and Kaufman, 2015). Mouse *Kcnq1ot1* RNA contains 890 bp silencing domain. When it inserts into an episomal plasmid, transcript from silence domain targets episomal plasmid to the nucleoli during mid S-phase, spread repressive histone modifications and silence flanking reporter genes(Mohammad *et al.*, 2008).

1.5: *cis/ trans*-acting factors involved in NADs organization

To understand the functional implications of the nucleolar heterochromatin compartment, it is necessary to thoroughly understand the molecular mechanisms that drive NAD-nucleolus interactions. NADs are typically 10kb- 10 Mb in size with a medium size of ~700 kb(Koningsbruggen *et al.*, 2010; Németh

et al., 2010; Dillinger *et al.*, 2016). The contact of kilobases of chromatin with the nucleolus suggests involvement of multivalent interactions. These interactions may be driven by primary DNA sequences, chromatin features of NADs and nucleolar targeting proteins/RNAs.

1.5.1: DNA sequences that target genomic regions to the nucleolus

It is like that the ability of NADs to interact with the nucleoli is at least in part encoded in the DNA sequences. In microscopy studies, active Pol III that contains Pol III transcribed tRNAs and 5S rDNA, forms distinct foci in the nucleolar periphery(Haeusler and Engelke, 2006). Recent sequencing analyses of purified nucleoli reveal that 5S rDNA is highly enriched in the NADs(Koningsbruggen *et al.*, 2010; Németh *et al.*, 2010; Dillinger *et al.*, 2016). A study shows that ectopic integration of 119bp 5S rDNA sequence into new genomic location can autonomously re-direct the host regions to the nucleolar periphery and results in transcriptional repression of reporter genes and endogenous genes proximal to integration sites. The extent of transcriptional repression is closely correlated with the frequency of nucleolus association (Fedoriw *et al.*, 2012b). 5S rDNA is transcribed by RNA polymerase III and is required for ribosome assembly for cell growth(Haeusler and Engelke, 2006). It remains to understand how the actively transcribed 5S rDNA genes escape the repressive heterochromatic environment of nucleolus periphery.

1.5.2: CTCF

The CCCTC-binding factor (CTCF) is a sequence specific - DNA binding protein with between 55,000-65,000 sites of enrichment throughout the human genome (Merkenschlager and Nora, 2016). In immortalized human leukemia cell line, CTCF interacts with nucleolar protein nucleophosmin and tethers an exogenous insulator element to the nucleolus (Yusufzai *et al.*, 2004). In female cell lines, CTCF depletion significantly relocalized Xi from the nucleolus(Yang *et al.*, 2015). Because CTCF depletion reduces expression of *Firre* which is also required for perinucleloar localization of Xi(Yang *et al.*, 2015), CTCF can regulate Xi perinucleolar localization through direct tethering and regulating *Firre* expression(Matheson and Kaufman, 2015).

1.5.3: Histone modifications as anchoring signals

As discussed above, in both *C.elegans* and mammalian cells, histone H3K9 methylations are implicated as anchoring signals for perinuclear chromatin(Towbin *et al.*, 2012; Bian *et al.*, 2013; Kind *et al.*, 2013a; Chen *et al.*, 2014; Harr *et al.*, 2015). NADs are also enriched in H3K9me3(Koningsbruggen *et al.*, 2010; Németh *et al.*, 2010; Dillinger *et al.*, 2016). In replicative senescent cells, most NADs-nucleolar associations are maintained but H3K9me3 enriched centromeric and pericentromeric repeats extensively dissociated from the nucleolus(Dillinger *et al.*, 2016). Further analysis of NADs purified from cells depleted of the H3K9 methyl transferase Sedb1, Suv39 or G9a is needed.

1.5.4: lncRNAs for nucleolar targeting of inactive X chromosome

X-chromosome inactivation represents a powerful model system for facultative heterochromatin that associates with nucleoli. Close proximity of Xi to lamina or nucleolus may facilitate initiation and maintenance of heterochromatic features and transcriptional silencing. In MEFs, Xi frequently associates with nucleolus during mid-late S phase. Reduced perinucleolar targeting of the Xi results in several features of compromised heterochromatin including decreased H3K27me3 enrichment and Xi reactivation at the single gene level (Zhang *et al.*, 2007).

Two lncRNAs have been identified tether Xi to the nucleolus. The first one is the *Xist* lncRNA which is essential for silencing and compaction of the X chromosomes. The Xist gene is located in the 2.3 Mb region called the X inactivation center (XIC) (Chureau *et al.*, 2002), which contains several noncoding genes that regulate *XIST*. In MEF, deletion of *Xist* from endogenous Xic loci significantly reduces Xi-nucleolar association. Conversely, autosomes carrying Xic transgenes preferentially associate with nucleoli and displayed S phase dependent association as the endogenous Xi did (Zhang *et al.*, 2007; Kelsey *et al.*, 2015). Chromatin context around the integration sites does not influence the Xi-nucleolus association. In human male HT1080 cells, ectopic *Xist* cDNA is integrated into different regions in autosomes and the active X chromosome. Upon *XIST* expression, all the integration sites show increased perinucleolar localization and silencing of a reporter gene(Kelsey *et al.*, 2015). However, the recruitment of repressive histone modifications is strongly

influenced by the pre-existing epigenetic features of integration sites (Zhang *et al.*, 2007; Kelsey *et al.*, 2015)

Another example is the lncRNA *Firre*. *Firre* is a strictly nuclear lncRNA which escapes X-chromosome inactivation(Hacisuleyman *et al.*, 2014; Yang *et al.*, 2015). It forms expression foci on both X chromosomes before and after X-chromosome inactivation(Yang *et al.*, 2015). In the mouse fibroblast, the *Firre* locus on the Xi contacts the nucleolus. Depletion of *Firre* RNA decreases perinucleolar localization of the Xi. (Yang *et al.*, 2015). Although H3K27me3 declustered on the Xi in *Firre* depleted cells, there are minimal effects on gene silencing, consistent with the idea that multiple functionally overlapping factors affect Xi heterochromatin localization and gene silencing(Csankovszki *et al.*, 2001)(Yang *et al.*, 2015). Insulator protein CTCF binds *Firre* locus specifically on Xi. However, depletion of *Firre* does not change the CTCT occupancy (Yang *et al.*, 2015). It implicates that *Firre* can target Xi to the nucleolus independent of CTCF. *Firre* interacts with nuclear matrix factor hnRNPU and facilitates trans-chromosome interactions among Xi and other five genomic loci (Hacisuleyman *et al.*, 2014). Further studies should explore whether these genomic foci are enriched to the nucleolar periphery as well.

1.5.5: Comparison between LADs and NADs organization

In Table 1.1, I summarized the similarities and differences between LAD and NAD organization.

Table 1.1: Features of LADs and NADs organization

	LADs	NADs
Known periphery/perinucleolar region regulators		
a. NL /nucleolar protein or RNA	Lamin B Lamin A/C (Kohwi et al., 2013; Shevelyov et al., 2009; Solovei et al., 2013)	Ki-67 nucleophosmin nucleolin Alu RNA (Timothy et al., 2017; Caudron-Herger *et al.*, 2015)
b. proteins interacting with NL/nucleolar proteins and chromatins	Lamin B receptor emerin (Chen et al., 2016; Amendola et al 2015; Zheng et al., 2015)	CAF-1 p150 (Corey et al., 2016)
c. Insulator elements	CTCF (Guelen et al., 2008)	CTCF (Yusufzai et al., 2004)
d. DNA sequence	beta-globin(*HBB*)locus (Bian et al.,2013)	119bp 5S rDNA (Fedoriw et al.,2012)
e. Chromatin modification	H3K9me C. *elegan*: MET-2 SET-25 (Towbin et al., 2012) Mammal: G9A Suv39H1 Suv39H2 (Bian et al.,2013; Chen et al.,2014b; Harr et al., 2015;Kind et al.,2013	?
f. lncRNA		*cis*: *XIST* *Firre* (Zhang et al.,1997; Yang et al.,2015)
Dynamics after mitosis	stochastically,	with preference

	with preference to NL and perinucleoar (Kind et al., 2013)	to NL and perinucleolar (Koningsbruggen et al., 2010)
Transcriptional activity	repress some but not all transgenes (Guelen et al., 2008;Peri-Hupes et al.,2010;Akhtar et al.,2013;	repress some but not all transgenes (Nemeth et al., 2010)
Cell Cycle dynamics	?	S phase specific: Xi Kcnq (Zhang et al., 2007; Mohammad et al., 2008)
Constitutive and Facultative	cLADs fLADs (Meuleman et al., 2013; Peri-Hupes et al., 2010)	?

1.6: G1/S phase checkpoint

Normal cell cycle progression through interphase and mitosis is regulated by coordinated activation of cell cycle proteins and checkpoint pathways. Proper activation and inactivation of cyclin dependent kinase (CDK) is essential to promote proper transition through the cell cycle, and checkpoints are the control mechanisms which ensure cells are qualified to progress through the next phase. Currently, there are three known checkpoints: the G1 checkpoint, G2/M checkpoint, and the spindle checkpoint. The G1/S cell cycle check point controls the commitment of cells to transition through the G1 phase to enter into the DNA synthesis S phase. Several distinct transcription factors regulate S phase entry. They interact and coordinate with each other to regulate the cell cycle progression.

1.6.1: E2F-Rb pathway

E2F transcription factors E2F1, E2F2, and E2F3 and the Retinoblastoma tumor suppressor protein (pRB) pathway are one of the major drivers for the G1/S transition. The canonical model for its regulation is simple. pRB is a chromatin associated protein. When in the hypophosphorylated state, pRB associates with E2F transcription factors to prevent expression of genes required for S phase. Hyper-phosphorylation of pRB releases E2Fs and thereby allows cell cycle progression(Dyson, 1998).

Besides sequestrating E2F transcription factors, pRB directly binds to the promoter and recruits a number of co-repressors to silence transcription. Examples of the proteins associated with pRB included histone deacetylases (HDAC1, HDAC2), DNA methyl transferase (DNMT1), chromatin remodeling complex BRG1, histone methyl transferases Suv39h1 and Suv4-20h1/h2 (Talluri and Dick, 2012).

pRB does not always imply transcription repression. Under certain conditions, E2F/pRB complexes could associate with transcriptionally coactivators. One study showed that upon DNA damage, pRB forms transcriptional active complex with transcription factor E2F1 and drives expression of pro-apoptotic genes (Ianari *et al.*, 2009). It indicates that pRB mediated transcription is context dependent. More than 300 proteins had been reported to associate with pRB(Morris and Dyson, 2001; Talluri and Dick, 2012). Depending on the stimuli, pRB can either recruit co-repressors or co-activators to

the binding regions. But how the different cellular processes dictate pRB's interactome is largely unknown.

pRB can function beyond G1/S checkpoint. In hTERT-RPE1 cells, depletion of pRB increased incidence of lagging chromosomes and abnormal chromosome segregation due to cohesion defects(Manning *et al.*, 2010). By direct binding methyltransferase Suv4-20h2(Gonzalo *et al.*, 2005), pRB facilitates H3K9me3 and H4K20me3 establishment at centromeric heterochromatin(Manning *et al.*, 2010). Depletion of pRB reduces H4K20me3 and loading of cohesion complex on centromeric regions. (Manning *et al.*, 2010; Manning *et al.*, 2014)

1.6.2: p21

The major role of p21 in the G1 checkpoint lies in its ability to bind and inactivate cyclin A /CDK2, cyclin E/CDK2, and cyclin D/CDK4 complexes(Xiong *et al.*, 1993; Labaer *et al.*, 1997; Gartel and Radhakrishnan, 2005).

p21 directly inhibits DNA synthesis by binding to PCNA, the sliding clamp required for processive DNA polymerase activity. In vitro, a competition between p21 and Pol δ or RFC for binding to central loop of PCNA efficiently inhibits Pol δ DNA replication (Waga and Stillman, 1998)

The effect of p21 on CDK is stoichiometry regulated and does not always inactivate CDK. Low levels of p21 can activate the CDK4/6 complex and facilitate S phase entry. One study shows that S130 phosphorylation on p21 is central for CDK activation. In the low p21 setting, CDK7 phosphorylates S130. When

phosphorylated, p21 associates with CDK4/6 and facilitates CDK4/6 activation by rendering T172 on CDK4/6 more accessible to CAK(Bisteau *et al.*, 2013).

As a universal CDK inhibitor, overexpression of p21 can potentially inhibit cyclin B1-CDK1 and cyclin A-CDK1/2 complex and arrest cells at G2/M transition(Baus *et al.*, 2003).

1.6.3: DREAM complex

During the G0, G1/S and G2/M phases, the RB-like pocket proteins p130 and p107, repressive E2F transcription factors E2F4 or E2F5, dimerization partner 1 (DP1), and five subunits of the multi-vulval class B (MuvB) complex regulate expression of cell cycle dependent genes through a common pathway. These factors form a large multi-protein complex termed DREAM complex (Sadasivam and DeCaprio, 2013; Guiley *et al.*, 2015; Fischer *et al.*, 2016).

DREAM complex changes its components through cell cycle progression. In serum-starved and quiescent G0 cells, p107 is not detectable. DREAM complex contains p130, E2F4 and MuvB complex. Knockdown or mutation of p130 increased p107 expression and formed a p107 DREAM complex instead(Hurford *et al.*, 1997; Litovchick *et al.*, 2007; Sadasivam and DeCaprio, 2013). When p107 and p130 are simultaneous depleted, the MuvB core is unable to form a functional DREAM complex during quiescence and prematurely enters into the cell cycle(Litovchick *et al.*, 2007). During S phase, MuvB dissociates from p130 and sequentially recruits BMYB and FOXM1 to late cell cycle promoters(Litovchick *et al.*, 2007). Increased activity of BMYB-MuvB-FOX1

up-regulates mitotic gene expression and promotes mitosis(Sadasivam and DeCaprio, 2013).

Expression of early cell cycle genes is co-regulated by E2F/Rb and DREAM complex(Fischer *et al.*, 2016). In serum-starved cells, DERAM binds to the promoters of E2F targets(Litovchick *et al.*, 2007). It recruits histone deacetylase HDAC1 and represses S phase-promoting transcripts(Rayman *et al.*, 2002). Disruption of DREAM complex by co-depletion of p130 and p107 in quiescent cells leads to derepression of E2F-targeted genes and premature G1 phase entry(Hurford *et al.*, 1997). When cells enter the cell cycle, E2F-binding sites were less bound by DREAM and switched to E2F binding(Litovchick *et al.*, 2007)(Sadasivam and DeCaprio, 2013). Transcription by active E2F transcription factors permits cell cycle gene expression and continuance of the cell cycle. (Shawna Miles 2017, Sada-sivam and DeCaprio 2013)

1.7: Concluding Remarks

1.7.1: Mechanisms for targeting genomic regions to the nucleolus

Heterochromatin is concentrated in three intranuclear regions: the nuclear periphery, the perinucleolar space and in pericentromeric bodies(Politz *et al.*, 2013; Padeken and Heun, 2014). Although many LADs overlap with NADs sequences and *in situ* hybridization studies show that PCH can overlap with PH or PNH in many tissue types(Koningsbruggen *et al.*, 2010; Kind *et al.*, 2013a; Politz *et al.*, 2016), some heterochromatic genomic regions, such as constitutive LADs (cLADs), preferential interact with NL(Meuleman *et al.*, 2013). Increased

NAD association with NL occurs upon nucleoli disruption(Ragoczy *et al.*, 2014). Peripheral positioned HBB transgenes shift to the pericentromeric compartment upon depletion of periphery targeting regions (Bian *et al.*, 2013).These results indicate that distribution across these different heterochromatin compartments is at least partly nonstochastic and involves specific targeting elements.

As nuclear lamina protein Lamin B can form the contact points for LADs(Shimi *et al.,* 2015), nucleolar proteins mediating NAD organization have been reported. In the plant *Arabidopsis thaliana*, cells from nucleolin mutant *(nuc1)* plants showed altered nucleolar morphology. Deep sequencing of purified nucleoli in *nuc1* cells revealed decreased nucleolar association of telomeric heterochromatin(Pontvianne *et al.*, 2016). In addition, in the cells expressing LacI-nucleolin (NCL) or LacI-nucleophosmin (NPM), LacO-tagged transgenes was targeted to the nucleolar periphery(Caudron-Herger *et al.*, 2015).However, not all the nucleolar proteins can target genomic loci to the nucleolus. Fibrillarin is localized in the dense fibrillar components of nucleolus. Fibrillarin is an rRNA 2'-O-methyltransferase and histone H2A glutamine methyltransferase(Reichow *et al.*, 2007). In the LacI-Lac system, fibrillarin cannot promote translocation of LacO transgenes to nucleoli(Caudron-Herger *et al.*, 2015). LacO array integrated proximal to the rDNA repeats on chromosome 13 frequently associates with nucleoli and can be visualized by LacI-GFP(Booth *et al.*, 2014). In this system, unbiased RNAi screen can identify proteins required for NADs localization. One challeng is that many proteins regulate NAD-nucleolus association, even at the

level of individual NADs. Depletion of individual proteins on the relocation may be modest due to redundancy.

Below, I suggest a step -wise NAD assembly model. First, similar types of NADs exhibit a high affinity to each other. Certain nucleolar protein/RNAs target NADs to the nucleolus via recognition of specific DNA sequences, chromatin features such as DNA methylation and histone modifications. Once in the nucleolus, association with nucleolar components such as Alu RNA, rDNA or proteins reduce the off-rate of the NADs from nucleolus and prolong its residence time. Some NADs have more "contacts points" with nucleolus and can interact with the nucleolus in most cell types, while the other NAD-nucleolus interactions occu in only certain cell types.

1.7.2: The functional distinction and redundancy among three repressive heterochromatin compartments

There is substantial overlap between the three heterochromatin compartments. [m6]A-Tracer technique to track the destination of parental LADs in the daughter cells reveals that some LADs that end up in the nuclear interior after mitosis become closely associated with nucleoli(Kind *et al.*, 2013a). Similarly, as a result of stochastic reshuffling following mitosis, mother NADs reposition in the nuclear periphery and thus become LADs in daughter cells(Koningsbruggen *et al.*, 2010). Furthermore, disruption of nucleoli causes a shift of associated genomic loci toward NL without gene derepression, indicating these regions are functionally equivalent as repressive compartments(Ragoczy *et al.*, 2014; Politz *et al.*, 2016).

However, three repressive heterochromatin compartments are not identical. In addition to the probabilistic distribution of heterochromatin, specific tethering elements preferentially position certain genomic loci at particular heterochromatin compartment. To better define the functional distinction and redundancy of heterochromatin compartment, it is essential to identify the constitutive and facultative LADs/NADs and correspondent targeting mechanisms.

1.7.3: S-phase dependent NAD-nucleolus association

Because LADs or NADs are typically several megabase in size, their ability to move in a given cell is limited(Gibcus and Dekker, 2013). *In vivo* tagging and tracking of dynamics of LAD-NL interactions in single cell shows that interphase LADs move within 1 μm from the NL. NL-contacting loci is rarely seen to move all the way to the nuclear interior. Even acidic–activating domain VP16 can disrupt H3K9me3 on the LADs and dislodge them further away from the NL, most of LADs still moved over a short distance from NL and are not found in the interior(Kind *et al.*, 2013a). With respect to cell cycle, chromatin mobility peaks in early G1 where it associates with organization elements and seeds heterochromatic compartment reorganization(Thomson *et al.*, 2004). During other phases of cell cycle, large chromatin segments at the scale of megabase is considerably less dynamic(Gibcus and Dekker, 2013).

NAD dynamics throughout the cell cycle has not been investigated in a genome-wide manner, but a microscopic study at a single cell level identified S phase dependent association between Xi and the nucleolus(Zhang *et al.*, 2007).

This movement is intriguing considering constrained chromosome mobility throughout interphase. Within one cell cycle, interphase Xi moves to the nucleolus and then moves away from it. lncRNA *Firre* and *XIST* are important in perinucleolar localization of Xi(Zhang *et al.*, 2007; Yang *et al.*, 2015). Progression of cells through replication is required for position LADs to the nuclear periphery. In the cells blocked at G1/S transition, the loci change their positions relative to NL(Shachar *et al.*, 2016) compared with asynchronous cells. But how the NADs-nucleolus interactions respond to the G1/S checkpoint is not studied yet.

Chapter II: Ki-67 affects heterochromatic characteristics of the inactive X chromosome

2.1: Abstract

Ki-67 maintains heterochromatin-associated repressive histone modification H3K9Me3 and promotes association of alpha-satellite to the nucleolus in HeLa cells. These results indicate its involvement in heterochromatin organization. In this chapter, I illustrate Ki-67 affects Xi-nucleolus association in cell-type-specific manner. Acute depletion of Ki-67 altered S phase specific perinucleolar localization of Xi in hTERT-RPE1 cells but not in virally-transformed 293T cells. Notably, in hTERT-RPE1 cells, upon Ki-67 depletion, Xi that were localized away from the nuclear lamina displayed several features of compromised heterochromatin, including increased Pol II association, transcription of repetitive DNA, and decreased H3K27me3 and H4K20me1 labeling. In contrast, in 293T cells, these heterochromatic characteristics of the inactive X chromosome remained unchanged.

2.2: Introduction

Nucleoli, the site of rDNA transcription and ribosome assembly, are the largest nuclear body in the nucleus. Notably, nucleolar periphery houses a subset of the cellular heterochromatin, which shares many loci with (Dillinger *et al.*, 2016) and is exchanging dynamically with lamina-associated heterochromatin regions(Kind *et al.*, 2013a; Koningsbruggen *et al.*, 2010; Ragoczy *et al.*, 2014).

The observation of only a specific subset of the genomes non-randomly associates with nucleoli raises the question whether there are trans-acting factors specifically targeting the genomic loci to the nucleolus.

X inactivation in female mammals is a classic example of facultative heterochromatin formation. Xi is usually localized to either the nucleolar periphery or to the nuclear lamina(Barr and Bertram, 1949; Chun-Kan Chen *et al.*, 2016; Zhang *et al.*, 2007). In MEFs, it frequently associates with nucleoli during the mid to late S phase(Zhang *et al.*, 2007). Association of Xi with the nucleolus ensures heterochromatin maintenance and gene silencing, rendering Xi a well-suited model to study the relationship of heterochromatin compartment and biological functions. Recently, studies have demonstrated that Ki-67 promotes movement of several repetitive genomic loci to the nucleolus. Thus, my goal was to test whether Ki-67 can promote association between Xi and the nucleolus as well.

2.3: Results

2.3.1: Depletion of Ki-67 decreases perinucleolar localization of the Xi in asynchronous hTERT-RPE1 cells but not in tumor-derived 293T cells

Ki-67 protein is localized to the nucleolus in interphase cells, and also regulates the association of repetitive DNA with the nucleolar periphery (Booth *et al.*, 2014; Matheson and Kaufman, 2015). A prominent example of heterochromatin association with nucleoli is the inactive X chromosome (Xi) in mammalian female cells (Zhang *et al.*, 2007). The perinucleolar space is a

subset of the heterochromatic compartment; another frequent location for heterochromatin is at the nuclear periphery, adjacent to the nuclear lamina (Politz *et al.*, 2016). Accordingly, the Xi is usually localized to one of these two preferred locations (Zhang *et al.*, 2007), Because Ki-67 depletion reduces alpha satellite localization to the perinucleolar region, we hypothesized that it might also affect the interphase localization of the Xi. We first examined Xi localization in asynchronous hTERT-RPE1 cells, a diploid retinal pigment epithelial cell line immortalized by an hTERT transgene (Bodnar *et al.*, 1998). We used immuno-RNA-FISH to detect Xi-associated lncRNA XIST and nucleolar protein fibrillarin. Indeed, Ki-67 depletion resulted in a partial but statistically significant reduction in Xi-nucleolar associations (Fig 2.1 A-D). This loss of nucleolar association was accompanied by an increase of similar magnitude in Xi-lamina associations. Similar results obtained with two distinct Ki-67 depletion reagents, one a synthetic siRNA and the other a cocktail of in vitro-diced dsRNAs non-overlapping the siRNA target, both of which efficiently depleted steady-state Ki-67 levels (Fig 2.5 G and Fig 2.6 G). However, in virally-transformed 293T cells, we observed no significant alteration in Xi-nucleolar associations (Fig 2.1 E-H), measured either as the total number of allele association, or the number of alleles associated per cell. Thus, we conclude that effects of Ki-67 depletion on Xi-nucleolar association are cell-type dependent.

Figure 2.1: Depletion of Ki-67 redistributes the Xi chromosome in asynchronous hTERT-RPE1 but not in 293T cells. Scale bars, 10 μm.

A. Fluorescence microscopy images of representative hTERT-RPE1 cells treated either with scramble control or Ki-67-targeted siRNAs as indicated. Cells were analyzed by RNA-FISH to detect XIST RNA (green) marking the Xi, and by immunofluorescence with anti-fibrillarin antibodies (red) to label nucleoli. DNA was stained with DAPI (blue).

B. Quantification of XIST association frequencies from panel A experiments. XIST associations with the indicated locations were counted; "total nucleolar" indicates the sum of XIST signals that are exclusively nucleolar plus those that also are on the nuclear periphery. Three biological replicate experiments were performed with mean percentage association and SDs graphed. Total cells assayed = 363 for si-scramble, 376 for siKi-67. Holm-Sidak corrected p-values comparing si-scramble and siKi-67 treatments are indicated, with p-values < 0.05 in red.

C. Fluorescence microscopy images of representative hTERT-RPE1 cells treated either with luciferase- or Ki-67-targeted esiRNAs as indicated. Cells were stained as in panel A.

D. Quantification of association frequencies from panel C experiments. Total cells assayed = 348 for esi-luciferase, 391 for esiKi-67.

E. Fluorescence microscopy images of representative 293T cells treated either with scramble control or Ki-67-targeted siRNAs.

F. Quantification of XIST association frequencies from panel E experiments. Total alleles assayed = 272 for si-scramble, 298 for siKi-67. Holm-Sidak adjusted p-values comparing association frequencies were > 0.97 for all comparisons.

G. Fluorescence microscopy images of representative 293T cells as panel E, except that cells were treated with in vitro-diced esiRNAs as depletion reagents.

H. Quantitation of XIST association frequencies from panel G experiments.

Total alleles assayed = 250 for esi-luciferase, 270 for esiKi-67. Holm-Sidak adjusted p-values comparing association frequencies were > 0.98 for all comparisons.

Figure 2.1: Depletion of Ki67 redistributes Xi chromosome within asynchronous hTERT-RPE1 but not in 293T cell. Scale bars, 10 μm.
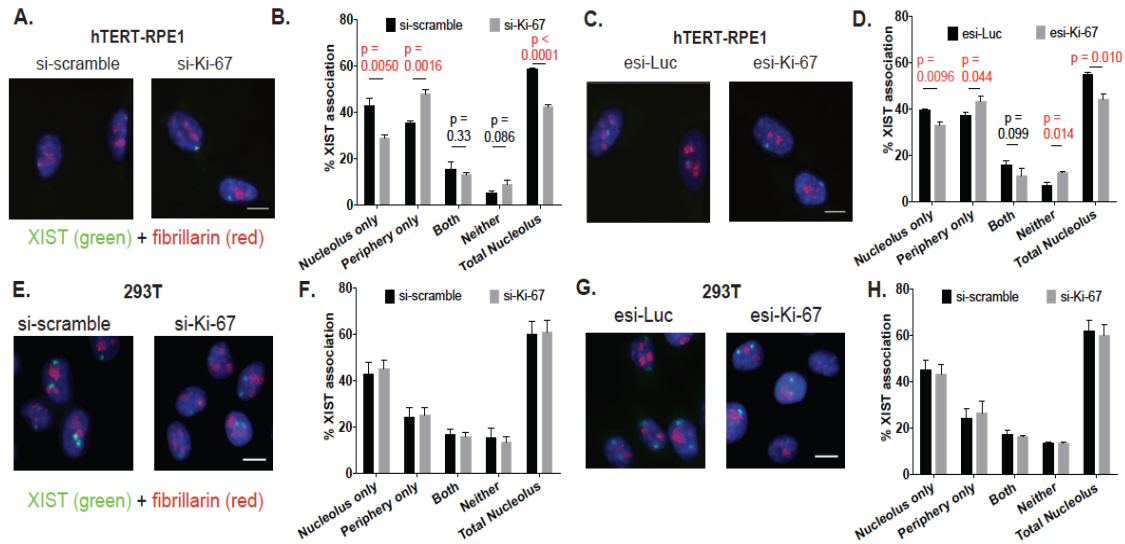
2.3.2: Altered Xi-nucleolus association dynamics in synchronized hTERT-RPE1 cells upon Ki-67 depletion

The Xi-nucleolar association is cell-cycle regulated, occurring most prevalently in S phase cells (Zhang *et al.*, 2007). We therefore examined Xi localization in synchronized cells using immuno-RNA-FISH experiments in which the Xi-associated lncRNA *XIST* was detected at the same time as the nucleolar protein fibrillarin. Cells were blocked near the G1/S transition of the cell cycle with hydroxyurea (HU) for 15 hours (Figure 2.2 A) (Zhang *et al.*, 2007), which provided efficient arrest. Cells were then released into drug-free media and

pulse-labeled with the deoxynucleotide analog EdU at two-hour timepoints across an 8-10-hour time course (Fig 2.2). In control cells treated with the scrambled siRNA, EdU labeling was first detected at the 2 hour time point, and displayed a typical early S phase pattern consisting of many small foci(Dimitrova and Berezney, 2002). At later time points, the pulse of EdU labeled larger foci, indicative of mid-late S phase patterns. Upon Ki-67 depletion, we observed a delay in the initial detection of EdU incorporation of approximately 2 hours (Fig 2.2 B). Notably, the Ki-67 depleted population also displayed a higher percentage of cells that did not incorporate EdU during the time course (Fig 2.2 C). Together, these data indicates that Ki-67 depletion affects S-phase in hTERT RPE-1 cells.

Next, we examined how Xi localization was altered during the synchronized cell time course (Fig 2.2 D-G). Consistent with published data from mouse cells (Zhang *et al.*, 2007), the frequency of Xi-nucleolar associations peaked in middle S-late S phase transition; this was true for the frequency of Xi associations that were exclusively at the nucleolus (Fig. 2.2D), and for the frequency of Xi chromosomes simultaneously associated with both the nucleolus and the lamina (Fig. 2.2E). These peaks occurred in both the control and Ki-67-depleted populations, with the Xi-nucleolar interaction peaks delayed two hours in the latter case. The two-hour shift correlates with the delay in S phase entry in the Ki-67-depleted cells (Fig 2.2).

As suggested by the Xi localization data from asynchronous cells (Fig 2.2 A-D), Xi associations with the nucleoli and lamina were inversely related, so that the peak of nucleolar associations (Fig 2.2 D-E) coincided with the lowest

frequencies of laminar associations (Fig2.2 F). We note that when the total Xi-laminar association frequencies were counted by summing the exclusively laminar associations (Fig. 2.2 F) plus those also associated with nucleoli simultaneously (Fig 2.2. E), we observed little change during the experiment (Figure 2.2 G). Thus, the biggest changes during S phase are lamina-associated Xi becoming transiently also associated with nucleoli (e.g. compare Fig. 2.2E and 2.2F). Together, these data indicated that cell cycle-regulated Xi-nucleolar associations are delayed in concert with S phase entry upon depletion of Ki-67 in female hTERT-RPE1 cells

Figure 2.2: Frequency of Xi-nucleolus association in synchronized hTERT-RPE1 cells. Scale bars, 5 μm

A. Schematic of assay. Cells were released from HU arrest for the indicated time periods, pulsed for 20 min with EdU, and analyzed by click chemistry for EdU incorporation and assayed for Xi-nucleolus association.

B. Representative cells from the indicated time points, showing EdU staining (green) to detect the progression of S phase. Total DNA is visualized with DAPI staining (blue). S phase cells were categorized into 3 sub-stages based on the number, size, shape and distribution of fluorescent-labeled replication foci. During early S phase, small and numerous replication foci were scattered in the nuclear interior, but excluded from nucleolus, nuclear periphery and other heterochromatic regions. At mid-S phase, replication takes place at the nuclear periphery and perinucleolar regions. Late in S phase, there are several large foci throughout the nucleus (Dimitrova and Berezney, 2002).

C. Distributions of EdU morphologies during the time course. Percentages of early S phase,middle S phase and late S phase EdU staining morphologies were counted in >300 total cells per time point.

D. Panels D-G: Frequencies of Xi associations versus time. All associations were measured in HU-synchronized cells with the averages and std. dev. from 3 independent experiments. At each time point, >300 cells were counted.

D. Xi-nucleolar only associations (Xi chromosomes associated with nucleoli but not lamina).

E. Xi chromosomes associated with both the lamina and nucleoli simultaneously.

F. Xi-lamina only associations (Xi chromosomes associated with lamina but not nucleoli). Note that Xi-nucleolar associations (panels I-J) peak and Xi-lamina only (panel K) associations reach a minimum when the majority of cells are in mid-late S phase, which is delayed in Ki67-depleted cells by 2 hr.

G. Xi-total laminar associations (Xi chromosomes associated either with the lamina or with both lamina and nucleoli simultaneously).

Figure 2.2:Frequency of Xi-nucleolus association in synchronized hTERT-RPE1 cells. Scale bars, 5 μm

D. Nucleolus Only — si-scr, si-Ki-67; % cells vs hours

E. Both Nucleolus and Lamina — si-scr, si-Ki-67; % cells vs hours

F. Lamina Only — si-scr, si-Ki-67; % cells vs hours

G. Total Lamina — si-scr, si-Ki-67; % cells vs hours
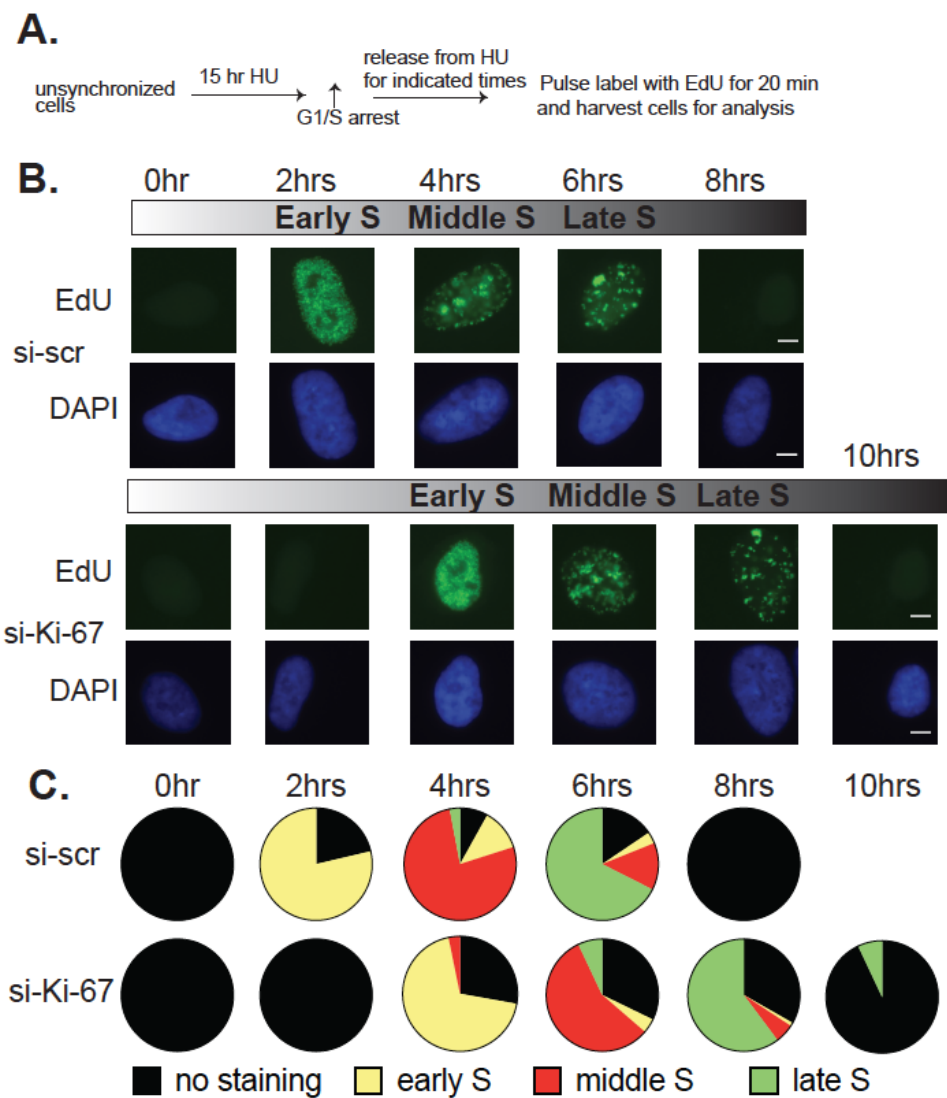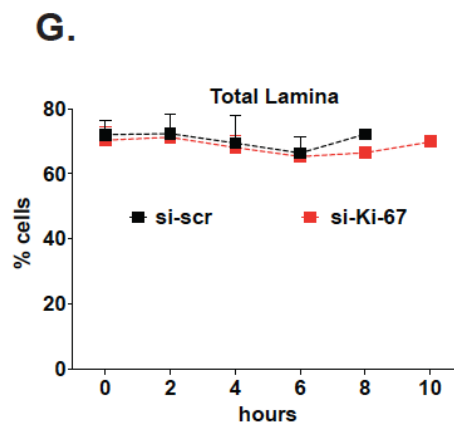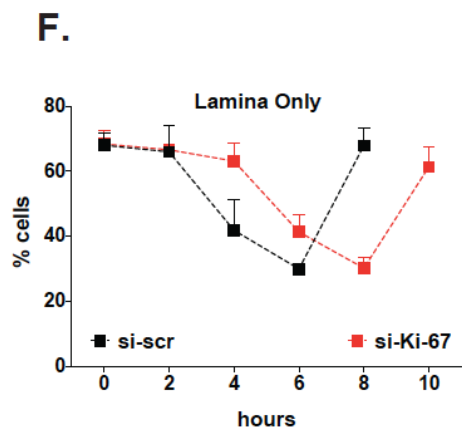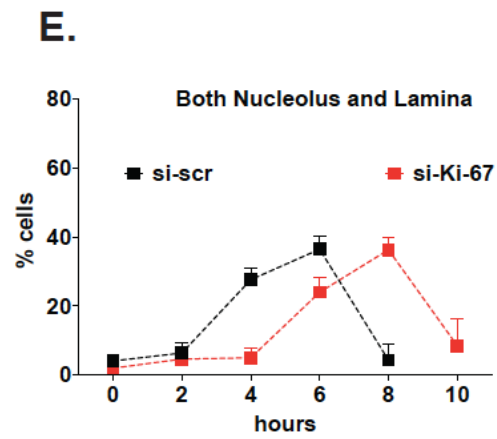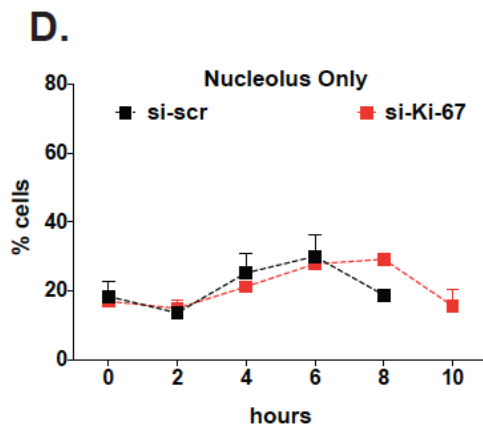
2.3.3: Ki-67 depletion leads to heterochromatin erosion on internalized Xi in hTERT-RPE1 cells but not in 293T cells

Ki-67 is required for the normal cellular localization of heterochromatin-associated histone modifications (Sobecki *et al.*, 2016), and for the interphase nucleolar association of heterochromatic loci (Booth *et al.*, 2014; Matheson and Kaufman, 2017a). Because the inactive X (Xi) chromosome is a well-studied example of facultative heterochromatin that associates with the nucleoli of female mouse (Zhang *et al.*, 2007) and human cells (Petersen *et al.*, 1962; Barr and Bertram, 1949; Bourgeois *et al.,1985*) we tested whether Ki-67 affected characteristics of Xi heterochromatin. Indeed, Ki-67 depletion in hTERT-RPE1 cells resulted in a subset of cells that displayed reduced staining intensity for antibodies recognizing H3K27me3 and H4K20me1, histone modifications that are enriched on the Xi (Lucchesi *et al.*, 2005; Kohlmaier *et al.,2004*)(Fig2.3 A, C, E, G). H3K27me3 is generated by the Polycomb PRC2 complex and is a keystone of facultative heterochromatic silencing (Cao *et al.,*2002; Di Croce *et al.*, 2013; Simon *et al.* 2013). H4K20me1 is generated by the PR-Set7/Set8/KMT5a enzyme (Beck *et al.*, 2012) and together with H3K27me3 is an early mark on Xi chromosomes during the process of XIST-mediated inactivation (Kohlmaier *et al.*,2004,Beck *et al.*, 2012). Notably, changes to either of these histone modifications were only observed in cells in which the Xi was localized away from the nuclear periphery (Fig. 2.3 B, D, F, H).

Increased levels of repetitive element-rich Cot-1-hybridizing transcripts and RNA polymerase II have previously been observed in breast cancer cell lines

that display perturbations in Xi chromatin (Chaligné *et al.*, 2015). We tested for changes in these properties in hTERT-RPE1 cells. We detected an increase in the frequency of cells that display Cot-1-hybridizing transcripts or RNA polymerase II on the Xi upon Ki-67 depletion in hTERT-RPE1 cells (Figures 2.5-2.6). As observed above for the histone modifications (Fig. 2.3), increased levels of Cot-1 RNA and Pol II within the XIST domain were only observed in cells in which the Xi was localized away from the nuclear periphery. Also, as for all other phenotypes detected, these changes were similar with either Ki-67 depletion reagents (Figs. 2.5-2.6). Changes in H3K27me3 and H4K20 me1 staining were not observed in 293T cells (Fig2.4).

Figure 2.3: H3K27me3 and H4K20me1 staining of the inactive X chromosome were altered upon Ki-67 depletion in a subset of hTERT-RPE1 cells. Scale bars, 5 μm.

A. Immuno-FISH analysis of H3K27me3 overlap with XIST in siRNA-treated hTERT-RPE1 cells. Note that in the si-Ki-67-treated cell, the H3K27me3 signal overlapping XIST displayed reduced intensity and was localized away from the nuclear lamina.

B. Quantitation of percentage of cells that display reduced H3K27me3 enrichment on the Xi in the panel A experiments. Enrichment was calculated as the ratio of the mean H3K27me3 signal overlapping XIST divided by the mean H3K27me3 signal from remainder of the entire nucleus. Cells with ratios less than 1.5 were defined as having reduced enrichment, as described previously (Chaligné *et al.*, 2015). Percentages were calculated for the total cell populations, as well as for the nuclear lamina-associated XIST foci and the non-lamina-associated foci, as indicated. Total cells assayed = 250 for si-scramble and 239 for si-Ki-67. Mean and SDs are graphed from three biological replicate experiments. p-values were determined by unpaired student's t tests.

C. Analysis of H3K27me3 enrichment on Xi as in panel A, for hTERT-RPE1 cells treated with in vitro-diced esiRNAs.

D. Quantitation as in panel B. Total cells assayed= 236 for esi-luciferase, 220 for esi-Ki-67.

E. Immuno-FISH analysis of H4K20me1 overlap with XIST in siRNA-treated hTERT-RPE1 cells. Note that the H4K20me1 signal colocalizing with XIST is reduced in the Ki-67-depleted cell.

F. Quantitation of the panel E experiments, as in panel B. The total cells assayed = 204 si-scramble and 216 for si-Ki-67.

G. Analysis of H4K20me1 in cells treated with esiRNAs.

H. Quantitation of the panel G experiments. Total cells assayed = 164 for esi-luciferase, 182 for esi-Ki-67.

I. Example of H3K27me3 signal intensity quantification.

Figure 2.3:H3K27me3 and H4K20me1 staining of the inactive X chromosome were altered upon Ki-67 depletion in a subset of hTERT-RPE1 cells. Scale bars, 5 μm.

G.

| H4K20me1 | XIST | H4K20me1 + XIST |

esi-Luc

esi-Ki-67

H.

Reduced H4K20me1 at XIST

■ esi-Luc ■ esi-Ki-67

p = 0.98   p = 1.8e^{-3} p = 3.3e^{-3}

% cell

Lamina Non-Lamina Total

I.

H3-K27me3

XIST mask

ratio = 1.98

nucleus mask

$$ratio = \frac{mean\ IF\ signal\ at\ XIST\ mask}{mean\ IF\ signal\ at\ nucleus\ mask}$$
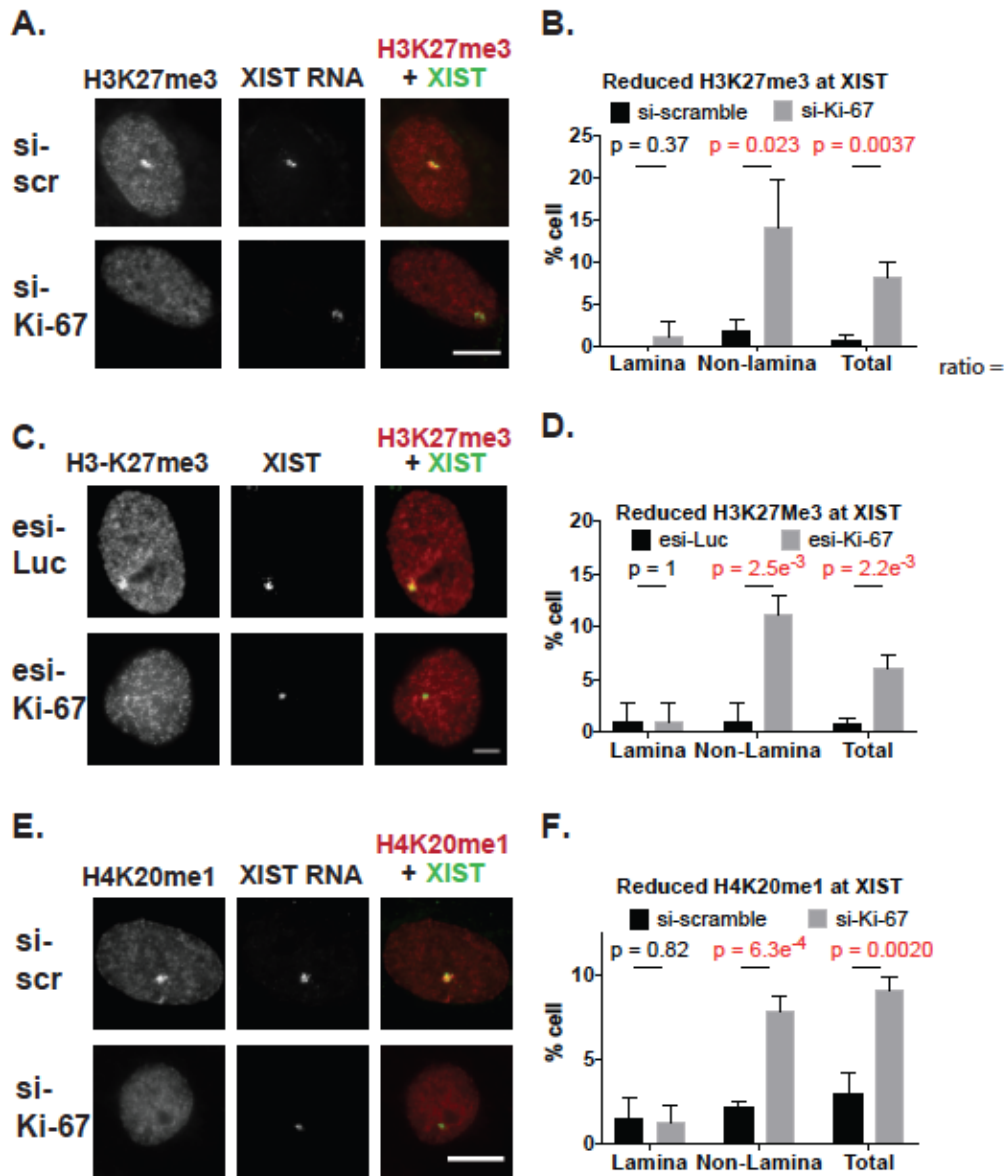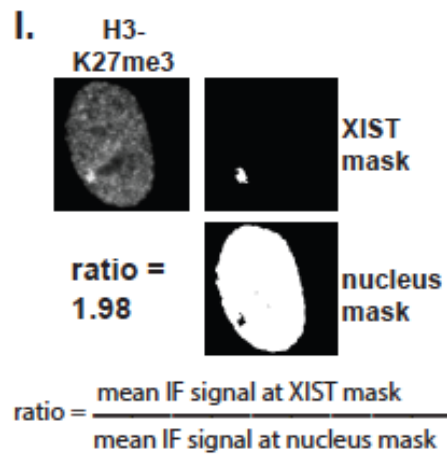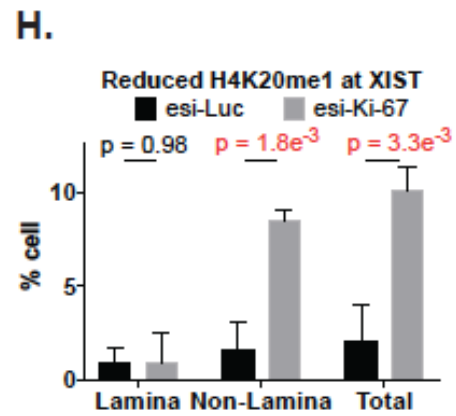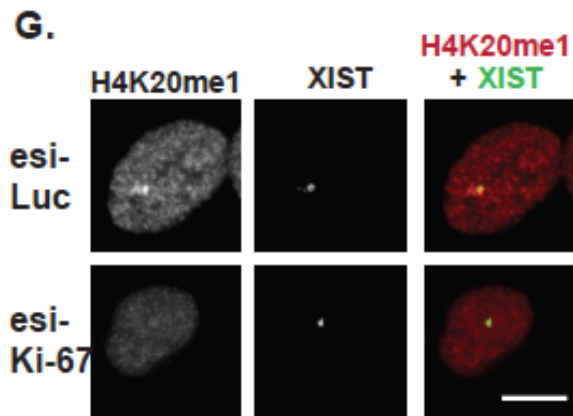
Figure 2.4: H3K27me3 and H4K20me1 staining of the inactive X chromosome were unaltered upon Ki-67 depletion in 293T cells. Scale bars, 5 μm.

A. Immuno-FISH analysis of H3K27me3 overlap with XIST in siRNA-treated 293T cells. Note that 293T cells have two Xi chromosomes. In these cells, the H3K27me3 foci overlapping XIST remained unchanged upon Ki67 depletion.
B. Quantitation of panel A. The total alleles assayed = 136 for si-scramble and 146 for si-Ki-67.
C, D. Analysis of H3K27me3 in esiRNA-treated 293T cells. Total alleles assayed = 196 for esi-luciferase, 198 for esi-Ki-67.
E. Immuno-FISH analysis of H4K20me1 overlap with XIST in 293T cells. In these cells, the H4K20me1 foci overlapping XIST remained unchanged upon Ki67 depletion.
F. Quantitation of panel E. The total alleles assayed = 180 for si-scramble and 162 for si-Ki-67.
G, H. Analysis of H4K20me1 in esiRNA-treated cells. Total alleles assayed = 180 for esi-luciferase, 162 for esi-Ki-67.

Figure 2.4: H3K27me3 and H4K20me1 staining of the inactive X chromosome were unaltered upon Ki-67 depletion in 293T cells. Scale bars, 5μm.
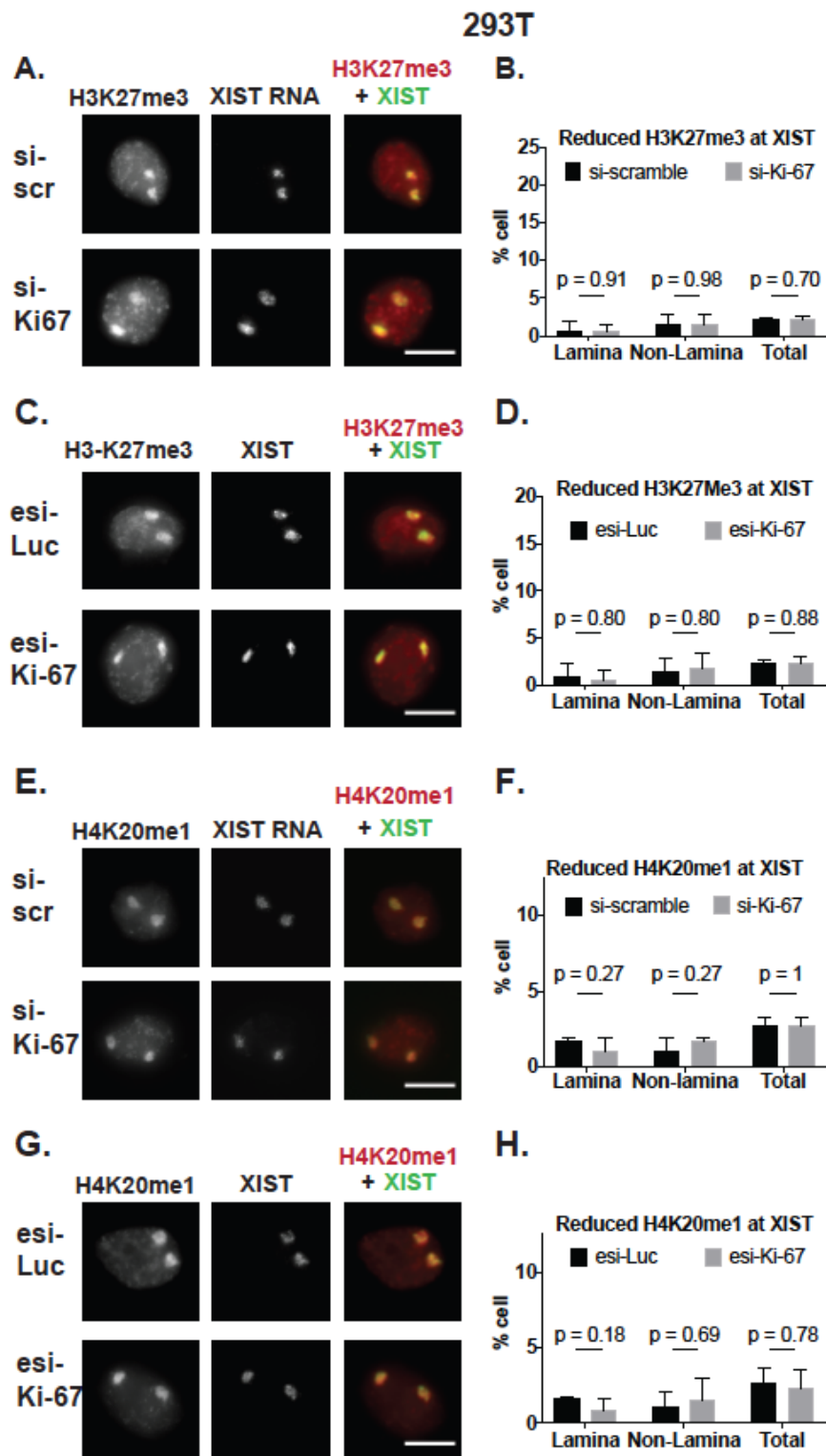
Figure 2.5: Analysis of Cot-1 and Pol II enrichment on Xi in siRNA-treated hTERT-RPE1 cells. Scale bars, 5 µm.

A-B Localization of Cot-1-hybridizing transcripts relative to XIST domains, when XIST is localized away from (A) or at (B) the nuclear lamina. A line scan (white arrow) across the XIST signal (green) was used to analyze Cot-1 hybridization levels (red); fluorescent densities across the line scan were plotted in the right-hand panels. Cot-1 RNA was considered to be reduced across the XIST domain when the average Cot-1 signal overlapping XIST was lower than the average Cot-1 signal across the nucleus. The average nucleus Cot-1 signal is depicted in dotted line. In the examples shown where Xi was within the cell interior (panel A), Cot-1 RNA was excluded from XIST in the si-scramble-treated cell, but not the siKi-67-treated cell. In contrast, siKi-67 treatment did not affect Cot-1 enrichment on Xi in cells where Xi was at the lamina (panel B).

C-D Analysis of RNA Pol II localization (red) relative to XIST (green) when XIST is localized away from (panel C) or at (panel D) the nuclear lamina. Exclusion was analyzed as in panels A-B.

E. Quantitation of Cot-1 RNA overlap with XIST RNA domains. Mean (and std. dev.) percent of cells displaying Cot-1 RNA overlapping XIST foci are plotted from three biological replicate experiments. The total cells assayed = 404 for si-scramble and 465 for si-Ki-67. p-values were determined by unpaired student's t tests.

F. Quantitation of percentage of cells showing presence of RNA Pol II at Xist RNA domain. The total cells assayed = 362 for si-scramble and 367 for si-Ki-67.

G. Immunoblot analysis of Ki67 depletion in siRNA-treated hTERT-RPE1 cells from above.

Figure 2.5: Analysis of Cot-1 and Pol II enrichment on Xi in siRNA-treated hTERT-RPE1 cells. Scale bars, 5 μm.
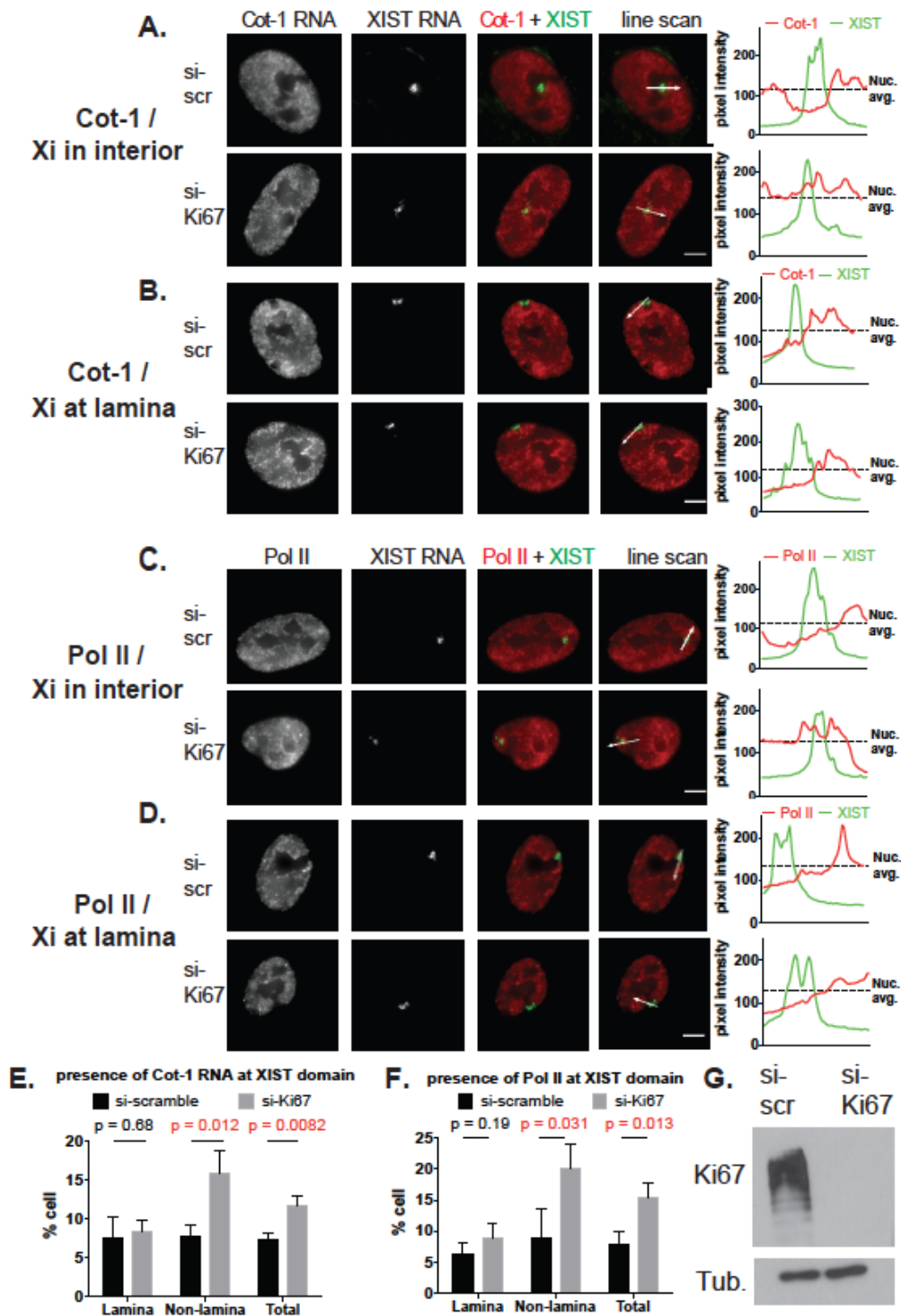
Figure 2.6: Analysis of Cot-1 and Pol II enrichment on Xi in esiRNA-treated hTERT-RPE1 cells. Analyses were performed as in Figure 12. Scale bars, 5 μm.

A, B. Cot-1. Total cells assayed= 178 for esi-luciferase, 180 for esi-Ki-67.

C, D. Pol II. Total cells assayed= 160 for esi-luciferase, 176 for esi-Ki-67.

E.   Quantitation of Cot-1 RNA overlap with XIST RNA domains from panels A-B.

F.   Quantitation of RNA Pol II at Xist RNA domain from panels C-D.

G. Immunoblot analysis of Ki-67 depletion in esiRNA-treated hTERT-RPE1 cells from above.

Figure 2.6: Analysis of Cot-1 and Pol II enrichment on Xi in esiRNA-treated hTERT-RPE1 cells. Scale bars, 5 μm.
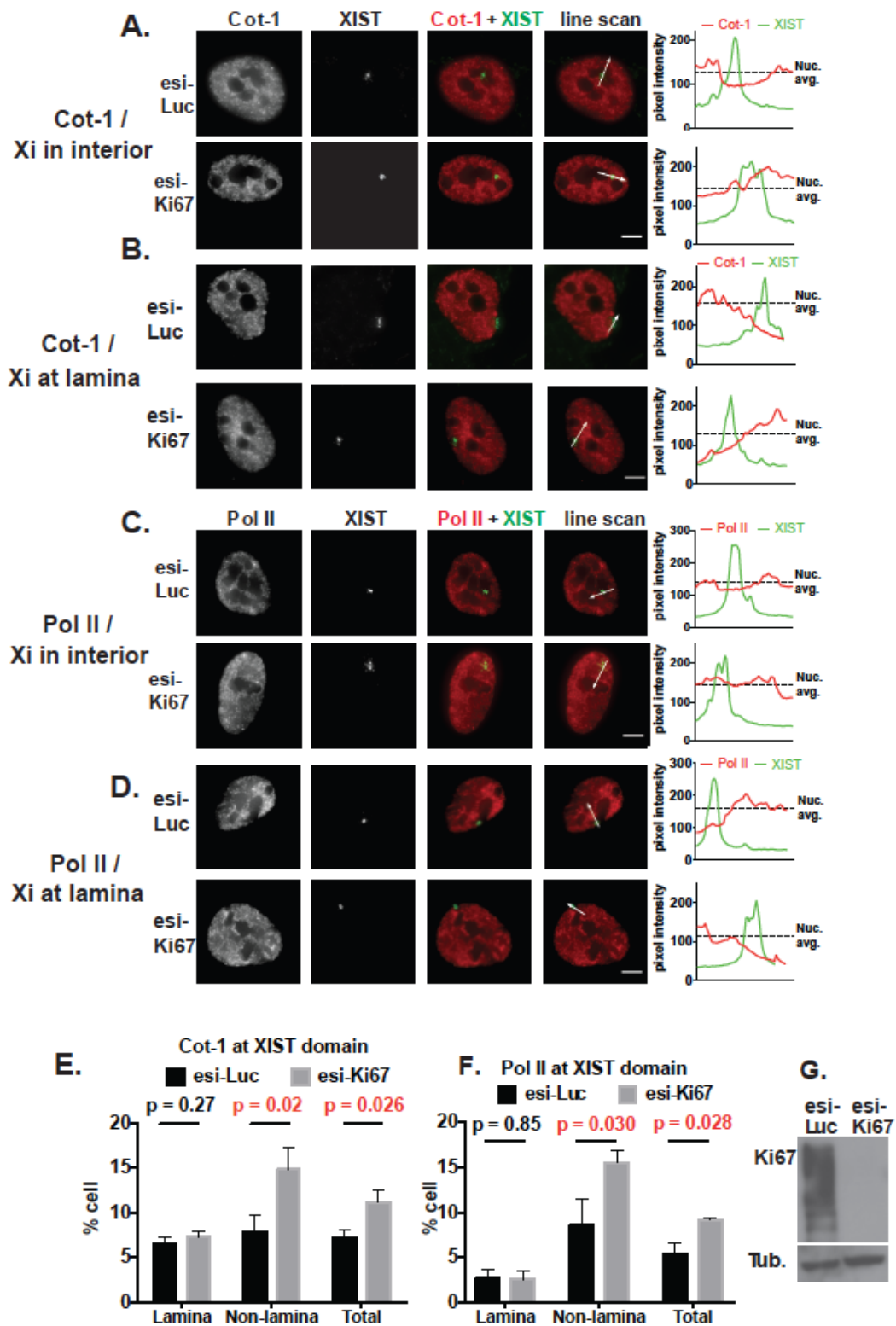
2.3.4: Some aspects of Xi structure and function were resistant to Ki-67 depletion.

Not all aspects of Xi heterochromatin were sensitive to Ki-67 depletion. For example, Ki-67 depletion did not alter the overall appearance of the XIST "cloud" that covers the Xi (Fig. 2.7 A). In addition, RT-PCR showed no significant down regulation of XIST transcript expression (Fig. 2.7 I). Also, there was no evidence for Xi chromosome-wide deprepression of transcription, as shown in the analysis of X-linked gene expression (Fig. 2.7 B), or in the analysis of allele-specific transcription of X-linked genes detected via analysis of known SNPs (Table 2.1). Furthermore, an additional mark associated with the Xi, the histone variant macroH2A, did not change in appearance upon depletion of Ki-67 (Fig. 2.7C-H). Together, the Xi data indicate that acute depletion of Ki-67 alters several, but not all, characteristics of Xi heterochromatin in hTERT-RPE1 cells.

Figure 2.7: Some aspects of Xi structure and function were resistant to Ki-67 depletion in hTERT-RPE1 cells. Scale bars, 10 μm.

A. XIST cloud in hTERT-RPE1 cells has similar appearance regardless of Ki-67 depletion. Cells were treated with the indicated siRNAs for 72 hrs and analyzed by RNA-FISH to localize XIST (green) and DAPI staining (blue). Scale bar: 10 μm.
B. Average RNA levels of X linked genes did not change upon Ki-67 depletion in hTERT-RPE1 cells. log2 FPKM analyses of RNA-seq data from two biological replicates for the two indicated siRNA treatments are shown.
C-H.   MacroH2A enrichment at the XIST domain was not altered upon Ki-67 depletion. hTERT-RPE1 cells were treated with siRNAs (C-E) or in vitro-diced esiKi-67 (F-H) for 72 hrs. Panels C, F: Cells were analyzed by immuno-RNA-FISH to localize XIST (green) and macroH2A (red). Scale bar: 10 **μ**m. Panels D, G: Quantitation of cells that displayed reduced macroH2A staining is shown. Total cells assayed= 248 for si-scramble, 291 for siKi-67, 218 for esi-luciferase, 236 for esiKi-67. Panels E, H: immunoblot analyses of Ki-67 depletions.
I. XIST expression does not altered upon Ki-67 depletion

Figure 2.7: Some aspects of Xi structure and function were resistant to Ki-67 depletion in hTERT-RPE1 cells. Scale bars, 10 μm
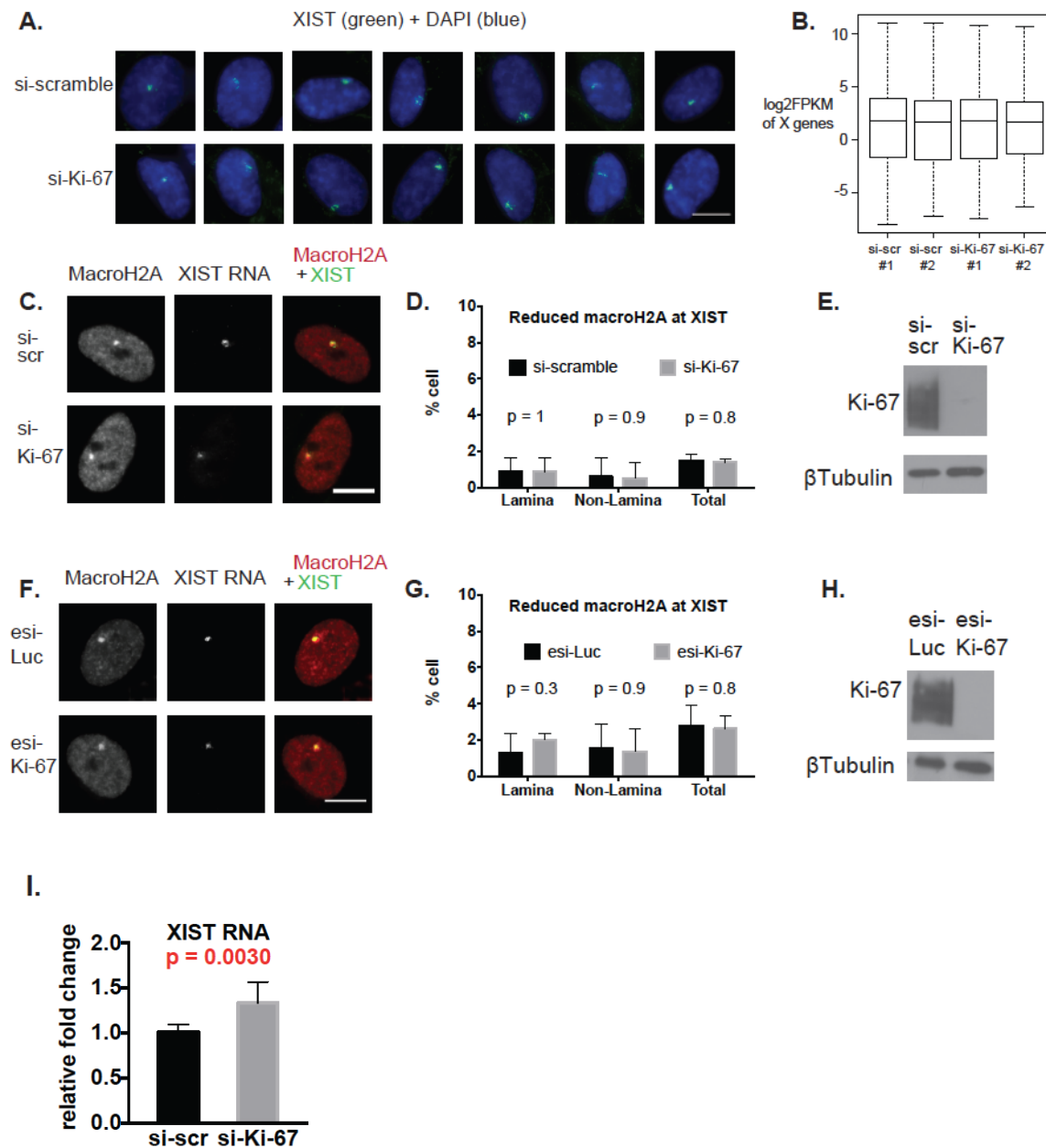
Table 2.1:Analysis of X-linked SNP in RNAseq data

seqnames	start	end	Symbol	Conclusion
chrX	110675623	110675623	CHRDL1	No evidence of escape in siKi67
chrX	54810072	54810072	MAGED2	weak evidence of biallelic expression (1 read/113 in siKi67)
chrX	54809928	54809928	MAGED2	No evidence of escape in siKi67
chrX	20125252	20125252	EIF1AX	biallelic expression
chrX	1011404674	101140674	CENPI	No evidence of escape in siKi67
chrX	101552926	101552926	ARMCX1	No evidence of escape in siKi67
chrX	24995899	24995899	POLA1	No evidence of escape in siKi67
chrX	104193.108	104193108	FAM199X	No evidence of escape in siKi67
chrX	109543785	109543785	NXT2	No evidence of escape in siKi67

2.3.5: Ki-67 does not affect perinucleolar localization of Xi in asynchronous mouse cell culture

We extend our investigation to the female mouse embryonic fibroblast cells. We performed immuno-RNA-FISH to detect Xi-associated lncRNA *Xist* and nucleolar protein fibrillarin. Asynchronous primary MEF transfected with a scramble control siRNA displayed ~45% of *Xist* alleles associate with nucleoli, which is consistent with previous report (Zhang *et al.*, 2007). Cells transfected with siRNA reagents directed against Ki-67 mouse RNA does not display altered Xi association frequencies with nucleoli (Fig 2.8 A-B). Efficient depletion of Ki-67 protein has been confirmed by the immunoblotting(Fig 2.8C). It indicates that Ki-67 does not regulate Xi-nucleolus association in mouse system.

Figure 2.8: Depletion of Ki-67 does not redistribute the Xi within asynchronous primary MEF. Scale bars, 10 μm.

A. Fluorescence microscopy images of representative primary MEF treated either with scramble control or Ki-67-targeted siRNAs as indicated. Cells were analyzed by RNA-FISH to detect XIST RNA (green) marking the Xi, and by immunofluorescence with anti-fibrillarin antibodies (red) to label nucleoli. DNA was stained with DAPI (blue).

B. Quantification of XIST association frequencies from panel A experiments. XIST associations with the indicated locations were counted; "total nucleolar" indicates the sum of XIST signals that are exclusively nucleolar plus those that also are on the nuclear periphery. One biological replicate experiment was performed. Total cells assayed = 95 for si-scramble, 106 for siKi-67.

C. immunoblot analyses of Ki-67 depletions

Figure 2.8: Depletion of Ki-67 does not redistribute the Xi chromosome within asynchronous primary MEF. Scale bars, 10 μm

A.

si_scramble si_Ki67

XIST(green) + Fibrillarin (red)

B.

C.

si- si-
scr Ki67

Ki67

tubulin
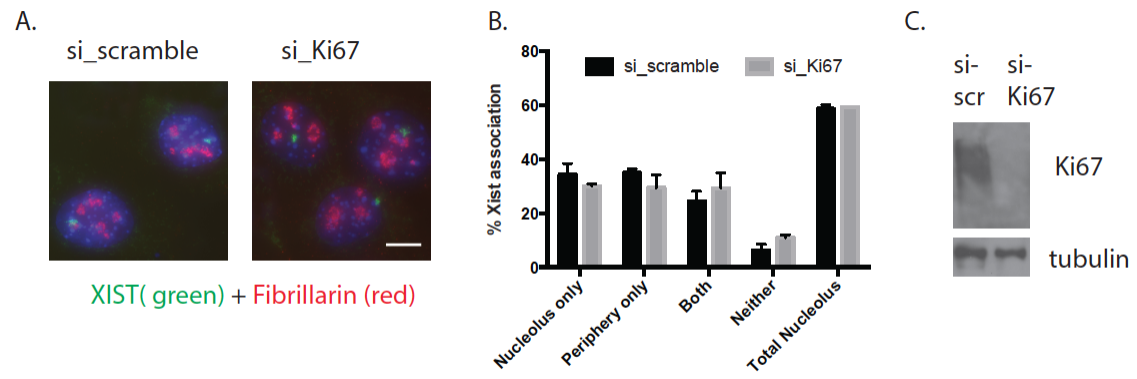
2.4: Discussion

2.4.1: Ki-67 contributes to the interphase localization of the Xi chromosome

Nucleoli are non-membrane bound organelles within the nucleus. Not only are these sites of synthesis and assembly of ribosome components, the periphery of these organelles plays an important role in higher order chromosome localization (Politz *et al.*, 2016; Chubb *et al.*, 2002). Specifically, the nucleolar periphery houses a subset of the cellular heterochromatin, which is largely overlapping with (Dillinger *et al.*, 2016) and exchanging dynamically with lamin-associated heterochromatin regions (Kind *et al.*, 2013; Koningsbruggen *et al.*, 2010; Ragoczy *et al.*, 2014). Like other heterochromatin regions, high resolution analysis of nucleolus-associated domains (termed NADs) in human cells reveals enrichment of satellite repetitive DNAs and repressive histone marks (Koningsbruggen *et al.*, 2010; Dillinger *et al.*, 2016; Németh *et al.*, 2010). Major questions in chromosome biology are how heterochromatin regions are partitioned to different intranuclear locations, and how these interactions are governed by cell cycle progression.

As a region of facultative heterochromatin, the mammalian inactive X (Xi) chromosome in female cells is enriched in NAD loci, usually localized to either the nucleolar periphery or to the nuclear lamina (Barr and Bertram, 1949; Zhang *et al.*, 2007; Dillinger *et al.*, 2016). In mouse cells, the Xi-nucleolar association is cell cycle-dependent, with frequencies peaking during mid-to-late S phase. A genetic deletion was used to show that the long non-coding RNA Xist, which is expressed from the Xi chromosome, is required for normal Xi-perinucleolar

localization. Deletion of Xist results in diminished H3K27me3 enrichment and increased synthesis of Cot-1-hybridizing, repeat-derived RNAs on the Xi (Zhang *et al.*, 2007). These data suggest that perinucleolar localization of Xi contributes to the maintenance of heterochromatin structure. More recently, depletion of long non-coding RNA Firre was shown to reduce association of the Xi to nucleolus, and also reduces H3K27me3 density on the Xi (Yang *et al.*, 2015). However, *Firre* depletion has minimal effects on Xi gene silencing, consistent with the idea that multiple functionally overlapping factors affect Xi heterochromatin localization and gene silencing.

Here, we discovered that Ki-67 affects the Xi-nucleolus interaction. Analysis of synchronized RPE-1 cells shows that the association appears more slowly in Ki-67-depleted cells, coincident with the delay in S phase entry. In addition to this delay, Ki-67 depletion alters some of the heterochromatin characteristics of the Xi, causing significantly increased levels of Cot-1-hybridizing RNAs and Pol II, and decreased enrichment of H3K27me3. This loss of heterochromatic properties is partial in the cell population, and we do not detect uniform reactivation of Pol II genes on the Xi (Table 2.1). These data are consistent with previous studies showing that multiple overlapping mechanisms maintain the inactive status of the Xi (Csankovszki *et al.*, 2001; Yang *et al.*, 2015). We note that XIST levels are not reduced upon Ki-67 depletion (Fig 2.7 I), suggesting that altered XIST levels are unlikely to explain the effect of Ki-67 on the Xi. Instead, our data is consistent with the view that Ki-67 is one of the factors

that contributes to the maintenance of heterochromatic structures of the Xi (Sobecki *et al.*, 2016) in this case in a manner coupled to S phase progression.

Recent data show that the nuclear lamina localization mediated by the interaction between XIST and the lamina B receptor facilitates the spreading of XIST on the Xi chromosome, which in turn contributes to transcriptional silencing (Chun-Kan Chen *et al.*, 2016). This raises the question of whether there are specific protein factors that contribute to the association of the Xi with the nucleolus in addition to the lncRNAs *XIST* and *FIRRE* (Zhang *et al.*, 2007; Yang *et al.*, 2015). Could Ki-67 be such a factor? One possibility consistent with our data is that Ki-67's primary role in Xi localization being related to S phase progression, which favors the Xi-nucleolar association via unknown mechanisms. However, one aspect of Ki-67 function here may not solely result from cell cycle progression regulation. It appears that the erosion of heterochromatic features on the Xi occurs in a significant fraction of Ki-67-depleted cells away from the nuclear lamina, but the lamin-associated Xi chromosomes are not altered. There are two possibilities to explain these data. First, it may be that lamina association confers protection from heterochromatin changes. Alternatively, those Xi chromosome that experience altered structures upon Ki-67 may preferentially relocalize away from the lamina. Because our shRNA-based experiments necessitate a 72-hour period to achieve strong Ki-67 depletion, there is likely passage through multiple mitoses for each cell during this period. As Ki-67 is a key component of the perichromosomal layer that envelopes each mitotic chromosome (Booth *et al.*, 2014; Cuylen *et al.*, 2016), it is tempting to speculate

that the loss of Ki-67 affects the reassociation of heterochromatic sequences with the nuclear lamina or nucleoli after mitotic exit.

2.5: Materials and methods

2.5.1: cell culture methods

hTERT-RPE1 cells (a kind gift from Dr. Judith Sharp) was cultured in DMEM-F12 medium (VWR 12001-600) with 10% fetal bovine serum (FBS, Hyclone #SH30910.03), 1% penicillin/streptomycin, 5% L-glutamine and 7.5% sodium bicarbonate solution.

293T cells were cultured in DMEM medium with 10% FBS, 1% penicillin/streptomycin, 5% L-glutamine. The cells were split 1:4 every 3 days

Primary MEF were cultured in DMEM medium with 10% FBS, 1% penicillin/streptomycin, 5% L-glutamine. The cells were split 1:3 every 2 days

For hydroxyurea treatment, hTERT-RPE1 cells were cultured in the presence of 2 mM hydroxyurea for 15 h, then washed with three times phosphate-buffered saline (PBS) and released into hydroxyurea-free medium and harvested at the indicated time points.

2.5.2: Immunofluorescence

Cells grown on glass coverslips were fixed in 4% paraformaldehyde for 10 min and then permeabilized with 0.5% Triton X-100 for 10 min at room temperature. The fixed cells were blocked in 5 % goat serum for 30 min, and incubated in primary antibody at 37 ^{O}C in a humidified chamber for 1h. The cells

were washed with PBS for 5 min three times, incubated with secondary antibody for 1 h at 37 ^{O}C in humidified chamber, followed by three PBS washes, 5 min each. Slides were then incubated with 130 ng/ml 4,6-diamidino-2-phenylindole (DAPI) for 5 min and mounted in Vectashield mounting medium (Vector Lab, H-1000)

Images were taken on a Zeiss Axioplan2 microscope with a 63× objective. Entire cells were imaged using 200 nm step-intervals and displayed as maximum intensity projections generated using AxioVision version 4.6.

The Xi-nucleolar association frequencies were scored in a blinded manner. Densitometry of individual immunostained cells was performed in Image J 10.2 macro script.

2.5.3: Immuno-RNA-FISH and RNA-FISH

The plasmid pGIA which contains human XIST exons 4, 5 and 6 was a gift from Dr Judith Sharp. Cot-1 probe was from Invitrogen (Sigma 11581074001). The probes were labeled either with biotin-14-dCTP or digoxigenin-11-dUTP using the BioPrime DNA labeling system (Invitrogen 18094-011).

For immunofluorescence (IF) combined with RNA-FISH, IF was performed first as above. Cells were then re-fixed in 4% paraformaldehyde for 10 min at room temperature. The cells were then dehydrated in 75%, 85%, 95% and 100% ethanol for 2 min each. Approximately 150 ng of each probe was mixed with 20 µg single-stranded salmon sperm DNA (Sigma-Aldrich) and 12 µg E. coli tRNA and then air-dried in a speed vacuum, resuspended in 20 ml 50% formamide / 50% hybridization buffer (20% Dextran Sulfate in 4× SSC), denatured at 80 ^{O}C for 10

min and pre-annealed at 37 ^{O}C for 30 min prior to hybridization. Hybridizations were performed overnight in a humidified chamber at 37°C. The next day, cells were washed for 20 min in 50% formamide in 2× SSC at 37°C and then for 20 min in 2× SSC at 37°C and 20 min in 1× SSC at 37°C. The hybridized probes were detected by incubation with either Alexa fluor-488 conjugated to streptavidin (Invitrogen S-32354) or Dylight 594 labeled anti-Digoxigenin/Digoxin (Vector Labs, DI-7594) at 1:500 dilutions for 60 min in a 37°C humid chamber. After incubation, slides were washed twice in 50% formamide, 2× SSC for 5 min and once in 1× SSC for 5 min in a 37°C humid chamber before DAPI staining as above.

2.5.4: siRNA

The siRNA targeting human Ki-67 is from the collection of Silencer Select Predesigned siRNAs (Thermo Fisher Scientific), and targets nucleotides 559-577 of the cDNA (NM_002417.4).

Its sequence is as follows:

sense CGUCGUGUCUCAAGAUCUAtt,

antisense UAGAUCUUGAGACACGACGtg

2.5.5. esiRNA methods

esiRNAs were generated using the DEQOR method (Surendranath *et al.*, 2013), with primers designed using the DEQOR database (http://deqor.mpi-cbg.de/deqor_new/input.html) to generate T7-tailed dsDNA templates from human cDNA in two rounds of PCR. RNA from hTERT-RPE1 cell line was used

to generate cDNA. In the 1st round of PCR, primers specific to the gene of interest (Luciferase, or Ki-67) were used in the following program: 95 °C for 3 mins, 16 cycles of (95 °C for 1 min, 65 °C -1 °C/cycle for 1 min, and 72 °C for 1 min) followed by an additional 15 cycles of (95 °C for 1 min, 60 °C for 1 min, and 72 °C for 1 min) and one final cycle at 72 °C for 5 mins. In the 2nd round of PCR, a T7 promoter-tailed primer was used to amplify the product of the 1st round with the following program: 95 °C for 2 mins, 4 cycles of (95 °C for 30 seconds, 42 °C for 45 seconds, and 72 °C for 1 min) followed by an additional 29 cycles of (95 °C for 30 seconds, 60 °C for 45 seconds, and 72 °C for 1 min) and one final cycle at 72 °C for 5 mins. The product of the 2nd round of PCR is used to transcribe ds esiRNA using T7 RNAP in presence of 25 mM NTPs and 40 mM Tris pH 7.9, 6 mM $MgCl_2$, 2 mM spermidine and 10 mM NaCl using the following thermocycler program: 37 °C for 5 hours 30 mins, 90 °C for 3 mins, Ramp 0.1 °C/second to 70 °C, 70 °C for 3 mins, Ramp 0.1 °C/second to 50 °C, 50 °C for 3 mins, Ramp 0.1 °C/second to 25 °C, 25 °C for 3 mins. After transcription and annealing, products were digested with 2U of RQ1 DNAseI for 15 minutes at 37 °C. esiRNAs were then generated by digesting dsRNAs with RNAse III (Fazzio *et al.*, 2008) and purified as described using Invitrogen RNA Mini Kits.

esiRNA targets Ki-67 repeat regions at nucleotides 3611-4047, 3979-4357, 4705-5098 and 6913-7347 of the cDNA (NM_002417.4).

Forward primer for hKi-67

gcgtaatacgactcactataggGTGCTGCCGGTTAAGTTCTCT

Reverse primer for hKi-67

gcgtaatacgactcactataggGCTCCAACAAGCACAAAGCAA

Forward primer for luciferase

gcgtaatacgactcactataggAACAATTGCTTTTACAGATGC

Reverse primer for luciferase

gcgtaatacgactcactataggAGGCAGACCAGTAGATCC

Cells were transfected with Lipofectamine RNAi MAX (Invitrogen Catalog number 13778100) following manufacturer's instructions.

For esiRNA transfection, 500ng of esiRNA targeting either luciferase control or Ki67 was transfected into 40×10^3 cells.

For siRNA transfection, 40 nM of either scramble or siKi67 was transfected into 40×10^3 cells.

The cells were harvested 72 hrs after transfection for immunoblotting, RT-qPCR, RNA-seq, FACS or FISH analysis.

2.5.6. Visualization of 5-ethynyl-2-deoxyuridine(EdU)-labeled nascent DNA

hTERT-RPE1 cells were grown on glass coverslips in DMEM/F12 media as described above. 5-ethynyl-2-deoxyuridine (EdU) was added to the culture medium at concentration of 10 mM for 20 min. After labeling, cells were washed three times with PBS. Cells were then permeablized in 0.5% Triton X-100 for 30 seconds and then fixed in 10% formaldehyde for 10 min. Cells were then rinsed twice with PBS and then incubated 30 min in 100 mM Tris-HCl pH 8.5, 1 mM $CuSO_4$, 100 mM ascorbic acid plus 50 mM carboxyrhodamine 110-azide for click-chemistry labeling. After staining, the cells on coverslips were washed three times with PBS plus 0.5% Triton X-100, 5 min each. Cells were then

counterstained with DAPI, mounted in Vectashield and imaged by fluorescence microscopy as above.

2.5.7: Immunoblotting

For immunoblotting, cells were collected 3 days after RNAi transfection. Whole-cell lysates were extracted in 20 mM Tris-HCl 7.5, 1% SDS and 10% glycerol supplemented with protease inhibitor cocktail (Sigma P8340-1ml). The lysates were sonicated in a Bioruptor set on high power for one 5 min cycle, with 30s on/30s off. 15 mg of each lysate were separated by SDS-PAGE, transferred to PVDF membrane and probed as described in the figure legends.

Table 2.2: Antibodies used for immunofluorescence and western blotting

Epitope	Species	Manufacturer	Catalog #	Immunofluorescence Dilution	Western Blot Dilution
Fibrillarin	Rabbit	Abcam	Ab5821	1:500	1:2000
BrdU	Mouse MoBu-1	Abcam	ab8039	$0.5 \ \mu g/10^6$ cells	
Ki-67	Rabbit	Abcam	Ab15580	1:500	1:2000
beta-tubulin	Mouse	Ubpbio	Y1060		1:10,000
Amersham ECL Rabbit IgG, HRP-linked whole Ab	Rabbit	GELife science	NA934		1:5000
IgG (H+L) Secondary Antibody, Alexa Fluor® 594	Rabbit	Life Techonologies	A-21207	1:2000	
Secondary Antibody, Alexa Fluor® 488	Rabbit	Life Technologies	A-21206	1:2000	

Streptavidin, Alexa Fluor® 488 Conjugate		Invitrogen	S-32354	1:500	
DyLight 594 Labeled Anti-Digoxigenin/Digoxin		Vector Labs	DI-7594	1:500	
macro H2A.1	rabbit	Abcam	Ab3726	1:500	
H4K20me1	Mouse	Active motif	39727	1:500	
RNA polymerase II	Mouse(CTD4H8)	Millipore	05-623	1:500	
H3K27me3	rabbit	Active motif	39535	1:500	

Chapter III: Ki-67 affects S phase gene expression and cell cycle progression in checkpoint proficient cells

3.1: Abstract

Although Ki-67 is widely used as a cell proliferation marker, whether it affects cell cycle progression has been controversial. I show here that depletion of Ki-67 in human hTERT-RPE1, WI-38, IMR90, and hTERT-BJ cell lines reduced the proportion of cells in S phase and coordinately downregulated genes related to DNA replication. These cell lines are able to induce the expression of checkpoint protein p21. On the contrary, in tumor-derived U2OS, HeLa, and 293T cells, I do not observed either the p21 induction or the alteration of the transcription and cell cycle distribution. Further more, additional co-depletion of p21 thoroughly suppressed the transcriptional and cell cycle defects in diploid and primary cell lines. Altogether, these results indicate that Ki-67 regulates cell cycle progression in p21 checkpoint proficient cells.

3.2: Introduction

Ki-67 was first identified via an antibody raised against Hodgkin lymphoma cell nuclei (Gerdes *et al.*, 1983). Because Ki-67 is generally expressed strongly in proliferating cells and poorly in quiescent cells (Gerdes *et al.*, 1984), anti-Ki-67 antibodies are frequently used to detect proliferative cells in clinical studies(Gerdes *et al.*, 1987; Dowsett *et al.*, 2011). In interphase cells, Ki-67 primarily localizes to the nucleolus(Verheijen *et al.*, 1989a; Kill, 1996; Cheutin *et al.*, 2003), whereas during mitosis, it coats the chromosomes(Verheijen *et al.*, 1989a; Saiwaki *et al.*, 2005; Takagi *et al.*, 2014). In the past few years, several studies have greatly increased our understanding of Ki-67 function. This is particularly true for its mitotic roles. Specifically, Ki-67 is required for formation of the mitotic perichromosomal layer(Booth *et al.*, 2014)(Sobecki *et al.*, 2016), a proteinaceous sheath that coats mitotic chromosomes(Van Hooser *et al.*, 2005; Booth *et al.*, 2016). As part of this layer, Ki-67's large size and highly positively-charged amino acid composition keeps individual mitotic chromosomes dispersed rather than aggregated upon nuclear envelope disassembly, thereby ensuring normal kinetics of anaphase progression (Cuylen *et al.*, 2016). At anaphase onset, Ki-67 binds protein phosphatase 1γ (PP1γ) to form a holoenzyme (Kumar *et al.*, 2016) important for targeting substrates that must be dephosphorylated during mitotic exit (Takagi *et al.*, 2014). In contrast to its structural role on the mitotic chromosomal surface, Ki-67 does not appear to affect nucleosomal spacing (Cuylen *et al.*, 2016) or condensation of individual mitotic chromosomes(Booth *et al.*, 2016; Cuylen *et al.*, 2016).

In addition to its expression in proliferating cells, other experiments suggested Ki-67 has a positive role in regulating cell proliferation. In early studies, antisense oligonucleotides targeting Ki-67 expression in human IM-9 multiple myeloma cells blocked [^{3}H]-thymidine incorporation, indicative of inhibition of proliferation (Schluter *et al.*, 1993). Likewise, Ki-67-targeted phosphorothioate anti-sense oligonucleotides that resulted in partial depletion of Ki-67 protein inhibited proliferation of human RT-4 bladder carcinoma and other tumor cell lines (Kausch *et al.*, 2003). More recently, siRNA-mediated depletion of Ki-67 resulted in reduced proliferation in human 786-0 renal carcinoma cells (Zheng *et al.*, 2006).

However, despite its utility as a proliferation marker, the contribution of Ki-67 to cell proliferation has recently been questioned. For example, in one recent study, genetic disruption of Ki-67 in human MCF-10A epithelial breast and DLD-1 colon cancer cells did not affect cell proliferation rates in bulk culture, although clonogenic growth of highly diluted cell populations was reduced (Cidado *et al.*, 2016). In another recent study, depletion of Ki-67 in human HeLa or U2OS cells did not alter cell cycle distribution (Sobecki *et al.*, 2016). These data raise the possibility that Ki-67 function may have different consequences in different cell types. Experiments here investigated cell-type specific Ki-67's involvement in cell cycle progression and molecular mechanism underlying the differences.

3.3:Results

3.3.1: Acute depletion of Ki-67 affects S phase gene expression and S phase progression in hTERT-RPE1 cells

To explore how Ki-67 impacts gene expression, we performed RNAseq analyses of hTERT-immortalized human diploid RPE1 cells depleted of Ki-67. Ki-67 depletion resulted in both reduced and increased RNA levels at different loci (SRR4252548, SRR5535471, SRR5535778, and SRR5535934). However, Reactome pathway analysis of RNA abundance changes showed that the most altered functional sets of genes included those involved in DNA replication and cell cycle progression (Figure 3.1 A). For example, levels of RNAs encoding all subunits of several protein complexes involved in S phase progression were concertedly reduced, including DNA replication clamp loader RFC (RFC1-5 genes), ssDNA-binding complex RPA (RPA1-3), the replicative helicase (MCM1-6), the GINS replication initiation complex (GINS1-4), the DNA polymerase alpha/primase complex, as well as the DNA replication clamp PCNA and the flap-endonuclease FEN1 involved in Okazaki fragment maturation. We confirmed reduced levels of a subset of replication-related RNA targets by RT-qPCR analyses (Figure 3.2A). Notably, the RT-qPCR data were very similar when obtained with two distinct Ki-67 depletion reagents, one a synthetic siRNA and the other a cocktail of in vitro-diced dsRNAs non-overlapping the siRNA target, both of which efficiently depleted steady-state Ki67 levels (Figures 3.2 A, B, I, J).

We also observed that fluorescence-activated cell sorting (FACS) analysis of Br-dUTP-labeled cells showed that the proportion of S phase cells decreased

upon depletion of Ki-67 in hTERT-RPE1 cells with either depletion reagent (Figure 3.2 C-D; quantified in Fig. 3.2 E, G). In contrast, proportions of G1 and G2/M populations were not significantly altered (Fig. 3.2F and 3.2 H). Therefore, Ki-67 is important for normal S phase distribution and gene expression in hTERT-RPE1 cells.

As an additional control for the direct effect of the siRNA treatment, we used CRISPR/Cas9 to mutate the siRNA target site in hTERT-RPE1 cells (Fig. 3.3 A-B). In a resulting homozygous mutant cell line (Figure 3.3 C), siKi-67 no longer depleted Ki-67 protein levels, but as expected the esiKi-67 reagent was still effective (Figure 3.3 D). We also observed that siKi-67 no longer altered candidate S phase RNA levels in the resistant cell line, but esiKi-67 did (Figure 3.3E). We conclude that the transcriptional response to acute depletion of the Ki-67 mRNA is due to loss of Ki-67 protein.

Figure 3.1: Characterization of RNA-seq data.

A. Scatter plots comparing the RPKM (Reads Per Kilobase of transcript per Million reads) RNA levels between two si-scramble RNAseq replicates. R: Pearson's correlation, note that a perfect correlation is R=1.

B. Scatter plots comparing the RPKM RNA levels between two si-Ki67 RNAseq replicates.

C. Distribution of fold changes in gene expression comparing RNAseq data from si-scramble and si-Ki67-treated hTERT-RPE1 cells. In this "MA" plot, the x-axis shows the mean log2 value for normalized counts of abundance levels for each RNA species. The y-axis shows the log2 fold change upon Ki-67 depletion. The symmetry of the plot above and below the y = 0 axis indicates that similar numbers of genes are up- and down-regulated upon Ki-67 depletion.

D. Reactome evaluation of RNAseq analysis of si-Ki-67 treated cells/ The PATH terms with a p-value<5e-05 are graphed

Figure 3.1: Characterization of RNA-seq data
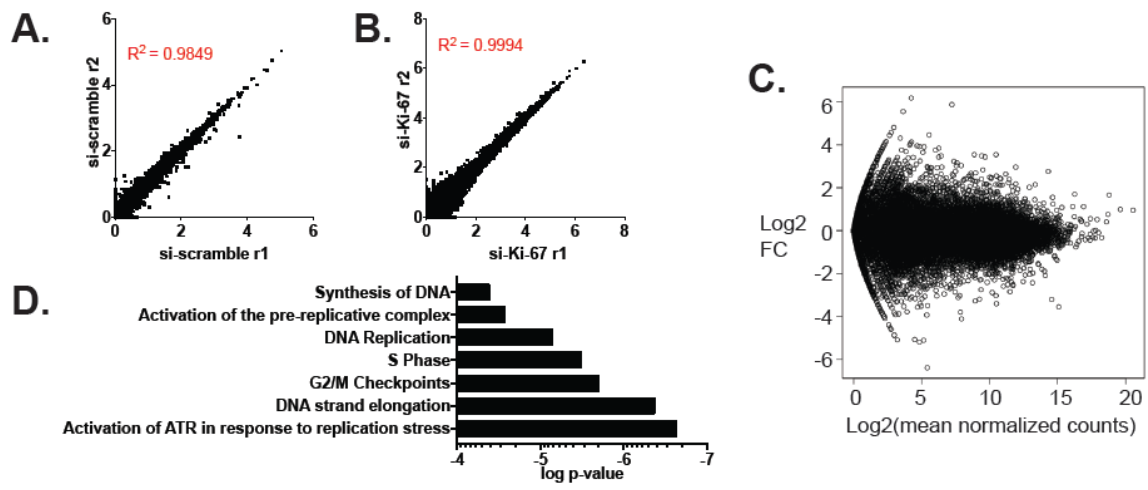
Figure 3.2: Ki-67 depletion in hTERT-RPE1 cells reduced S-phase-related mRNA abundance and the proportion of cells in S phase.

A. RNA levels of DNA replication genes are coordinately down-regulated in siKi-67-treated cells. RT-qPCR measurements are presented as fold change relative to the scramble siRNA control after normalization. *MKI67* mRNA levels indicate effectiveness of the siRNA treatment. Data are mean ± std. dev. of 3 biological replicates.
B. Analysis of RNA levels as in panel E, except that cells were treated with in vitro-diced esiRNAs as depletion reagents.
C. FACS analysis of siRNA-treated cells. Cells were pulsed with BrdU for 20 min, and analyzed via two-dimensional flow cytometry monitoring BrdU incorporation (y-axis) and DNA content (x-axis). G1 (lower left), G2 (lower right), and S-phase populations (upper box) are boxed in each sample, with percentages of the total population shown. Data shown are from one representative experiment of three biological replicates performed.
D. FACS analysis as in panel G, except that cells were treated with esiRNAs.
E. Quantification of percentage of cells in S-phase in siRNA-treated hTERT-RPE1 populations from three biological replicate BrdU-labeling experiments. p-value comparing si-scramble and si-Ki-67 treatments is indicated, calculated via an unpaired, two-tailed parametric t test.
F. Quantification of percentage of cells in G1 or G2/M phase from the same three experiments analyzed in panel I.
G. Quantification of percentage of S-phase cells as in panel I, except that cells were treated with in vitro-diced esiRNAs.
H. Quantification of percentage of cells in G1 or G2/M phase from the same three experiments analyzed in panel K.
I. Immunoblot analysis of Ki-67 depletion in siRNA-treated hTERT-RPE1 cells from panel D. Marker molecular weights are indicated on the left.
J. Immunoblot analysis of Ki-67 depletion in esiRNA-treated hTERT-RPE1 cells from panel F.

Figure 3.2: Ki-67 depletion in hTERT-RPE1 cells reduced S-phase related mRNA abundance and the proportion of cells in S phase
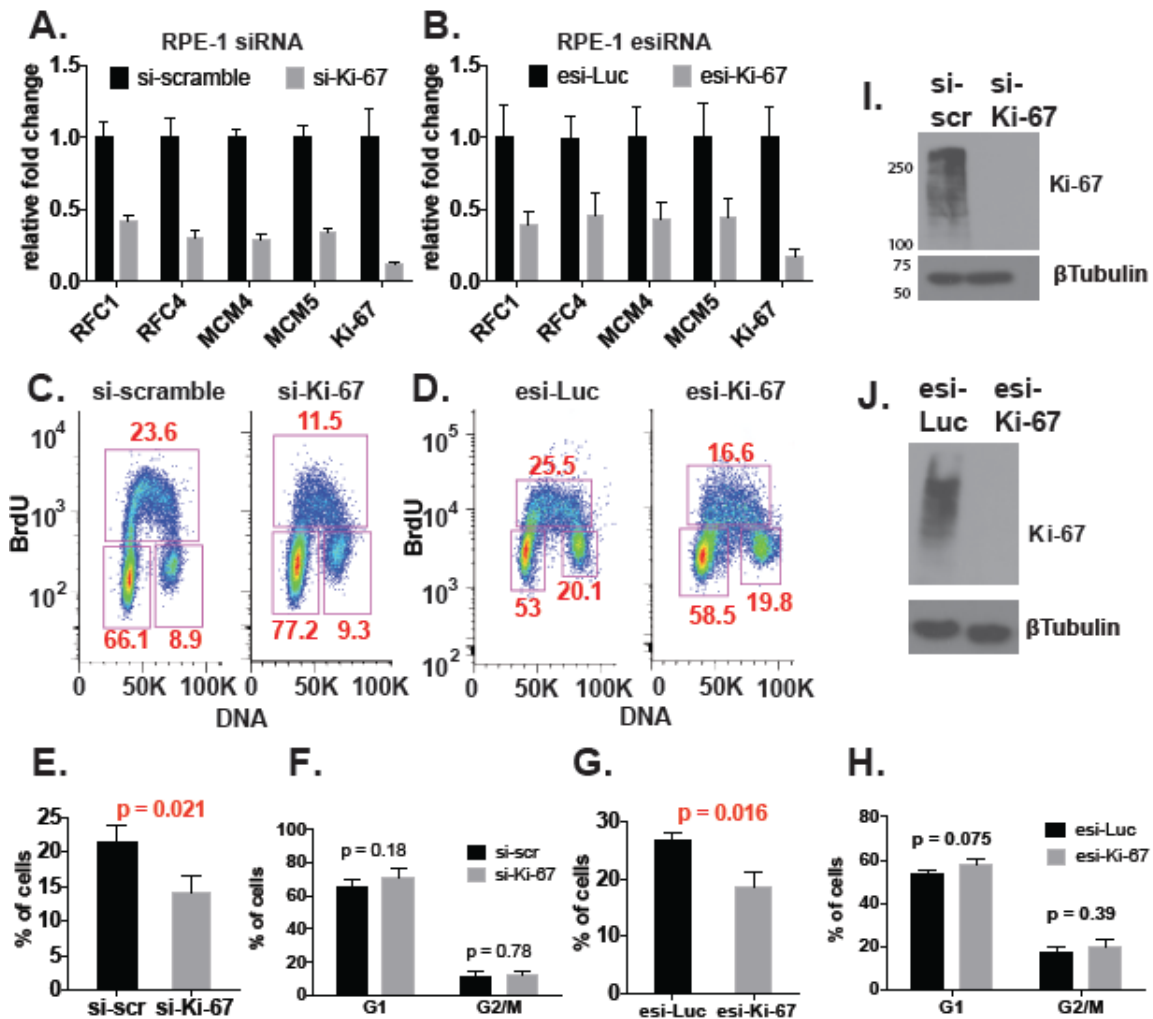
Figure 3.3: Validation of specificity and effectiveness of Ki-67 depletion reagents.

A. CRISPR/Cas9-based strategy for generating siRNA-resistant mutations in the endogenous Ki-67 gene. The si-Ki-67 target (green) and sgRNA-directed cleavage site (red triangle) are indicated on the upper diagram of the endogenous locus. Altered nucleotides (red) and the novel EcoO109I restriction site are shown on the lower diagram of the repair template.
B. DNA sequence analysis of a PCR product from wild-type hTERT-RPE1 cells and si-Ki-67-resistant clone #7.
C. EcoO109I digestion of the same PCR product sequenced in panel B.
D. Immunoblot analysis of clone #7 treated with the indicated reagents.
E. RT-qPCR analysis of clone #7.
F-L. Immunoblot analyses of the indicated cell lines, treated with the indicated RNA depletion reagents

Figure 3.3: Validation of specificity and effectiveness of Ki-67 depletion reagents
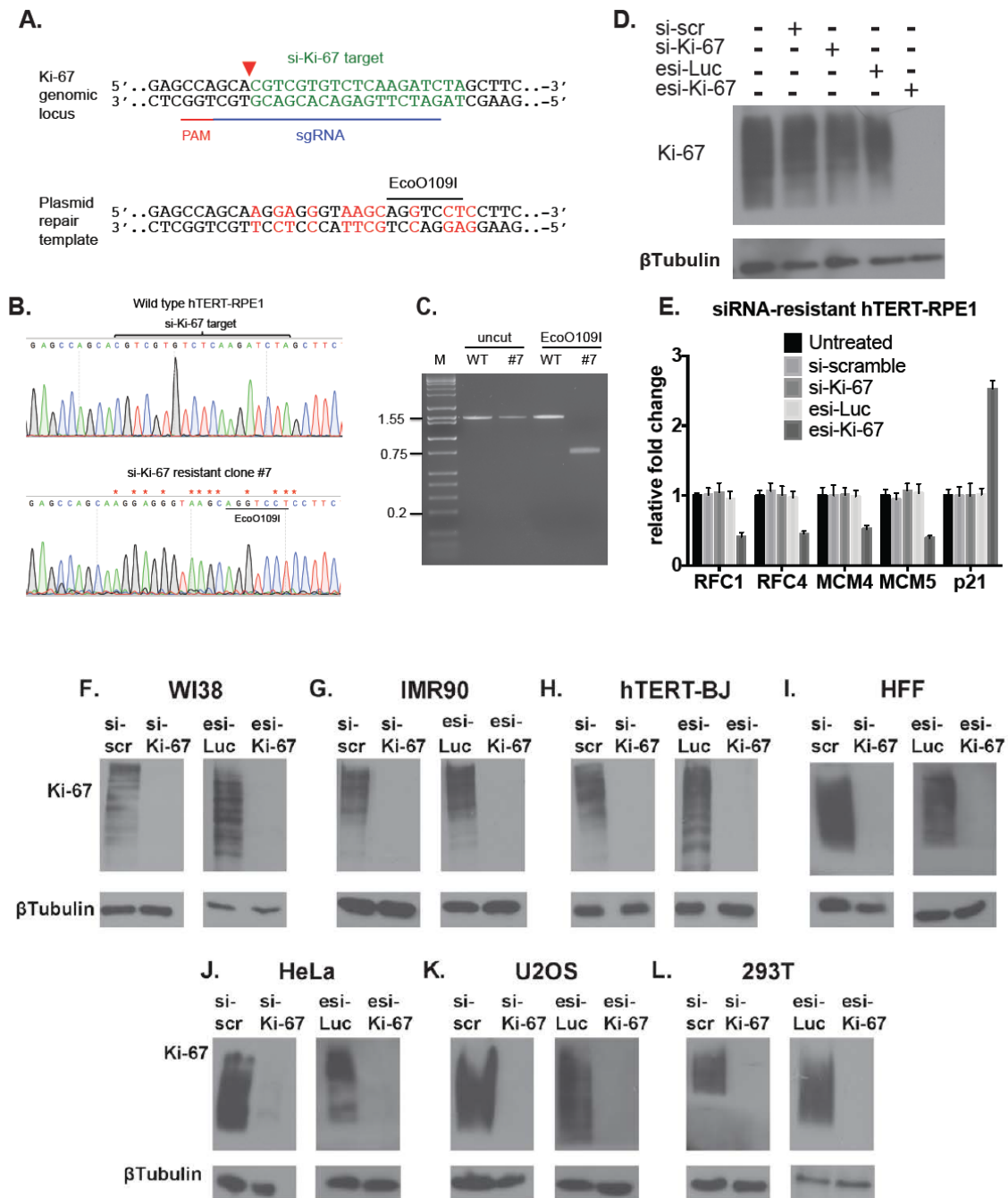
3.3.2: Acute depletion of Ki-67 affects S phase gene transcription and the proportion of cells in S phase in diploid fibroblasts and primary cells, but not in tumor derived cell lines.

Recent studies challenge the view that Ki-67 is important for human cell proliferation; for example, depletion of Ki-67 had minimal effects on the cell cycle distribution of tumor-derived HeLa or U2OS cells (Sobecki *et al.*, 2016). Because our data indicated that Ki-67 contributes to normal cell cycle progression in hTERT-RPE1 cells, we hypothesized that the contribution of Ki-67 to cell cycle progression would be cell type-dependent, and may be related to checkpoint function. To explore this idea, we depleted Ki-67 in several additional cell lines. We compared diploid, non-immortal WI-38 and IMR90 fibroblasts, hTERT-immortalized BJ fibroblasts, and primary human foreskin fibroblasts (HFFs) with tumor-derived cell lines: virally-transformed kidney (293T) or cervical carcinoma (HeLa) cells, and osteosarcoma U2OS cells. Importantly, we confirmed that all these cells could be efficiently depleted of Ki-67 protein using both of our depletion reagents (Figure 3.3 F-L).

In all of the experiments with the non-tumor-derived cells, we observed reduced replication factor RNA levels and fewer cells in S phase, similar to our results in hTERT-RPE1 cells, and these results were independent of which Ki-67 depletion reagent was used (Figures 3.4-3.5). In contrast, in the tumor-derived cell lines, Ki-67 depletion did not result in uniform down regulation of the S phase genes tested, nor were there changes in cell cycle distribution (Figures 3.6-3.7). These data are consistent with RNAseq data sets in HeLa and U2OS cells

(Sobecki *et al.*, 2016) that did not display concerted downregulation of DNA replication genes. We conclude that the effects of Ki-67 depletion on RNA levels and cell cycle distribution are cell type-dependent.

Figure 3.4: siRNA-mediated Ki-67 depletion affected S-phase gene expression and cell cycle distribution in diploid human cells.

WI-38 (panels A-D), IMR-90 (panels E-H), hTERT-BJ (panels I-L) cell lines and human primary fibroblasts (HFF, panels M-P) were analyzed.
A, E, I, M.   RT-qPCR analysis, as in Figure 1E.
B, F, J, N.   FACS analysis, as in Figure 1G.
C, G, K, O.   Quantification of percentage of S-phase cells, as in Figure 1I.
D, H, L, P.   Quantification of percentage of G1 and G2/M phase cells as in Figure 1J.

Figure 1 3.4: siRNA-mediated Ki-67 depletion affected S-phase gene expression and cell cycle

distribution in diploid human cells
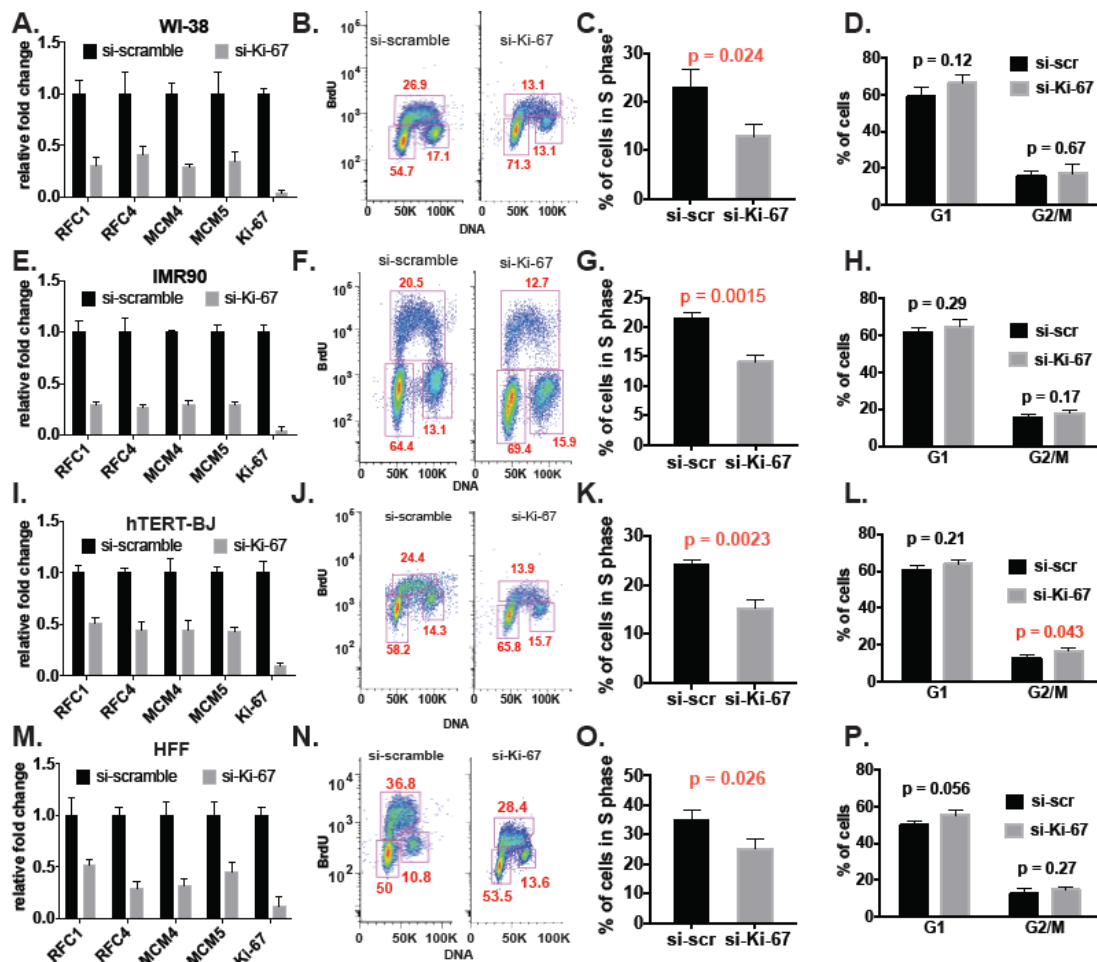
Figure 2 3.5: esiRNA-mediated depletion of Ki-67 in diploid cells resulted in the same phenotypes observed with siRNA treatments
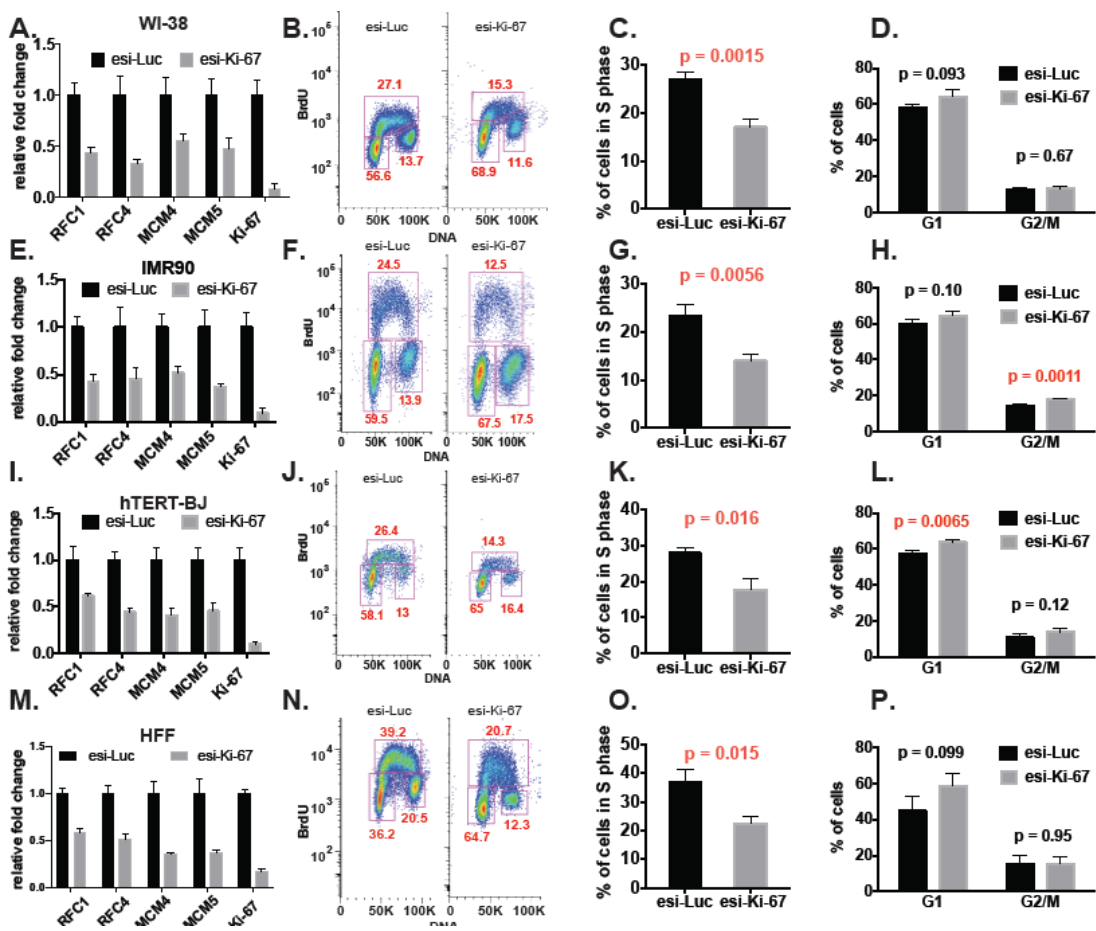
Figure 3.6: Ki-67 depletion did not affect S-phase gene expression and cell cycle distribution in HeLa (panels A-D), U2OS (panels E-H), and 293T (panels I-L) cell lines.

Panels A, E, I: RT-qPCR analysis. Panels B, F, J: FACS analysis. Panels C, G, K: Quantification of percentage of S-phase cells. Panels D, H, L: Quantification of percentage of G1 and G2/M phase cells.

Figure 3.6: Ki-67 depletion did not affect S-phase gene expression and cell cycle distribution in HeLa, U2OS and 293T cell lines.
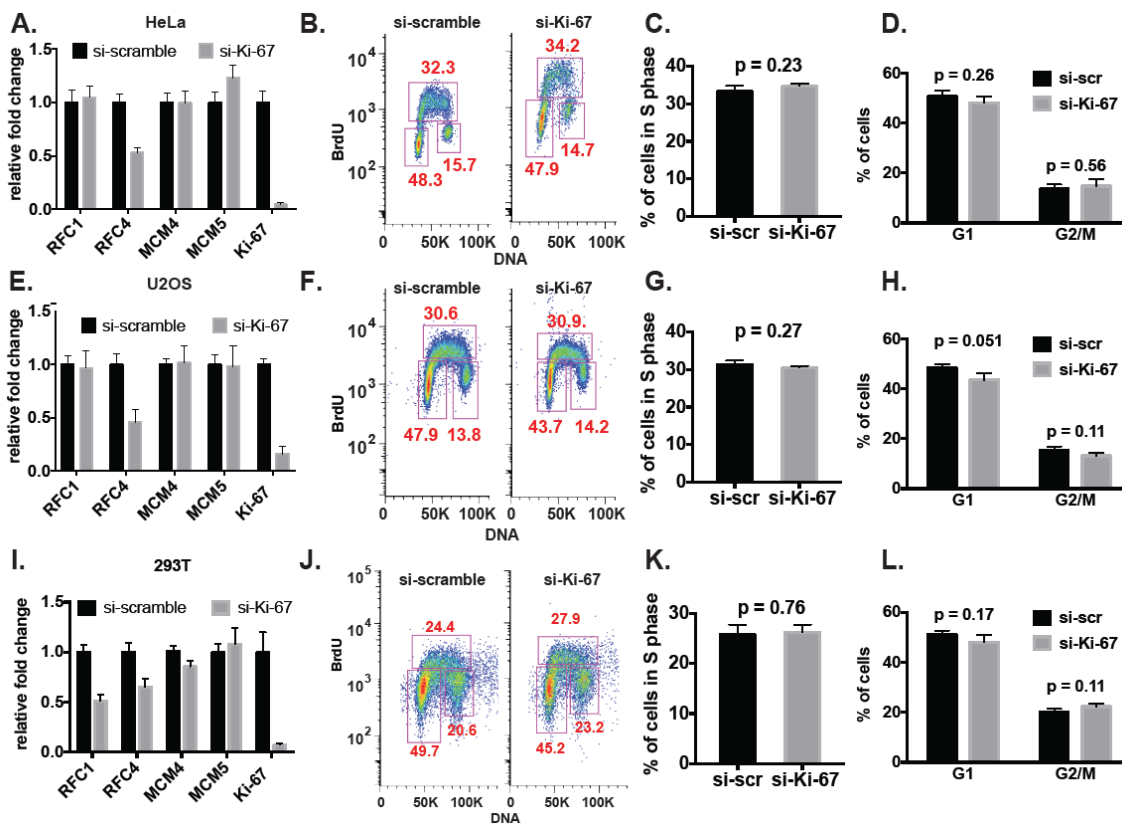
Figure 3.7: esiRNA-mediated depletion of Ki-67 in insensitive-cells resulted in the same phenotypes observed with siRNA treatments. Cells and assays were the same as Figure 3.6
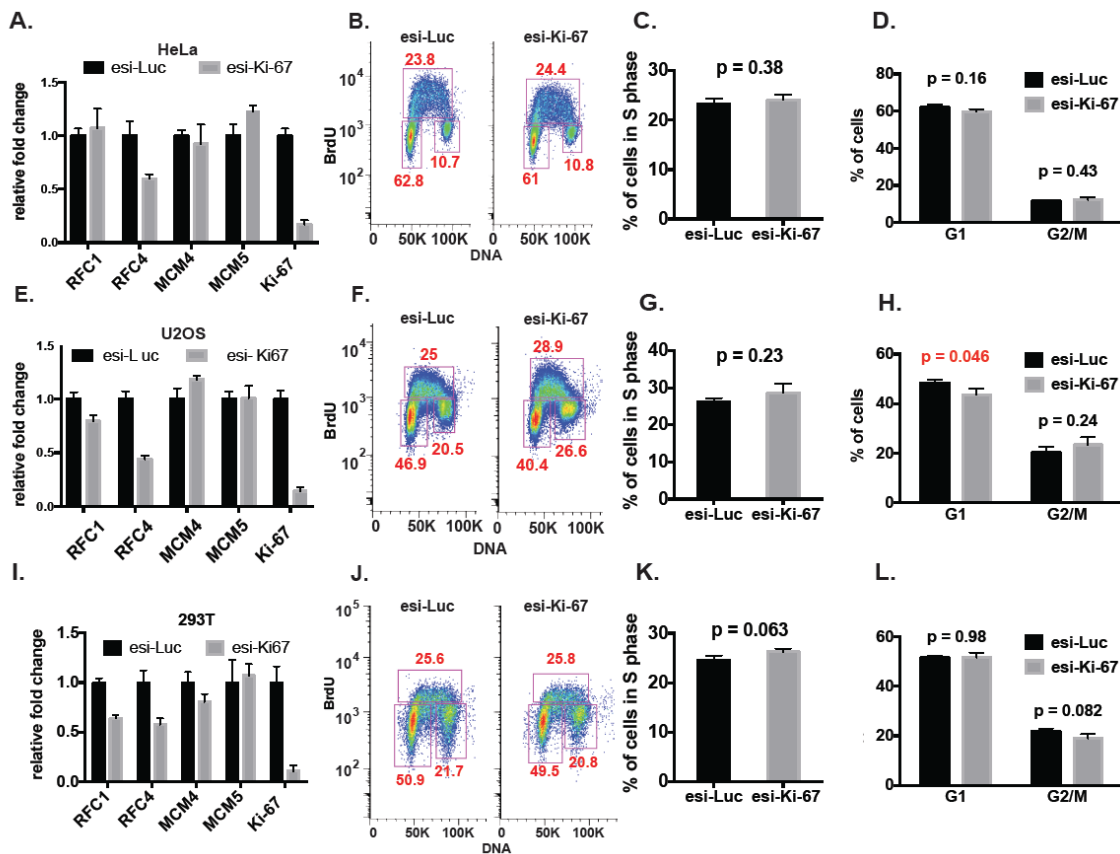
3.3.3: Rb partially contributes to transcriptional down regulation caused by Ki-67 depletion

Because Ki-67 depletion did not affect S phase transcription or cell cycle progression in tumor-derived cell lines, our data suggested that functional checkpoints are required for sensitivity to Ki-67 depletion. Consistent with this idea were comparisons of our RNAseq data with metadata analyses of genes regulated by cell cycle status or by E2F transcription factors (Fischer *et al.*, 2016) that are important for G1/S cell cycle phase transcription(Fischer *et al.*, 2016; Sadasivam and DeCaprio, 2013; Bertoli *et al.*, 2013). These meta-analyses aggregated multiple datasets, finding that coherent patterns of regulation in multiple datasets strongly predicted regulatory network connections that could be missed in single experiments. Of the cell cycle-regulated genes identified in that study, we find those that peak during G1/S phase were more frequently downregulated than upregulated upon Ki-67 depletion (Fig. 3.8 A). Consistent with this observation, E2F target RNA levels (Fig. 3.8 B) were much more frequently downregulated than upregulated upon Ki-67 depletion. These comparisons were consistent with the idea that checkpoint activation contributed to the observed delay in S phase entry and transcriptional phenotypes in Ki-67-depleted cells.

To test this, we performed experiments co-depleting checkpoint proteins. First, we took advantage of a derivative of hTERT-RPE1 cells that have an integrated, doxycycline-inducible shRNA that targets the RB mRNA (Manning *et al.*, 2014). Rb levels remained unchanged in these cells in the absence of

doxycycline (Fig. 3.8 C), and siRNA-mediated depletion of Ki-67 resulted in reduced S phase-related RNA levels as was observed previously (Fig. 3.8D). Addition of doxycycline to deplete Rb, together with a control scrambled siRNA leaving Ki-67 levels unchanged, did not significantly alter S-phase related target RNA levels (Fig. 3.8D). In contrast, simultaneous depletion of Rb and Ki-67 resulted in RNA levels at two of the four loci tested that were significantly elevated compared to those in cells depleted of Ki-67 alone (Fig. 3.8D). FACS analysis indicated that Rb depletion was insufficient to significantly change the cell cycle profile of Ki-67-depleted cells (Fig. 3.8E-F). We conclude that depletion of Rb only partially relieves the cellular response to Ki-67 depletion in hTERT-RPE1 cells.

Figure 3.8: Rb contributes to transcriptional downregulation caused by Ki-67 depletion.

A.   Summary of transcriptional changes of cell cycle target genes (based on Table S10 in (Fischer *et al.*, 2016)). The "Adjusted Cell Cycle Score" on the y-axis indicates values based on meta-analysis of 5 different cell cycle expression data sets, plus information regarding binding by Rb/E2F and MMB/FOXM1 transcription factors. Negative values indicate frequent detection of G1/S expression and binding by Rb/E2F, and positive values indicate frequent detection of G2/M expression and binding by MMB-FOXM1.

B. p-values of transcription changes of E2F target genes (based on Table S9 in (Fischer *et al.*, 2016)), with the greater score on the x-axis representing higher frequency of detection as an E2F target. As expected from panel A, E2F targets are commonly downregulated upon Ki-67 depletion.

C. Immunoblot analysis hTERT-RPE1 Tet-sh-Rb cells. Cells were treated with either vehicle (Rb+) or 2 μg/ml doxycycline (Rb-) as indicated for 72 h to induce sh-Rb expression, and were also incubated in the presence of either si-scramble (Ki-67+) or siKi-67 (Ki-67-).

D. RT-qPCR analysis of DNA replication genes in cells treated as in panel C. Measurements are presented as fold change relative to the scramble siRNA control without doxycycline induction. Data are mean ± std. dev. of 3 biological replicates. p-values were calculated via unpaired, two-tailed parametric t tests and corrected for multiple comparisons using the Holm-Sidak method.

E. Percentage of S phase cells calculated from three BrdU labeling experiments. p-values were calculated via unpaired, two-tailed parametric t tests.

F. FACS analysis of a representative BrdU labeling experiment.

G. p-values of transcription changes of DREAM target genes (based on Table S7 in (Fischer *et al.*, 2016)), with the greater score on the x-axis representing more frequent detection as a DREAM target.

Figure 3.8: Rb contributes to transcriptional downregulation caused by Ki-67 depletion
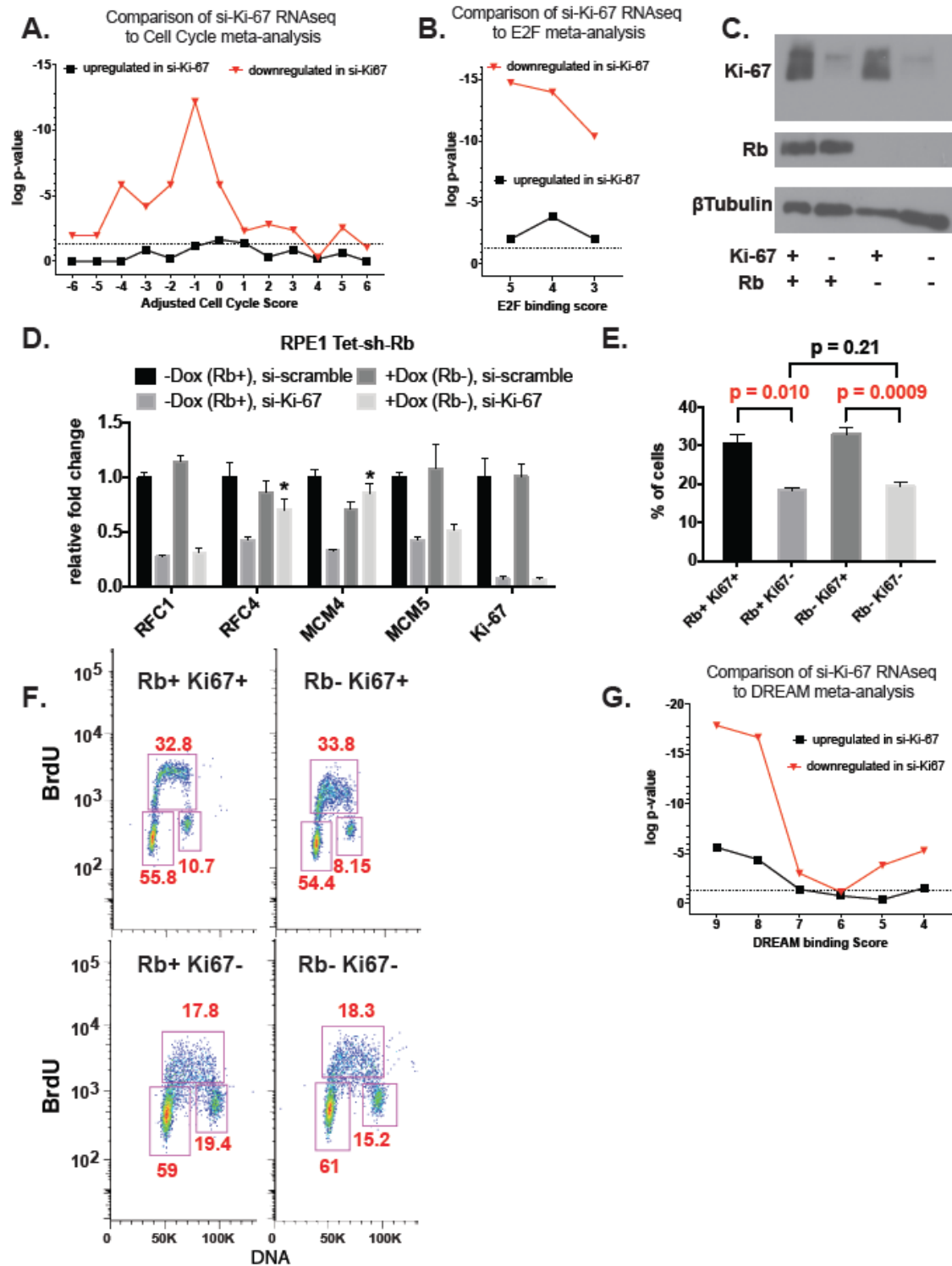
3.3.4: Co-depletion of p21 suppresses transcriptional and cell cycle progression responses to Ki-67 depletion

As depletion of Rb only partially relieves the cellular response to Ki-67 depletion in hTERT-RPE1 cells, we reasoned other factors must contribute. One clue was provided by comparison of the si-Ki-67 RNAseq data to metadata analysis of binding by subunits of the DREAM complex transcription repressor (Fischer *et al.*, 2016). We observed that genes with the highest predicted probability of DREAM binding were very frequently downregulated upon Ki-67 depletion (Fig. 3.8G). In mammalian cells, DREAM is a master regulator of cell cycle-dependent gene expression, repressing both G1/S and G2/M targets, and gene repression by DREAM requires the p21 checkpoint protein(Sadasivam and DeCaprio, 2013; Litovchick *et al.*, 2007; Schmit *et al.*, 2007). p21 is a potent universal CDK inhibitor (CKI). During G1 and S phases, it directly binds to and inhibits the kinase activity of cyclin E-CDK2, cyclin B1-CDK1 and cyclin D-CDK4/6 complexes (Xiong *et al.*, 1993; Gartel *et al.,* 2005; Labaer *et al.*, 1997). Furthermore, p21 also directly inhibits DNA synthesis by binding to PCNA, the sliding clamp required for processive DNA polymerase activity (Waga and Stillman, 1998). Therefore we hypothesized that p21 could be important for the response to Ki-67 depletion (Fig 3.10).

Consequently, we next tested effects of Ki-67 depletion on the *CDKN1A* gene, which encodes p21. Our RNAseq data indicated increased *CDKN1A* RNA levels in Ki-67 depleted hTERT-RPE1 cells (log2 fold change = +0.48, p = 0.016), although multiple hypothesis testing indicated that these values did not achieve

the stringent statistical significance cutoff of q < 0.05. RT-PCR measurements of *CDKN1A* RNA levels demonstrated a significant increase in four diploid cell types, but not in 293T cells (Fig. 3.9A). We note that induction of *CDKN1A* RNA was dependent on having an intact siRNA target site in the Ki-67 gene, indicating this is a direct effect of Ki-67 depletion (Figure 3.3E). Consistent with the increased RNA levels, we detected elevated p21 protein levels in hTERT-RPE1 but not 293T cells (Fig. 3.9B).

p21 is a direct target of transcriptional induction by the tumor suppressor p53, and the cell lines examined thus far therefore implicated active p53 in the sensitivity to Ki-67 (El-Deiry *et al.*, 1993; Deng *et al.*, 1995). To examine this relationship further, we compared the effects of Ki-67 depletion in additional cancer cell lines, including two expressing wild-type p53, MCF7 and HCT116, and also MDA-MB-231 cells which express a mutant p53 defective for p21 induction (Junk *et al.*, 2008). In MCF7 breast adenocarcinoma cells, we observed that Ki-67 depletion elevated p21 RNA and protein levels (Fig. 3.9 G,H), and down-regulated replication-related RNAs (Fig. 3.9H). In contrast, in HCT116 colorectal carcinoma and MDA-MB-231 breast adenocarcinoma cells, Ki-67 depletion did not increase p21 expression or cause concerted down-regulation of S phase genes. (Fig. 3.9 G, I, J). Because HCT116 and MDA-MB-231 cells differ in their p53 status, we conclude that p53 status cannot always predict the response to Ki-67 depletion. Instead, we find that induction of p21 upon Ki-67 depletion is a consistent hallmark of this form of checkpoint activation.

To assess the functional consequence of p21 induction, we performed co-depletion experiments in hTERT-RPE1 cells (Fig. 3.9D). We observed that cells simultaneously depleted of both Ki-67 and p21 no longer displayed the reduced levels of any of the four S phase-related mRNAs analyzed (Fig. 3.9D). Furthermore, FACS analysis of the co-depleted cells showed that there was significant restoration of the percentage of cells in S phase upon codepletion of p21 with Ki-67 (Fig. 3.9E-F). We conclude that induction of p21 is functionally important for the effects of Ki-67 depletion on cell cycle distribution in hTERT-RPE1 cells.

Figure 3.9: Cell-type-specific induction of a p21-dependent checkpoint upon depletion of Ki-67.

A. RT-qPCR analysis demonstrates cell-type specific induction of *CDKN1A* (p21) RNA upon Ki-67 depletion. (left panel) Indicated cells were treated with either si-scramble or si-Ki-67 for 72 hrs. (right panel) Same, except cells were treated with esiRNAs.
B. Cell-type specific induction of p21 protein levels upon Ki-67 depletion. hTERT-RPE1 and 293T cells were treated with the indicated siRNA or in vitro-diced esiRNA depletion reagents. p21 protein levels were quantified as a ratio to β-tubulin and normalized to levels in control-treated cells. Quantification was done in Image J 10.2.
C. Immunoblot analysis of hTERT-RPE1 cells depleted of the indicated proteins via siRNA treatments. Marker molecular weights are indicated on the right.
D. RT-qPCR analysis of DNA replication genes in hTERT-RPE1 cells from panel C. Asterisks indicate values in the si-p21 + si-Ki-67 samples that were significantly different ($p < 0.05$) from the siKi-67 samples. p-values were calculated via unpaired, two-tailed parametric t tests and corrected for multiple comparisons using the Holm-Sidak method.
E. Percentage of S phase cells calculated from three BrdU labeling experiments. p-values were calculated via unpaired, two-tailed parametric t tests.
F. FACS analysis of a representative BrdU labeling experiment.
G. Immunoblot analysis of additional siRNA-treated cell lines testing for p21 induction.
H. RT-qPCR analysis of the indicated genes in MCF7 cells. p-values calculated as in panel D were < 0.05 for all genes.
I. RT-qPCR analysis of the indicated genes in MDA-MB-231 cells.
J. RT-qPCR analysis of the indicated genes in HCT-116 cells.
K. co-depletion of p53 and Ki-67 in hTERT-RPE1 cells leads to synthetic lethality

Figure 3.9: Cell-type-specific induction of a p21-dependent checkpoint upon depletion of Ki-67
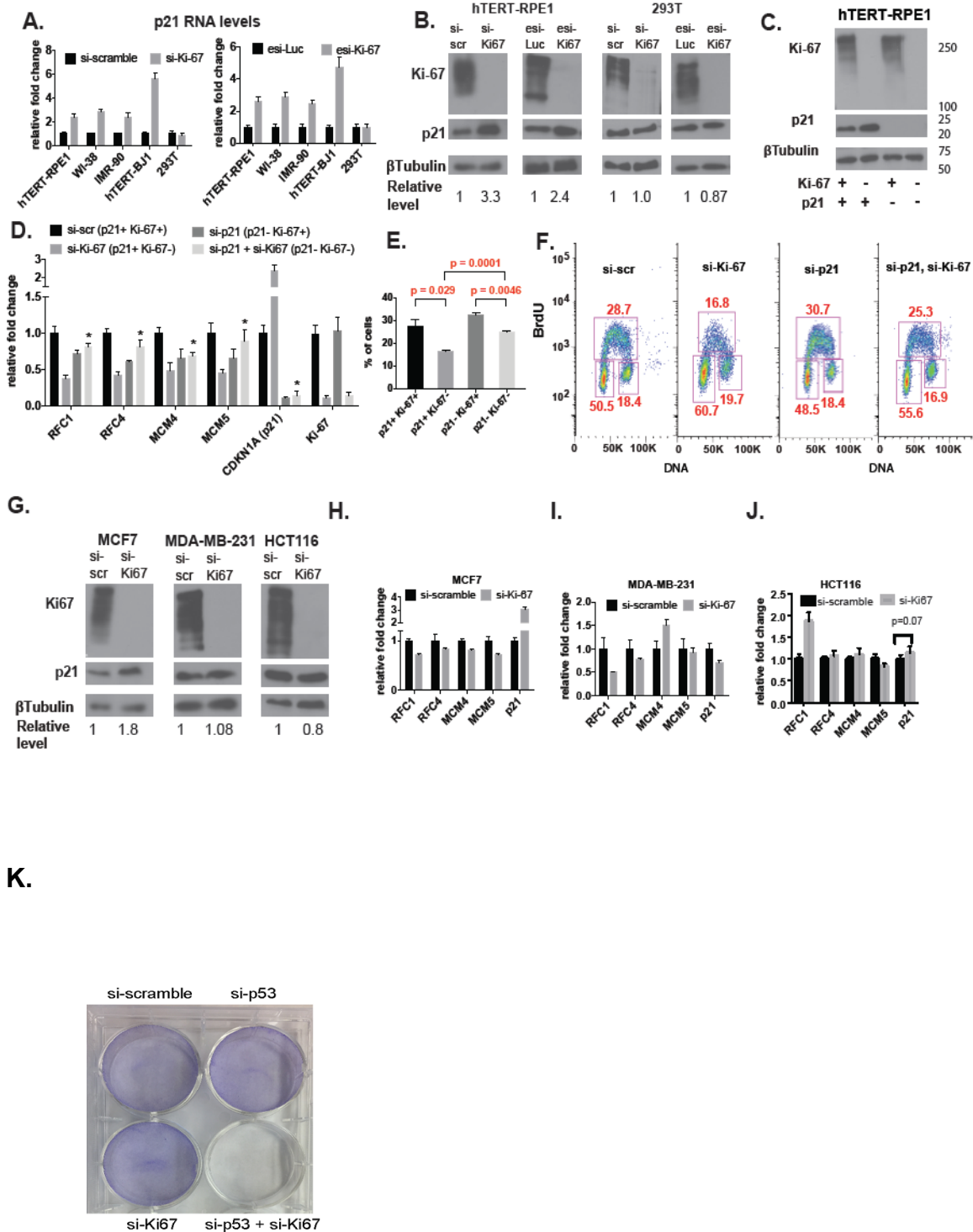
Figure 3.10: Model. In "Ki-67 sensitive" cells, depletion of Ki67 leads to p21 induction. The elevated p21 levels are predicted to downregulate the Rb/E2F and DREAM target G1/S cell cycle genes and inhibit DNA synthesis by binding to PCNA. Together, these effects delay S phase entry

Figure 3.10: Model
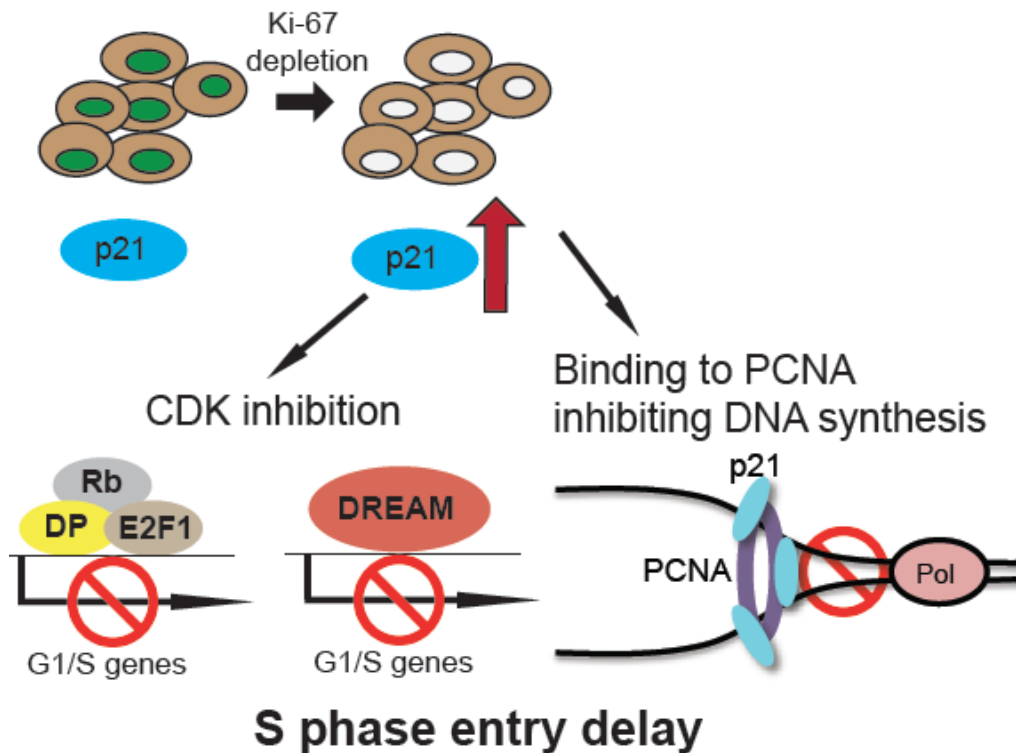
3.4: Discussion

3.4.1: Cell-type specific responses to Ki-67 depletion

Our studies show that Ki-67 expression is important for normal S phase progression in primary human foreskin fibroblasts, non-transformed fibroblast lines (WI-38 and IMR90), hTERT-immortalized BJ fibroblasts, and hTERT-immortalized RPE1 cells (Bodnar *et al.*, 1998), a human female retinal pigment epithelial cell line with a diploid karyotype (Ma *et al.*, 2015). In contrast, in cancer-derived 293T, U2OS and HeLa cells, depletion of Ki-67 did not cause defects in cell proliferation. Therefore, we conclude that Ki-67 is required for normal cell cycle progression in some but not all cell lines. Our data distinguish two types of responses to depletion of Ki-67 in human cells, depending on whether cells are able to mount a p21-dependent checkpoint.

hTERT-BJ fibroblasts were sensitive to Ki-67 depletion in our assays; however, a previous study indicated that shRNA-mediated Ki-67 depletion did not affect hTERT-BJ cell cycle re-entry after starvation (Sobecki *et al.*, 2016). We note that two other assays used in the previous study are insensitive to the cell cycle progression delays that we observe upon Ki-67 depletion. First, one-dimensional flow cytometry of propidium iodide-stained asynchronous populations cannot detect the S phase delays we detect in BrdU labeling experiments; second, a 3 hour EdU pulse is too long to capture the 2-hour S phase entry delay. Together, our data indicate that the effects of Ki-67 on S phase progression are transient in sensitive cell types and therefore best observed using short pulses of labeled deoxynucleotides.

3.4.2: Characteristics of checkpoint activation caused by Ki-67 depletion

Meta-analyses of our RNAseq data showed that Ki-67 depletion in hTERT-RPE1 cells resulted in frequent repression of Rb/E2F-regulated, G1/S expressed genes. However, depletion of the Rb checkpoint protein only partially relieved transcriptional repression and did not restore normal percentages of S phase cells, indicating that additional factors were responsible for the altered cell cycle profile in Ki-67 depleted cells.

A strong candidate for such a factor is the DREAM complex, which represses G1/S-expressed cell cycle genes in a p21-dependent manner(Fischer *et al.*, 2016; Benson *et al.*, 2014). We noticed frequent downregulation of DREAM complex targets in Ki-67-depleted cells, which lead us to test whether sensitivity to Ki-67 depletion was also p21-dependent. Notably, both the transcriptional alterations and cell cycle perturbations caused by Ki-67 depletion were partially relieved by simultaneous depletion of p21. Importantly, cell lines that induce p21 upon Ki-67 depletion are those that inhibit transcription of DNA replication genes and delay entry into S-phase. Thus, this study implicates a p21-dependent checkpoint in cells sensitive to Ki-67 depletion.

A recent study shows that PD0332991, a small molecule CDK4/CDK6 inhibitor (CDKi), depletes Ki-67 protein levels in some but not all cell lines (Sobecki *et al.*, 2017). In "CDKi-sensitive" cells, this compound causes G1 cell cycle arrest via an Rb-mediated checkpoint, inhibiting Ki-67 and cyclin A gene transcription while proteasome-mediated degradation destroys existing Ki-67 protein molecules. CDKi-sensitivity appears similar to many of the responses we

observe upon Ki-67 depletion, and CDKi-sensitive cells include IMR90 and primary fibroblasts that we found to be "Ki-67 sensitive". MCF7 breast adenocarcinoma cells are also CDKi-sensitive (Sobecki *et al.*, 2017), and we find that upon Ki-67 depletion MCF7 cells induce p21 and down-regulate DNA replication genes. In contrast, HeLa and U2OS cells are not sensitive to either CDKi or Ki-67 depletion. Thus, depletion of Ki-67 via CDKi treatment (Sobecki *et al.*, 2017) or via siRNA (this work) often leads to similar outcomes.

However, there is a counterexample to these correlations. CDKi treatment blocks S phase entry and depletes Ki-67 in MDA-MB-231 breast adenocarcinoma cells (Sobecki *et al.*, 2017). In contrast, upon Ki-67 depletion, MDA-MB-231 cells did not display either p21 induction or transcriptional down-regulation of S phase genes. Therefore, proteasome-mediated degradation of Ki-67 via CDK4/6 inhibition is not equivalent to siRNA-mediated Ki67 depletion in all cell types. We hypothesize that a key difference is related to induction of p21 in "Ki-67-sensitive" cell lines. p21 contributes to G1/S arrest via multiple mechanisms. As a CDK inhibitor(Xiong *et al.*, 1993; Gartel and Radhakrishnan, 2005), p21 blocks CDK-mediated Rb phosphorylation thereby inhibiting E2F-driven transcription(Brugarolas *et al.*, 1999). Likewise, it maintains activity of the transcriptionally repressive DREAM complex which contain Rb-related p107/p130 "pocket protein" subunits(Fischer *et al.*, 2016; Sadasivam and DeCaprio, 2013). p21 also directly interacts with PCNA and directly inhibits DNA synthesis (Waga and Stillman, 1998). Therefore, the lack of p21 induction in MDA-MD-231 cells may be the key factor explaining the lack of "Ki-67 sensitivity"

in this cell line. Future experiments will be required to determine whether the activation of the DREAM complex or direct inhibition of DNA synthesis machinery is more important for the "Ki-67-sensitive" phenotype associated with p21 induction.

Regarding the defect in p21 induction in MDA-MB-231 cells, we note that they express a gain-of-function R280K allele, which dominantly blocks p21 induction (Junk *et al.*, 2008). Thus, p53 status is likely a critical aspect of the different cell cycle responses to Ki-67 depletion in many cell lines. However, sensitivity to Ki-67 depletion cannot always be predicted strictly by p53 status. For example, HCT116 cells express wild-type p53 (Junk *et al.*, 2008) but are not sensitive to the CDKi PD0332991 (Sobecki *et al.*, 2017), or to Ki-67 depletion (Fig. 9J). Because Ki-67 expression predicts the differential response of different cell lines to CDKi treatment during xenograft tumor formation (Sobecki *et al.*, 2017), understanding how different checkpoint mutations alter Ki-67 expression and sensitivity to its depletion are important goals for developing stratified approaches to cancer therapies.

Table 3.1: The summary of similarities and differences between CDKi sensitivity and Ki-67 sensitivity

Cell line	Rb status	p53 status	p21 induction	CDKi sensitivity	Ki-67 sensitivity
IMR-90	+	+	+	+	+
MCF-7	+	+	+	+	+
HDF	+	+	+	+	+
hTERT-RPE1	+	+	+	unknown	+
MDA-MB-231	+	-	-	+	-
MDA-MB-436	-	-	unknown	-	unknown
HCT116	+	+	-	-	-
HeLa	low	+	-	-	-
U2OS	-	+	-	-	-

3.5: Material and Methods

3.5.1: Flow cytometry

Cells were pulsed labeled with 50mM bromodexoyuridine (BrdU) for indicated time. Cells were then washed twice with PBS, fixed in 70% ethanol at $4^{O}C$ for 1 hour. Post-fixed cells were denatured in 2N HCl/0.5% Triton-X for 30 minutes. After denaturation, cells were washed once in 0.1M sodium tetraborate for 2 minutes and once in PBS/1%BSA. After that, cells were resuspended in anti-BrdU antibody for 1hr followed by three washes with 0.5% Tween 20/1%BSA/PBS. The cells were incubated with secondary antibody for 30 minutes and counterstained with propidium iodide at the concentration of 50 mg/ml in PBS and acquired on a LSR II (BD Biosciences). The data was analyzed with FlowJo software (TreeStar, Ashland,OR)

3.5.2: RNA isolation and real time quantitative PCR

Total RNA from cells 72 hours post transfection was isolated using Trizol (Invitrogen 15596026) following manufacturer's instructions and purified using the RNeasy kit (Qiagen 74104). One microgram of RNA was subjected to reverse transcription with SuperScript II Reverse Transcriptase (Invitrogen 18064014). qPCR reactions were performed on an Applied Biosystem StepOnePlus machine (Life Technologies) using FAST SYBR mix (KAPA Biosystem). The program used is as follows: hold 98°C for 30 s, followed by 40 cycles of 95°C for 10 s and 60°C for 30 s. All the signals were normalized with beta-actin as indicated in the figure legends and the $2^{-\Delta\Delta Ct}$ method was used for

quantification (Life technologies). Primer sequences are designed by Primer3Plus software (Untergasser *et al.*, 2012; Andreas Untergasser et al.,2012).

Table 3.2: Primers for q-PCR

This table shows the forward and reverse primers used for q-PCR to particular targets used in Chapter III.

Target	Forward Primer	Reverse Primer
MCM4	TGACCGTTACCCTGACTCAA	CACACTTGGCACTGGAAGAA
MCM5	CTGGGGGAGTACTGGATTGA	ATGACCTGGATGTCCTGGAG
RFC1	GACACAGAAGCGGGAGAAAC	TGATGACTTGGAATGTTGCTG
RFC4	GACCACCTGGAACTGGAAAA	CTGAGCGACTTCCTGACACA
p21	CAGCAGAGGAAGACCATGTG	GGCGTTTGGAGTGGTAGAAA
Ki-67	TGCTCTGGGTTACCTGGTCT	GGCTTCTCCCCTTTTGAGAG
PIPB	TCTCCGAACGCAACATGAAG	ACACCTTGACGGTGACTTTGG

3.5.3:RNAseq: sample preparation and analysis

RNA was isolated as described above. Libraries from two replicates were constructed in a strand-specific manner via dUTP method by BGI and sequenced using Illumina-HiSeq 2000/2500 platform (BGI) as single-end 50-base reads. 29M and 31 M mapped reads were obtained from two controls, 28M and 29M were from two Ki67 knockdown replicates. Reads were aligned to the human reference genome (hg19) using Tophat 2.0.14. (Trapnell *et al.*, 2009; Kim *et al.*, 2013). Differential expression analysis was determined by cufflinks 2.2.1 (Trapnell *et al.*, 2010). In addition, the reactome analyses were performed using Bioconductor package ChIPpeakAnno (version 3.2.0) (Zhu *et al.*, 2010; Zhu, 2013). Genes that showed differential expression with p value < 0.05 between control and Ki-67 depletion samples were selected for the reactome analysis.

3.5.4: Accession Numbers

The data discussed in this publication have been deposited in NCBI's Sequence Read Archive (SRA, http://www.ncbi.nlm.nih.gov/sra/) and are accessible through SRA Series accession number SRR4252548, SRR5535471, SRR5535778, and SRR5535934.

3.5.5: Antibodies

mouse anti-p21 antibody (Abcam ab109520) at 1:1000 for immunoblotting

mouse anti-Rb antibody(4H1) cell signaling 9309 at 1:1000 for immunoblotting

CHAPTER IV: DISCUSSION

4.1: Scientific questions addressed by this dissertation

The mechanism by which perinucleolar heterochromatin attaches to the nucleolar periphery are not well understood, and even less is known if any NAD associations are sensitive to the G1/S checkpoint status of the cells examined.

Previous work from the Kaufman group demonstrates that Ki-67 promotes localization of alpha-satellite 17 to the nucleolus(Matheson and Kaufman, 2017a; Matheson and Kaufman, 2015). This leads to the question of whether Ki-67 targets other genomic regions to the nucleolus. Inactive X chromosome represents a premier example of facultative heterochromatin formation and maintenance. In unsynchronized female hTERT-RPE1 cells, depletion of Ki-67 significantly reduces the association of Xi to the nucleolus. This is accompanied by increased transcription of Cot-1 hybridizing DNA repetitive elements and reduced H3K27me3 and H4K20me1 enrichment on the Xi in a subset of cells in which the Xi was localized away from the nuclear periphery. In contrast to hTERT-RPE1 cells, no alteration of perinucleolar Xi localization or erosion of heterochromatin features is observed in 293T cells. Therefore, the impaired maintenance of epigenetic features in hTERT-RPE1 cells on non-laminar Xi chromosomes could indicate the laminar associations protect from this type of

erosion. Alternatively, these observations could indicate that movement away from the lamina is required for downstream alteration.

In MEF cells, perinucleolar localization of Xi is S phase dependent(Zhang *et al.*, 2007). To study the dynamics of the association, I synchronized the hTERT-RPE1 cells at the G/S transition and tracked the Xi –nucleolus association through the S phase progression. In the Ki-67 depleted cells, the frequency of Xi-nucleolar association peaks later than the control cells. I found a ~ 2hrs delay of S phase entry which correlates with the delay of interaction peak.

Although Ki-67 expression is tightly correlated to proliferation, its requirement for cell proliferation has been questioned. I applied two-dimensional fluorescence –activated cell sorting (FACS) analysis to examine the cell cycle in hTERT-RPE1 cells. 15 minutes pulse of labeled deoxynucleotides is sensitive to detect changes of proportion of S phase cells. In hTERT-RPE1 cells, depletion of Ki-67 indeed reduced the proportion of cells in S phase.

To understand the mechanism of regulation, I applied RNA-seq analysis of control and Ki-67 depleted hTERT-RPE1 cells. I observed coordinated downregulation of DNA replication genes. I further analyzed Ki-67 contribution to cell cycle on multiple non-immortalized and tumor derived cell lines. My data distinguished two types of response to Ki-67 depletion in human cells, depending on whether cells are able to mount a p21 dependent checkpoint. This discovery yields many more questions: With respect to the cell cycle, do Ki-67 depleted cells accumulate DNA damage? In addition to G1/S checkpoint, is G2/M checkpoint impaired? With respect to the heterochromatin compartment, how are

NAD-nucleolus interactions governed by cell cycle regulation? In the following chapter I will discuss experiments that may answer these questions and future studies that build upon these results.

4.2: How does Ki-67 promote NADs organization?

Ki-67 affects nucleolar localization of heterochromatin in multiple ways. The first of these appears to be restricted to G1/S checkpoint-proficient cells. By regulating the S phase progression in p21 checkpoint proficient cells, Ki-67 affects the S phase dependent association between Xi and the nucleolus. Paternal Kcnq locus visits the nucleolus during S phase in placental cell (Mohammad *et al.*, 2008). It is likely that Ki-67 can also influence its localization in the same manner as Xi.

Not all heterochromatin effects of Ki-67 depletion are dependent on cell cycle checkpoints. For example, depletion of Ki-67 in HeLa cells does not alter cell cycle, but the nucleolar association frequency of alpha satellite DNA was significantly reduced(Matheson and Kaufman, 2017a). Therefore, Ki-67 promotes NAD localization even in checkpoint-deficient cells. How does Ki-67 promote these interactions? There are several possibilities that are not mutually exclusive.

First, Ki-67 directly interacts with other NADs targeting elements. CAF-1 p150, the largest subunit of histone chaperones complex Chromatin Assembly Factor-1 (CAF-1) is one candidate. CAF-1 p150 is required for nucleolar macromolecular association(Smith *et al.*, 2014). In HeLa cells, CAF-1 p150 depletion disrupts localization of multiple nucleolar proteins and decreases the

association of NADs, including α-satellite DNA, D4Z4 macrosatellites, and the array of 5S rDNA(Smith *et al.*, 2014). Proteomics analysis of CAF-1 p150 detects Ki-67 as an interaction partner. During the interphase, a subset of CAF-1 p150 co-localize with Ki-67 and regulates Ki-67 localization(Smith *et al.*, 2014; Matheson and Kaufman, 2017a). These results indicate that Ki-67 and p150 may act in the same pathway to facilitate NAD targeting. To test this hypothesis, future studies should examine the association between alpha-satellite and the nucleolus in the Ki-67 mutant cell lacking p150 binding motif.

In addition, Ki-67 can interact with chromatin features of NADs. NADs are enriched in the repressive histone modifications H3K9me and H3K27me3. In the absence of Ki-67, H3K9Me3 and H4K20Me3 become less focally clustered(Sobecki *et al.*, 2016). Methylation of H3K9 is recognized by HP1(Jacobs and Sepideh, 2002; Nielsen *et al.*, 2002). Ki-67 directly binds HP1 with high affinity(Scholzen *et al.*, 2002). In HeLa cells, Ki-67 partly overlaps with HP1 and ectopic expression of HP1 relocalizes endogenous Ki-67 to the sites of high HP1 concentration. It suggests a model which Ki-67 maintains the repressive histone modifications of HP1-bound heterochromatin and attach them to the nucleolus. Depletion of Ki-67 may interfere with heterochromatin silencing marks within the NADs, resulting in mislocalization of NADs loci away from the nucleolus. Thus, future studies should map the domains on Ki-67 which are required for HP1 interaction or H3K9me3 maintenance. A series of cell lines with endogenous Ki-67 domain mutations can be generated using CRISPR/cas9

genome editing technology and NADs localization should be examined in these cell lines.

The LR domain of Ki-67 can bind to DNA (Takagi *et al.*, 1999; Scholzen *et al.*, 2002) and Ki-67 may recognize primary of sequences of DNA. There has been no systematic analysis of NAD relocalization in repsonse to Ki-67 depletion, so it is not known if there are unforessen specificities regarding this activity. It will be particularly interesting to know if any NAD associations are sensitive to the G1/S checkpoint status of the cells examined. The lack of ChIP grade antibodies for Ki-67 did not allow a ChIP-based approach to map its binding sites. A TAG-proteogenomic approach provide unbiased information on assoication with specific histone variants and modifications as well as the genomic binding regions of Repo-Man(de Castro *et al.*, 2017). Similarly, GST-tagged, full length Ki-67 or GST alone can be used as bait to isolate HeLa nucleosomes with high affinity for Ki-67. After elution, the chromatin bound fraction can be used either to separate the histone bands for mass spectrometry analysis or to extract DNA for sequencing. An tag such as FLAG or v5 can be inserted into the endogenous loci of Ki-67 by CRISPR/cas9 genome editing technology. Through these experiments whether Ki-67 prefers to target specific sequences or sequences with speficic chromatin features to nucleolus can be identified.

4.3: Further investigation into NADs organization during differentiation and cell cycle

Nuclear reorganization regulates developmental timing and gene expression. During development, the repressive compartments often change

form and composition(Almouzni and Probst, 2011; Peric-Hupkes *et al.*, 2010). The subsequent differentiation of mouse embryonic stem cells (mESC) via lineage-committed neural precursor cells (NPC) into terminally differentiated astrocytes (AC) represents a good system for studying NAD organization during development(Peric-Hupkes *et al.*, 2010). In this system, future studies should compare NADs identified via deep sequencing of nucleoli purified from mESC, NPC and AC.

Another system is to compare olfactory receptors between basal and sustentacular cells from the main olfactory epithelium and olfactory sensory neuron (OSNs). Olfactory receptor genes were considered to be NADs by deep sequencing of purified nucleoli from somatic cells(Koningsbruggen *et al.*, 2010; Németh *et al.*, 2010; Dillinger *et al.*, 2016). As the neurons develop, one of 2800 receptor genes is expressed whereas the remaining receptors are repressed and clustered with one another into heterochromatin loci(Imai *et al.*, 2010). It will be interesting to investigate whether repressed genes or expressed genes associate with different nuclear compartments during neuron development.

Although the FISH-microscope experiments have identified two S phase related NADs, an unbiased genome-wide analysis of NADs dynamics during the cell cycle has not reported. Two methods can address this question from population level and single cell level.

The nucleolus can be purified from synchronized cell population. Beginning in telophase, nucleoli reforms around individual NORs and form multiple small nucleoli. Nucleolar fusion then occurs, resulting in the formation of

larger mature nucleoli in late G1 phase (Pederson, 2011; McStay, 2016). So far no reports show successful biochemical purification of immature nucleoli, thus purifying nucleoli from S and G2 phase is a major focus.

NADs are heterogeneous in their chromatin compositions, regulatory functions, and the way they interact with the nucleolus. Therefore, single-cell mapping may reveal the NAD-nucleolus interactions that cannot be easily inferred from population-averaged maps. Combinations of Dam-Lamin B1 and ^{m6}A tracer enable the visualization of LAD-NL interactions in individual cell(Kind *et al.*, 2013b). However, major difficulties in performing nucleolar DamID arise due to the structure of the nucleolus. Unlike the nucleus, the nucleolus is a nonmembrane-bound subnuclear organelle. Nucleolus continuously exchanges macromolecules with the nucleoplasm. Imaging nucleolar protein-fluorescent protein fusions in live cells revealed that most nucleolar proteins shuttle between the nucleolus and the nucleoplasm at fast pace(Pederson and Tsai, 2009; Mangan *et al.*, 2017). For a DamID fusion protein, the best candidate protein should possess the following characteristics. First, the protein should have a relatively long retention time in the nucleolus. Second, the protein should reside in the granular component (GC) that is the outer regions of the nucleolus. Nucleophosmin/B23 is one candidate. Nucleophosmin/B23 is abundant in the GC of the nucleolus(Sirri *et al.*, 2008). When S125, the CDK2 phosphorylation site is mutated, S125A-B23 is less mobile and has a higher affinity for the nucleolus (Negi and Olson, 2006). Since nucleolus itself is a highly dynamic structure, it is

possible that NADs have a relatively higher motility than LADs on average during the interphase.

4.4: Why association occurs specifically in S-phase?

During S phase, proper chromatin states are re-established and epigenetic modifications are transmitted to the daughter strands. Intuitively, repressive perinucleolar localization may facilitate de novo incorporation of repressive chromatin factors. But other nuclear functions may be related to this process.

First is DNA replication timing. NADs show a strong overlap with domains replicating late during S phase. However, it is not clear whether it reflects the heterochromatic nature of NADs or whether nucleolus interactions can at least in part dictate DNA replication timing. For example, late replicating DNA on large chromosomes tends to localize to the periphery(Ragoczy *et al.*, 2014). Future studies should test whether embedding Xi into larger late replication domains would affect localization of integration sites in HT1080 male cells.

Another possible function is DNA repair. Double strand breaks (DSBs) arise spontaneously during DNA replication. In mammalian cells, two repair pathways are responsible for DSB: the error prone non-homologous end joining pathway (NHEJ) and error free homologous recombination(HR) (Ferguson *et al.*, 2000; Kolodner *et al.*, 2002). HR occurs mainly in S phase when a sister chromatid that can be used as a template for repair is present(Branzei and Foiani, 2008) . During the G2 phase, both processes can operate. Although HR is a main pathway in repairing breaks within heterochromatin (Geuting *et al.*, 2013;

Kakarougkas *et al.*, 2013), artificial tethering a DSB site to the NL delays DNA damage response and causes a shift from HR repair to NHEJ(Lemaître *et al.*, 2014). Whether S phase dependent nucleolar localization would influence DNA damage response activation and choice of repair pathway is not studied yet. To answer this question, future studies should induce the DSB on Xi and follow the repair process when it is tethered to NL or nucleolus. The autosomes bearing the Xic transgenes associate with nucleolus in mid-late S phase as endogenous Xi did in HT1080 cells(Kelsey *et al.*, 2015). Thus, synchronized S phase cells can enrich nucleolus associated Xi. If a LacO array is integrated into the Xic transgenes, expression of GFP-Emerin-LacI can reposition Xi transgene to nuclear periphery. To create spatially defined DSB, I-SceI locus can be integrated to the LacO-Xic and express I-SceI endonuclease under the control of a doxycycline-induced promoter(Lemaître *et al.*, 2014). The impact of nuclear compartments on DNA damage response efficiency can be assessed by comparing the kinetics of induction of γH2AX and 53BP1 via immunostaining. To evaluate which repair pathway it chooses, recruitment of Ku80 and XRCC4 is to mark NHEJ(Leiber, 2010; Britton *et al.*, 2013) and recruitment of BRCA1, Rad51 and Rad54 is to mark HR(Chen *et al.*, 2008; Heyer *et al.*, 2010). Furthermore, in order to investigate the contribution of NHEJ and HR in repairing the I-SceI breaks at the nucleolus, future studies should deplete NHEJ or HR and assess the degree of persistent breaks by γH2AX staining

4.5: To investigate how p53 and Ki-67 double depletion leads to lethality

Co-depletion of p21 suppressed the transcriptional and cell cycle defects in diploid hTERT-RPE1 cells upon Ki-67 depletion. As p21 is a downstream effector of the tumor-suppressor p53(Fischer *et al.*, 2016), I hypothesized that suppression of p53 should also suppress the transcriptional downregulation and reduced S population in Ki-67 depleted hTERT-RPE1 cells as p21 did. Surprisingly, simultaneous depletion of p53 and Ki-67 results severe cell death as observed from crystal violet staining (Fig 3.9K). p53 depletion alone leads to modest growth deficiency in hTERT-RPE1 cells. These data suggest that p53 has p21-independent functions that are essential for viability in the absence of Ki-67. The master tumor suppressor p53 frequently mutated in human cancers (Petitjean *et al.*, 2007). Whereas p53 mutations are not directly druggable(Reinhardt *et al.*, 2009), its synthetic lethal partners may implicate direct drug targets. Therefore, discovering of the mechanisms that govern the p53-Ki-67 synthetic lethality has the potential therapeutic implications. I hypothesize that Ki-67 depleted cells represent a particularly sensitive context in which the importance of p53 is exacerbated.

First, loss of p53, if in conjunction with ATR/ATM suppression, would continue proliferation of damaged cells that finally confers apoptosis(Reinhardt *et al.*, 2007). Future studies should analyze whether DNA damage checkpoints are intact in Ki-67 depleted cells. In both Ki-67 wild type or Ki-67 depleted cells, upon commonly used DNA-damaging agents cisplatin, doxorubicin and camptothecin, γH2AX phosphorylation, 53BP1 foci and cleaved caspase-3 can be visualized by

immunofluorescence(Lukas *et al.*, 2011b; Lukas *et al.*, 2011a; Gurpinar and Vousden, 2015) . Phospho-Chk1 ad phospho-Chk2 can be quantified by immunoblotting(Gurpinar and Vousden, 2015). Cells with co-depletion of MAPKAP Kinase-2 (MK2) and p53 lost intra-S and G2/M checkpoint following treatment of DNA damage reagent. Thus, the phosphorylation status of MK2 will also be examined(Reinhardt *et al.*, 2007).

In addition, loss of the G2/M checkpoint in the context of p53-deficiency sensitizes cells to various forms of DNA damage(Bunz *et al.*, 1998). Therefore, future studies will determine whether Ki-67 depleted cell has a functional G2/M checkpoint. Under genotoxic stress such as cisplatin or irradiation that activates G2/M checkpoint, the progression of Ki-67 depleted cells into M phase can be monitored by the proportion of mitotic cells. It can be performed by FACS analysis of propidium iodide-stained cells. H3 pSer-10 or pSer-28 level is another mitotic index that can be quantified by immunoblotting(Johansen and Johansen, 2006; Goto *et al.*, 1999).

Third, recent studies have shown that p53 null but not p21 null cells are deficient in resolving DNA topological conflicts between DNA replication and transcription(Yeo *et al.*, 2016). It renders p53 deficient cells sensitive to topoisomerase II inhibitor. Depletion of Ki-67 results in increased sensitivity to a topoisomerase II inhibitor doxorubicin (Cidado *et al.*, 2016). It is possible that Ki-67 and p53 double knockdown produces additive and unresolved replication stress that leads to cell death. Accumulation of TOP2A-DNA complex is an indicator of DNA topological states. It can be detected by dot-plot from CsCl

gradient fractionated cell extract(Yeo *et al.*, 2016). Therefore, future studies will focus to investigate the formation of TOP2A-DNA complex in Ki-67 depleted cells. In addition, the domains of Ki-67 that is synthetically lethal with p53 depletion can be mapped and the interactors involved in this process can be found out.

4.6: Whether Ki-67 depletion induces DNA damage and when does the DNA damage occur during the cell cycle?

Induction of p21 and delayed S phase entry in hTERT-RPE1 cells indicate the cells impose a response program to repair damaged DNA or to prevent further proliferation of damaged cells. However, one study did not detect accumulation of 53BP1 foci in Ki-67 depleted HeLa cells(Booth *et al.*, 2014). It may be due to the blunted DNA damage response in highly transformed cells since we did not detect alterations of cell cycle and transcription in virally transformed HeLa cell line. In addition, previous study focused on the mitotic cells, it is possible that at the time point they investigated, cells that underwent DNA damage do not have enough reaction time to form damage foci but the lesion will transferred to daughter cells where they become sequestered in 53BP1 nuclear bodies(Lukas *et al.*, 2011a). To address this question, cells throughout the cell cycle would be immunostained for γH2AX phosphorylation and 53BP1 foci(Lukas *et al.*, 2011b; Lukas *et al.*, 2011a; Gurpinar and Vousden, 2015). Chk1 and Chk2 checkpoint kinase phosphorylation would be quantified by immunoblotting (Gurpinar and Vousden, 2015).

As to when this damage occurs, there are several possibilities. During mitosis, Ki-67's large size and high density of positive charge rendered it as a

surfactant preventing chromosomes from collapsing into a single chromatin mass(Cuylen *et al.*, 2016) Loss of spatial separation between mitotic chromosomes impair spindle assembly and chromosome alignment during the metaphase. In addition, although Ki-67 depleted cells can continue to divide after mitotic defects, the subsequent second division becomes more problematic(Booth *et al.*, 2014). During interphase, Ki-67 promotes a subset of NAD loci to nucleolar periphery(Booth *et al.*, 2014; Matheson and Kaufman, 2017a). NADs repositioned away from repressive nucleoli periphery are more likely undergoing heterochromatin erosion. Determining the precise phase at which damage occurs will be difficult, as damage from preceding phase can mount during consecutive cell cycle(S. Pedersen *et al.*, 2016)

Appendix A: CAF-1 p150 does not organize mitotic chromosome periphery in mouse cells

Introduction

Mitotic chromatin must reorganize and condense for segregation. A proteinaceous sheath referred as perichromosomal layer (PCL) coats mitotic chromosomes(Hernandez-verdun and Gautier, 1994; Van Hooser *et al.*, 2005). Immunocytochemistry revealed that this structure associates with chromosome surface that consists of several proteins, including nucleolar protein nucleolin, fibrillarin, nucleophosmin and Ki-67, nuclear matrix proteins Ku proteins and ribonucleoproteins (RNPs) (Hernandez-verdun and Gautier, 1994; Van Hooser *et al.*, 2005). The persistent association of proteins on PCL from prophase till telophase implied that they are involved in determining the spatial relationship and interaction between chromosome during mitosis and early G1. Investigating the mechanism driving the movement of these proteins from the nucleus to the chromosome periphery and back to in the reforming nucleus will link mitotic chromosome structure to interphase genome organization.

Ki-67 is one of the earliest proteins to bind the perichromosomal layer in mitosis(Endl and Gerdes, 2000; Saiwaki *et al.*, 2005). On the onset of nucleoli disassembly in prophase, Ki-67 relocalizes to the PCL and accumulates on PCL until telophase(Takagi *et al.*, 2014). During mitosis, acute depletion of Ki-67 prevents all nucleolar proteins tested accumulating on the PCL in HeLa

cells(Booth *et al.*, 2014). Impaired PCL assembly results in deficient nucleologenesis and uneven distribution of nucleolar proteins in the daughter cells(Booth *et al.*, 2014).

CAF-1 p150, the largest subunit of histone chaperone Chromatin Assembly Factor (CAF-1) regulate Ki-67 nucleolar localization during interphase and normal levels of Ki-67 accumulation on the PCL during mitosis in HeLa cells(Smith *et al.*, 2014). This activity was mapped to the sumoylation interacting motif (SIM) within p150, which is dispensable for chromatin assembly but required for the Ki-67 localization and the association of nucleolus association domains (NADs) with nucleolus during interphase(Smith *et al.*, 2014).

CAF-1 p150 and Ki-67 are highly conserved between human and mouse(Kumar *et al.*, 2016). We began exploring the CAF-1 p150/Ki-67 hierarchy in several mouse cell types

Results

Ki-67 localization throughout the cell cycle in mouse cell culture

In human cells, Ki-67 has three distinct nuclear localization patterns, which appear at different stages of cell cycle. In the early G1 phase, Ki-67 localizes to hundreds of distinct foci, which colocalize with heterochromatic satellite repeats. (Bridger *et al.*, 1998). Ki-67 relocalized to the reformed nucleoli during the interphase(Verheijen *et al.*, 1989b; Kill, 1996; Traut *et al.*, 2002; Cheutin *et al.*, 2003). Third, Ki-67 localizes to the PCL during mitosis(Endl and Gerdes, 2000; Saiwaki *et al.*, 2005; Booth *et al.*, 2014). Via immunofluorescence, I first

examined Ki-67 localization in mouse embryonic stem cells (mESCs) E14 cells. In the interphase, I found that Ki-67 is distributed among the whole nucleus (Fig A1 Top Right). I did not observed predominant nucleolus localization. During the mitosis, Ki-67 robustly associated with the PCL (Fig A1, Top Left). I observed the similar Ki-67 localization pattern in NIH3T3 cells (Fig A1 Bottom).

Figure A.1: Ki-67 's localization throughout the cell cycle in mESC E14 and NIH3T3 cells

mESC E14(Top) or NIH 3T3 (bottom) were subjected to immunofluorescence using antibodies recognizing Ki-67 (Green) and nucleophosmin (red). DAPI staining is shown to identify nuclei. Left: a mitotic nuclei. Right: an interphase nuclei. Scale bar 10 μm

Figure A.1: Ki-67 localization throughout the cell cycle in mESC E14 and NIH3T3 cells
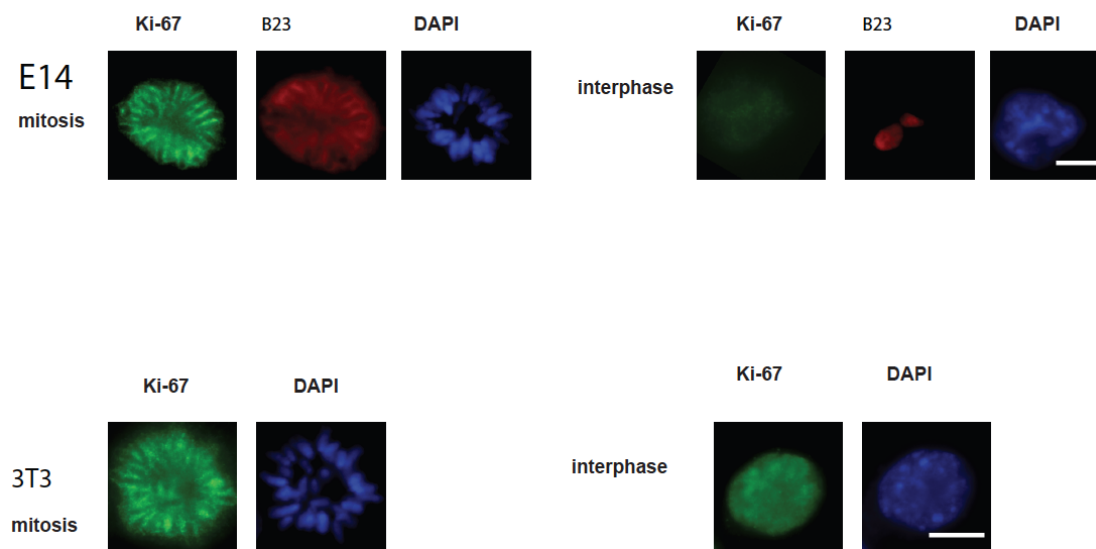
In NIH3T3 cells, Ki-67 depletion does not relocalize nucleophosmin from PCL

In the HeLa cells, Ki-67 is required from the localization of other known PCL proteins (Booth *et al.*, 2014). I next investigate whether it is true in NIH 3T3 cells. I used RNAi to deplete Ki-67 in NIH3T3 cells and determined distribution of endogenous nucleophosmin/B23 in the mitotic cells. Nucleophosmin/B23 accumulates on the PCL on both control and Ki-67 depleted cells.

Figure A.2: Depletion of Ki-67 does not dislocalize nucleophosmin on mitotic chromosomes in NIH3T3 cells

NIH3T3 cells were treated with si scramble (Top) or siRNA targeted Ki-67 (middle) for 72 hr and were subjected to immunofluorescence using antibodies recognizing Ki-67 (green) and nucleophosmin (red). DAPI staining is shown to identify nuclei. Scale bar: 10 μm

Figure A.2: Depletion of Ki-67 does not dislocalize nucleophosmin on mitotic chromosomes in NIH3T3 cells

Ki67

si_src

10 µm

B23

si_Ki67

si_
scr

si_
Ki67

250

Ki67

100

Tubulin

75

50
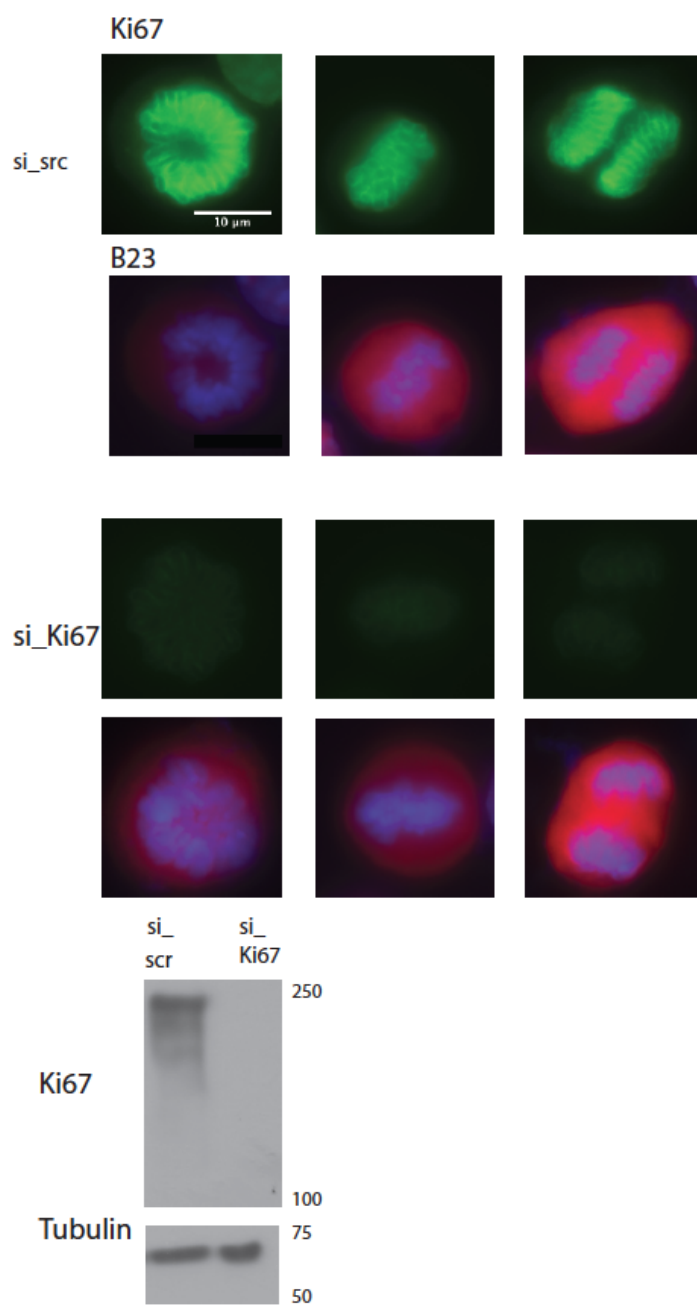
Loss of CAF-1 p150 does not impair Ki-67 localization neither in interphase nor mitosis

I then investigate whether p150 regulates Ki-67 localization in the mouse cells. In NIH 3T3 and E14 cells, I efficiently depleted p150 via synthetic siRNA (Fig A3 D,E). Because prolonged p150 depletion leads to strong inhibition of cell proliferation(Houlard *et al.*, 2006), I limited my acute depletion experiments to the first 72h after siRNA treatment when I did not observe alteration in cell growth. Upon p150 depletion, I did not observe dispersion of Ki-67 neither in the interphase nuclei nor from the PCL during the mitosis in NIH3T3 cells (Fig A3 B, C). In mESC E14 cells, p150 depletion does not alter Ki-67's accumulation on PCL (Fig A3 A). These observations reveal that mouse CAF-1 p150 did not regulate at least a subset of nucleoloar proteins localization in interphase and mitosis.

Figure A.3: Depletion of CAF-p150 does not alter Ki-67 localization neither in the interphase nor the mitosis in mESC E14 and NIH3T3 cells.

mESC E14 cells were treated with si scramble or siRNA targeted p150 for 72 hr and were subjected to immunofluorescence using antibodies recognizing Ki-67 (green) DAPI staining is shown to identify nuclei. Scale bar 10 μm

      A. E14 cells in mitosis
      B. NIH3T3 cells in mitosis
      C. NIH3T3 cells in interphase
      D. Immunoblot analysis of E14 cells treated with the indicated RNA depletion reagents
      E. Immunoblot analysis of NIH3T3 cells treated with the indicated RNA depletion reagents

Figure A.3: Depletion of CAF-1 p150 does not alter Ki-67 localization neither in the interphase nor the

mitosis in mESC E14 and NIH3T3 cells
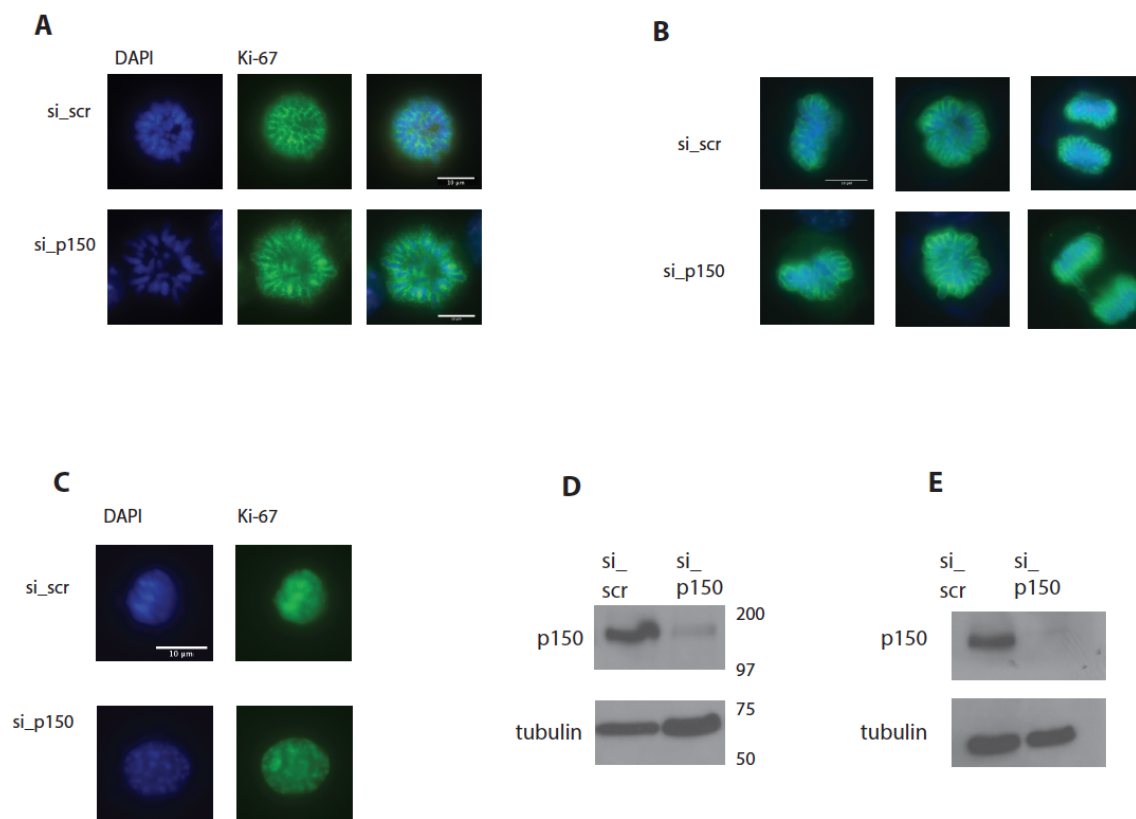
Discussion

Ki-67 has long been reported to localize in the nucleoli in mammalian cells during the interphase(Verheijen *et al.*, 1989b; Kill, 1996; Traut *et al.*, 2002; Cheutin *et al.*, 2003). In the mouse Swiss-3T3 fibroblasts, by immunostained with an affinity-purified polyclonal antibody, Ki-67 is first seen as small foci in the early G1 phase and then accumulates as large foci that overlap with nucleolar marker fibrillarin until mitosis(Starborg *et al.*, 1996). However, in both mESC E14 and NIH 3T3 cells, by using two different mouse Ki-67 antibody, I did not observe the predominant nucleolar localization of Ki-67. Instead, in both mouse cell lines, Ki-67 dispersed within the whole nucleus including nucleoplasm. A subset of it accumulates in the heterochromatin regions labeled by DAPI.

The localization pattern does not alter in either paraformaldehyde fixation or methanol/acetone fixation. The specificity of antibodies has been confirmed by Ki-67 depletion experiment. In Ki-67 depleted cells, there is a dramatic decrease in fluorescence intensity of Ki-67 staining compared with control cells, but the signal intensity of B23 does not change, suggesting that reduced Ki-67 signal intensity is due to the decreased protein levels which can be specifically detected by the antibodies rather than a reflection of overall reduced epitope accessibility affected by RNAi. The discrepancy raises the possibility that Ki-67 may have different localizations in different cell types.

Materials and Methods

Cell culture methods

mESCs lines used in this study were E14. E14 was grown under feeder-free conditions. E14 cells (a kind gift from Dr. Thomas Fazzio) was cultured in DMEM- medium (VWR 10-017-CV) with 10% fetal bovine serum (FBS, Hyclone #SH30910.03), 1% penicillin/streptomycin, 2mM L-glutamine, 1% nonessential amino acids (Corning25-025-CI) and 10^6 units /L LIF (homemade). The cells were split 1:8 every 3days.

NIH 3T3 were cultured in DMEM medium with 10% FBS, 1% penicillin/streptomycin, 5% L-glutamine. The cells were split 1:3 every 2 days

siRNA experiments

Cells were transfected with Lipofectamine RNAi MAX (Invitrogen Catalog number 13778100) following manufacturer's instructions.

For siRNA transfection, 40 nM of either scramble or siKi67 or siCAF-1 p150 was transfected into 40×10^3 cells.

The siRNA targeting mouse Ki-67 and mouse p150 is from the collection of Silencer Select Predesigned siRNAs (Thermo Fisher Scientific) and targets nucleotides 1569-1587 of the cDNA (NM_001081117.2) or nucleotides 2750-2769 of the cDNA (NM_ 013733.3),

mouse si-Ki67 sequence is as follows:

sense CGUUGAUAUCAGCAACUUUtt,

antisense AAAGUUGCUGAUAUCAACGga

mouse CAF-1 p150 sequence is as follows:

sense CAGACUGUAUGAUCAUAGAtt,

antisense CGAGUGUGGUCAUUAUCGAtt

Table A.1: Antibodies used for immunofluorescence and western blotting

Epitope	Species	Manufacturer	Catalog #	Immunofluorescence Dilution	Western Blot Dilution
CAF-1 p150	Goat	Santa Cruz	sc-10206		1:200
Nucleophosmin	Mouse	Abcam	Fc82291	1:500	
Ki-67	Rabbit	Abcam	Ab66155	1:500	1:2000

Appendix B: Loss of CAF-1 impairs heterochromatin organization and retrotransposon repression in mouse embryonic stem cells

Introduction

Totipotent cells can generate a full organism including embryonic tissues as well as extraembryonic tissues. In the mouse, only the zygote and 2-cell stage blastomere are totipotent(Ishiuchi and Torres-Padilla, 2013). Totipotent 2-cell (2C)-like cells have also shown to occur spontaneously in embryonic stem cell (ESC) cultures at rare frequency(Macfarlan *et al.*, 2012). After five divisions from blastomere, mouse embryos reach the blastocyst stage, which is initially composed of the pluripotent inner cell mass and differentiated trophectoderm(Marikawa and Alarcon, 2009). The transition from a totipotent state to a pluripotent state is accompanied by the massive chromatin rearrangement and epigenetic reprogramming, which are required for specific gene expression(Guo and Morris, 2017).

CAF-1 is a three-subunit protein complex that deposits the DNA replication-linked histone H3 variant H3.1 into chromatin during S phase(Krude, 1995; Shibahara and Stillman, 1999; Smith and Stillman, 1989) . Via interaction with HP1 and methyl-CpG binding protein MBD, CAF-1 is important in the

heterochromatin establishment and maintenance (Murzina *et al.*, 1999; Quivy *et al.*, 2004; Sarraf and Stancheva, 2004; Uchimura *et al.*, 2006; Quivy *et al.*, 2008; Houlard *et al.*, 2006). CAF-1 p150 homozygous-null embryos lack chromocenters and arrested at the 16-cell stage. In mESC cells, depletion of CAF-1 p150 displayed similar abnormal heterochromatin organization (Houlard *et al.*, 2006). These results indicate that CAF-1 plays a vital role during early embryonic development. Loss of chromocenters is a landmark feature of 2-cell stage(Probst *et al.*, 2007). Here, I investigated how CAF-1 affects totipotency.

Results

Acute depletion of CAF-1 leads loss of chromocenters and transcriptional activation of major satellite in mouse embryonic stem cells

To examine the function of CAF-1 in mouse cells, I transfected siRNA which targeted the large subunit of CAF-1 p150 in mouse embryonic stem cells (mESCs) E14. Significant knockdown was achieved by 48 hr after transfection (Fig B1 B). I did not observed strong inhibition of cell proliferation at this time point. Prolonged p150 depletion leads to cell death; therefore, I limited my acute depletion experiment to the first 48h after siRNA treatment.

The heterochromatin organization of cells lacking CAF-1 was compared with cells treated with control siRNA. In mESCs, the pericentric heterochromatin domains cluster together and form higher-order chromatin structure termed chromocenters, which are visualized as DAPI-dense foci in interphase nuclei (Guenatri *et al.*, 2004). In control mESCs treated with scramble siRNA, I

observed the well-defined DAPI-stained foci. As previous reported, these structures were not detected in p150-depleted mESCs E14 cells (Houlard *et al*., 2006)(Fig B1 A).

In mouse, pericentric and centric chromosomal regions are mainly composed of large blocks of major and minor satellite repeats. To address whether the altered chromocenter morphology leads to deficiency of transcription repression, I analyzed the transcriptional activity of pericentric regions by RT-PCR. Depletion of p150 resulted in a strong upregulation of major and minor satellite transcription (Fig B1 C).

Figure B.1: Loss of CAF-1 p150 results in severe alterations of heterochromatin organization in mESCs E14. Scale Bar 10 μm

A: Abnormal heterochromatin organization in CAF-1 p150 depleted mESCs E14. mESC E14 were transfected with si scramble or siRNA targeted mouse p150. DAPI staining is shown to identify nuclei (Blue). In the mESC transfected with si scramble, chromocenters are visualized as DAPI-dense foci. In the mESC transfected with si p150, DAPI-dense foci were barely detectable. Scale Bar 10 μm

B. RNAi knockdown efficiency for p150 was confirmed by western blot. The whole cell extracts after the siRNA transfection were analyzed with the indicated antibodies

C. RT-qPCR analysis of major and minor satellites after p150 knock down.

RT-qPCR measurements are presented as fold change relative to the scramble siRNA control after normalization. Data are mean ± std. dev. of 3 biological replicates

Figure B.1 Loss of CAF-1 p150 results in severe alterations of heterochromatin organization in mESC

E14. Scale Bar 10 μm
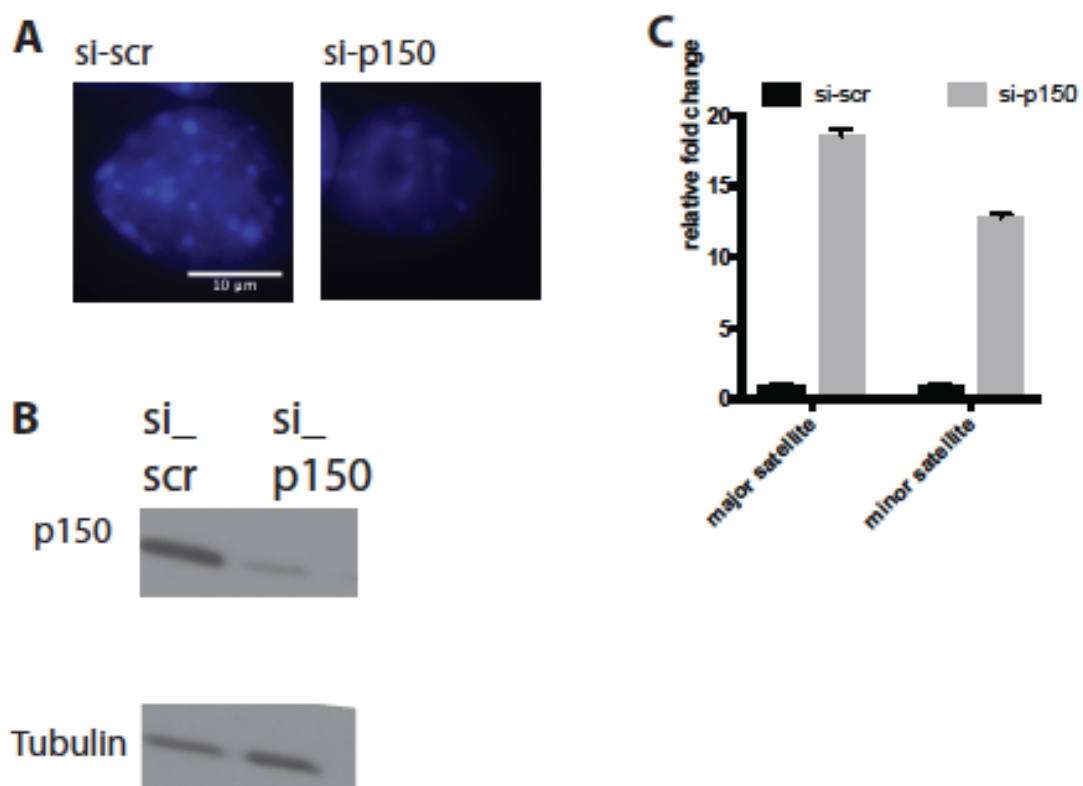
CAF-1 repressed transcription of endogenous retrotransposons in mouse embryonic stem cells

Loss of chromocenters and activation of the major satellite repeats are the hallmark features of totipotent cells(Probst *et al.*, 2007). I therefore ask if CAF-1 depletion affects the expression of 2-cell specific genes in mESCs E14 cells. RNAi for p150 indeed resulted in strong upregulation of the 2-cell specific transcripts *Zscan4*, *Eif1a,* as well as MERVL (Fig B2), a particular retrotransposon whose expression peaks in two-cell stage embryo and depressed after implantation. Other active retrotransposons such as IAP and LINE1 were not significantly unaffected (Fig B2), suggesting that p150 depletion does not affect global transcription of all repetitive elements in mESCs E14.

Figure B.2: CAF-1 p150 depletion specifically affects 2C-cell transcripts in mESC E14 cells
RT-qPCR analysis as Figure B.1

Figure B.2: CAF-1 p150 depletion specifically affects 2C-cell transcripts in mESC E14 cells
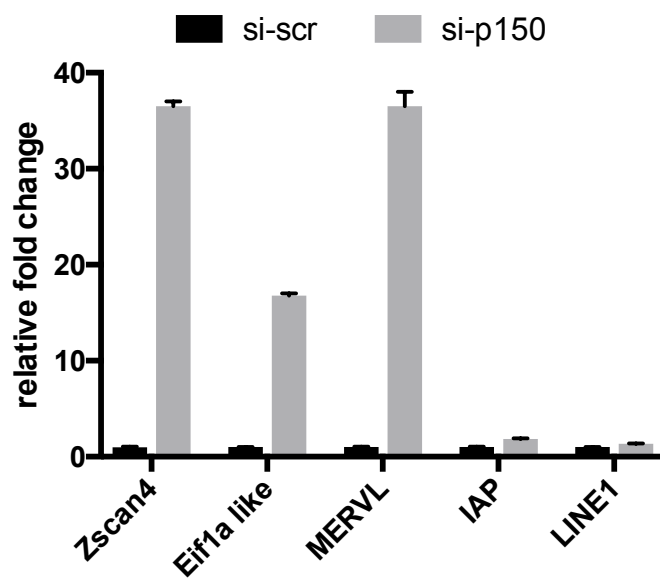
Discussion

Several lines of evidence put CAF-1 in the center of cellular plasticity. One study reported that depletion of either p150, or p60, two different subunits of CAF-1 complex significantly increased the proportion of 2C-like cells(Ishiuchi *et al.*, 2015). 2C-like cells displayed several properties of totipotent 2C cells in the ESC cultures. Depletion of CAF-1 leads to increased H3.1/H3.2 mobility and higher levels of specific 2C-like transcription (Ishiuchi *et al.*, 2015). Another study shows that by suppressing CAF-1 dependent nucleosome assembly, the efficacy of reprogramming of mouse fibroblasts to induced pluripotent stem cells (iPS cells) has increased by several orders of magnitude(Cheloufi *et al.*, 2015). The increased reprogramming efficiency results from a more accessible chromatin structure upon CAF-1 p150 depletion. It facilitates association of transcription factors at promoters of pluripotent factors and depletion of H3K9me3 at reprogramming –resistant regions. These results strongly suggest that by removal of the basic unit of the chromatin itself, probably concomitantly erasing the epigenetic and other chromatin features, prime cell at a state with more plasticity.

It is unclear how does newly established global "open chromatin structure" result in transcriptional depression at specific promoter elements. Transcription repression is maintained through DNA methylation or repressive histone modifications or both. It is possible that different regions rely on different mechanisms thus have different sensitivity to histone disturbance. For example, in the mESC cells, depletion of CAF-1 dilutes nucleosome, concomitantly dilutes

repressive histone modification on MERVL, thus derepresses the MERVL and favors the transition from ESC to 2C-like cells (Ishiuchi *et al.*, 2015)while during the morula stage, depletion of CAF-1 does not alter the MERVL expression(Hatanaka *et al.*, 2015). The repression mechanisms of MERVL between morula and blastocyst will help to elucidate the differences.

Materials and Methods

Table B.1: Primers for q-PCR

Target	Forward Primer	Reverse Primer
Zscan4	GAGATTCATGGAGAGTCTGACTGATGAGTG	GCTGTTGTTTCAAAAGCTTGATGACTTC
Eif1a like	AACAGGCGCAGAGGTAAAAA	CTTATATGGCACAGCCTCCT
MERVL	CTCTACCACTTGGACCATATGAC	GAGGCTCCAAACAGCATCTCTA
IAP	AAGCAGCAATCACCCACTTTGG	CAATCATTAGATGCGGCTGCCAAG
LINE1	GGACCAGAAAAGAAATTCCTCCCG	CTCTTCTGGCTTTCATAGTCTCTGG
Major satellite	GCACACTGAAGGACCTGGAATATG	GATTTCGTCATTTTTCAAGTCGTC
Minor satellite	TCTCCGAACGCAACATGAAG	ACACCTTGACGGTGACTTTGG
Minor satellite	CATGGAAAATGATAAAAACC	CATCTAATATGTTCTACAGTGTGG

GAPDH	CATGGCCTTCCGTGTTCCTA	GCCTGCTTCACCACCTTCTT

BIBLIOGRAPHY

Akhtar, A., and Gasser, S. M. (2007). The nuclear envelope and transcriptional control. Nat Rev Genet *8*, 507–517.

Almouzni, G., and Probst, A. V (2011). Heterochromatin maintenance and establishment: lessons from the mouse pericentromere. Nucleus *2*, 332–338.

Anguera, M., Sun, B., and Lee, J. (2006). X-Chromosome Kiss and Tell : How the Xs Go Their Separate Ways. Cold Spring Harb Symp Quant Biol *71*, 429–437.

Barr, M. L., and Bertram, E. G. (1949). A morphological distinction between neurones of the male and female, and the behaviour of the nucleolar satellite during accelerated nucleoprotein synthesis. Nature *163*, 676.

Baus, F., Gire, V., Fisher, D., Piette, J., and Dulić, V. (2003). Permanent cell cycle exit in G2 phase after DNA damage in normal human fibroblasts. EMBO J. *22*, 3992–4002.

Beck, D. B., Burton, A., Oda, H., Ziegler-Birling, C., Torres-Padilla, M. E., and Reinberg, D. (2012). The role of PR-Set7 in replication licensing depends on Suv4-20h. Genes Dev. *26*, 2580–2589.

Benson, E. K., Mungamuri, S. K., Attie, O., Kracikova, M., Sachidanandam, R., Manfredi, J. J., and Aaronson, S. a (2014). p53-dependent gene repression through p21 is mediated by recruitment of E2F4 repression complexes. Oncogene *33*, 3959–3969.

Bertoli, C., Skotheim, J. M., and de Bruin, R. A. M. (2013). Control of cell cycle transcription during G1 and S phases. Nat. Rev. Mol. Cell Biol. *14*, 518–528.

Bian, Q., Khanna, N., Alvikas, J., and Belmont, A. S. (2013). β-Globin cis-elements determine differential nuclear targeting through epigenetic modifications. J. Cell Biol. *203*, 767–783.

Bisteau, X., Paternot, S., Colleoni, B., Ecker, K., Coulonval, K., de Groote, P., Declercq, W., Hengst, L., and Roger, P. P. (2013). CDK4 T172 Phosphorylation Is Central in a CDK7-Dependent Bidirectional CDK4/CDK2 Interplay Mediated by p21 Phosphorylation at the Restriction Point. PLoS Genet. *9*.

Bodnar, A. G., Ouellette, M., Frolkis, M., Holt, S. E., Chiu, C. P., Morin, G. B., Harley, C. B., Shay, J. W., Lichtsteiner, S., and Wright, W. E. (1998). Extension of life-span by introduction of telomerase into normal human cells. Science (80-.). *279*, 349–352.

Booth, D. G. *et al.* (2014). Ki-67 is a PP1-interacting protein that organises the mitotic chromosome periphery. Elife *3:e01641*.

Booth, D. G., Beckett, A. J., Molina, O., Samejima, I., Masumoto, H., Kouprina, N., Larionov, V., Prior, I. A., and Earnshaw, W. C. (2016). 3D-CLEM Reveals that a Major Portion of Mitotic Chromosomes Is Not Chromatin. Mol. Cell *64*, 790–802.

Booth, D. G., and Earnshaw, W. C. (2017). Ki-67 and the Chromosome Periphery Compartment in Mitosis. Trends Cell Biol. *xx*, 1–11.

Bostick, M., Kyong, K. J., Esteve, P.-O., Clark, A., Pradhan, S., and Jacobsen, S. E. (2007). UHRF1 plays a role in maintaining DNA methylation in mammalian cells.

Science (80-.). *317*, 1760–1764.

Bourgeois, C. A., Laquerriere, F., Hemon, D., Hubert, J., and Bouteille, M. (1985). New data on the in situ position of the inactive X chromosome in the interphase nucleus of human fibroblasts. Hum. Genet. *69*, 122–129.

Branzei, D., and Foiani, M. (2008). Regulation of DNA repair throughout the cell cycle. Nat. Rev. Mol. Cell Biol. *9*, 297–308.

Bridger, J. M., Kill, I. R., and Lichter, P. (1998). Association of pKi-67 with satellite DNA of the human genome in early G 1 cells. *6*, 13–24.

Britton, S., Coates, J., and Jackson, S. P. (2013). A new method for high-resolution imaging of Ku foci to decipher mechanisms of DNA double-strand break repair. J. Cell Biol. *202*, 579–595.

Brown, C. J., Hendrich, B. D., Rupert, J. L., Lafrenière, R. G., Xing, Y., Lawrence, J., and Willard, H. F. (1992). The human XIST gene: Analysis of a 17 kb inactive X-specific RNA that contains conserved repeats and is highly localized within the nucleus. Cell *71*, 527–542.

Brugarolas, J., Moberg, K., Boyd, S., Taya, Y., Jacks, T., and Lees, J. A. (1999). Inhibition of cyclin-dependent kinase 2 by p21 is necessary for retinoblastoma protein-mediated G1 arrest after gamma-irradiation. Proc Natl Acad Sci *96*, 1002–1007.

Bunz, F., Dutriaux, A., Lengauer, C., Waldman, T., Zhou, S., Brown, J. P., Sedivy, J. M., Kinzler, K. W., and Vogelstein, B. (1998). Requirement for p53 and p21 to sustain G2 arrest after DNA damage. Science (80-.). *282*, 1497–1501.

Cao, R., Wang, L., Wang, H., Xia, L., Erdjument-Bromage, H., Tempst, P., Jones, R. S., and Zhang, Y. (2002). Role of histone H3 lysine 27 methylation in Polycomb-group silencing. Science (80-.). *298*, 1039–1043.

de Castro, I. J. *et al.* (2017). Repo-Man/PP1 regulates heterochromatin formation in interphase. Nat. Commun. *8*, 14048.

Caudron-Herger, M., Pankert, T., Seiler, J., Németh, A., Voit, R., Grummt, I., and Rippe, K. (2015). Alu element-containing RNAs maintain nucleolar structure and function. EMBO J. *34*, 2758–2774.

Chaligné, R. *et al.* (2015). The inactive X chromosome is epigenetically unstable and transcriptionally labile in breast cancer. Genome Res. *25*, 488–503.

Cheloufi, S. *et al.* (2015). The histone chaperone CAF-1 safeguards somatic cell identity. Nature *528*, 218–224.

Chen, L., Nievera, C. J., Lee, A. Y.-L., and Wu, X. (2008). Cell Cycle-dependent Complex Formation of BRCA1.CtIP.MRN Is Important for DNA Double-strand Break Repair. J. Biol. Chem. *283*, 7713–7720.

Chen, X., Yammine, S., Shi, C., Tark-Dame, M., Göndör, A., and Ohlsson, R. (2014). The visualization of large organized chromatin domains enriched in the H3K9me2 mark within a single chromosome in a single cell. Epigenetics *9*, 1439–1445.

Cheutin, T., O'Donohue, M.-F., Beorchia, A., Klein, C., Kaplan, H., and Ploton, D. (2003). Three-dimensional organization of pKi-67: a comparative fluorescence and electron tomography study using FluoroNanogold. J. Histochem. Cytochem. *51*, 1411–1423.

Chierico, L., Rizzello, L., Guan, L., Joseph, A. S., Lewis, A., and Battaglia, G.

(2017). The role of the two splice variants and extranuclear pathway on Ki-67 regulation in non-cancer and cancer cells. PLoS One *12*, 1–20.

Chubb, J. R., Boyle, S., Perry, P., and Bickmore, W. A. (2002). Chromatin motion is constrained by association with nuclear compartments in human cells. Curr. Biol. *12*, 439–445.

Chun-Kan Chen, Mario Blanco, Constanza Jackson, Erik Aznauryan, Noah Ollikainen, Christine Surka, Amy Chow, Patrick McDonel, Andrea Cerase, and Mitchell Guttman (2016). Xist recruits the X chromosome to the nuclear lamina to enable chromosome-wide silencing. Science (80-.).

Chureau, C., Prissette, M., Bourdet, A., Cattolico, L., Jones, L., Avner, P., and Duret, L. (2002). Comparative Sequence Analysis of the X-Inactivation Center Region in Mouse , Human , and Bovine. Genome Res. *12*, 894–908.

Cidado, J. *et al.* (2016). Ki-67 is required for maintenance of cancer stem cells but not cell proliferation. Oncotarget *7*, 6281–6293.

Csankovszki, G., Nagy, A., and Jaenisch, R. (2001). Synergism of Xist RNA, DNA methylation, and histone hypoacetylation in maintaining X chromosome inactivation. J. Cell Biol. *153*, 773–783.

Cuylen, S., Blaukopf, C., Politi, A. Z., Müller-Reichert, T., Neumann, B., Poser, I., Ellenberg, J., Hyman, A. A., and Gerlich, D. W. (2016). Ki-67 acts as a biological surfactant to disperse mitotic chromosomes. Nature *535*, 308–312.

Demmerle, J., Koch, A. J., and Holaska, J. M. (2012). The nuclear envelope protein emerin binds directly to histone deacetylase 3 (HDAC3) and activates HDAC3 activity. J. Biol. Chem. *287*, 22080–22088.

Deng, C., Zhang, P., Harper, J. W., Elledge, S. J., and Leder, P. (1995). Mice lacking p21CIP1/WAF1 undergo normal development, but are defective in G1 checkpoint control. Cell *82*, 675–684.

Dillinger, S., Straub, T., and Nemeth, A. (2016). Nucleolus association of chromosomal domains is largely maintained in cellular senescence despite massive nuclear reorganisation. bioRxiv.

Dimitrova, D. S., and Berezney, R. (2002). The spatio-temporal organization of DNA replication sites is identical in primary, immortalized and transformed mammalian cells. J. Cell Sci. *115*, 4037–4051.

Dowsett, M. *et al.* (2011). Assessment of Ki67 in Breast Cancer: Recommendations from the international Ki67 in breast cancer working Group. J. Natl. Cancer Inst. *103*, 1656–1664.

Durocher, D. *et al.* (1999). The FHA domain is a modular phosphopeptide recognition motif. Mol. Cell *4*, 387–394.

Durocher, D., and Jackson, S. P. (2002). The FHA domain. FEBS Lett. *513*, 58–66.

Dyson, N. (1998). The regulation of E2F by pRB-family proteins. Genes Dev. *12*, 2245–2262.

Eissenberg, J. C., and Elgin, S. (2014). HP1a: A structural chromsomal protein regulating transcription. Trends Genet. *30*, 103–110.

El-Deiry, W. S., Tokino, T., Velculescu, V. E., Levy, D. B., Parsons, R., Trent, J. M., Lin, D., Mercer, W. E., Kinzler, K. W., and Vogelstein, B. (1993). WAF1, a potential mediator of p53 tumor suppression. Cell *75*, 817–825.

Endl, E., and Gerdes, J. (2000). Posttranslational modifications of the Ki-67 protein coincide with two major checkpoints during mitosis. J. Cell. Physiol. *182*, 371–380.

Fazzio, T. G., Huff, J. T., and Panning, B. (2008). An RNAi screen of chromatin proteins identifies Tip60-p400 as a regulator of embryonic stem cell identity. Cell *134*, 162–174.

Fedoriw, A. M., Calabrese, J. M., Mu, W., Yee, D., and Magnuson, T. (2012a). Differentiation-Driven Nucleolar Association of the Mouse Imprinted Kcnq1 Locus. *2*, 1521–1528.

Fedoriw, A. M., Starmer, J., Yee, D., and Magnuson, T. (2012b). Nucleolar association and transcriptional inhibition through 5S rDNA in mammals. PLoS Genet. *8*.

Ferguson, D. O., Sekiguchi, J. M., Chang, S., Frank, K. M., Gao, Y., DePinho, R. A., and Alt, F. W. (2000). The nonhomologous end-joining pathway of DNA repair is required for genomic stability and the suppression of translocations. Proc. Natl. Acad. Sci. U. S. A. *97*, 6630–6633.

Finlan, L. E., Sproul, D., Thomson, I., Boyle, S., Kerr, E., Perry, P., Ylstra, B., Chubb, J. R., and Bickmore, W. A. (2008). Recruitment to the nuclear periphery can alter expression of genes in human cells. PLoS Genet. *4*.

Fischer, M., Grossmann, P., Padi, M., and DeCaprio, J. A. (2016). Integration of TP53, DREAM, MMB-FOXM1 and RB-E2F target gene analyses identifies cell cycle gene regulatory networks. Nucleic Acids Res. *44*, 6070–6086.

G.B, P., and A. J, T. (1962). Number of nucleoli in female and male human cells in tissue culture. Exp. Cell Res. *28*, 590–592.

Gartel, A. L., and Radhakrishnan, S. K. (2005). Lost in transcription: p21 repression, mechanisms, and consequences. Cancer Res. *65*, 3980–3985.

Gerdes, J., Lemke, H., Baisch, H., Wacker, H. H., Schwab, U., and Stein, H. (1984). Cell cycle analysis of a cell proliferation-associated human nuclear antigen defined by the monoclonal antibody Ki-67. J Immunol *133*, 1710–1715.

Gerdes, J., Schwab, U., Lemke, H., and Stein, H. (1983). Production of a mouse monoclonal antibody reactive with a human nuclear antigen associated with cell proliferation. Int. J. Cancer *31*, 13–20.

Gerdes, J., Stein, H., Pileri, S., Mt, R., Gobbi, M., Ralfkiaer, E., Km, N., Pallesen, G., Bartels, H., and Palestro, G. (1987). Prognostic relevance of tumour-cell growth fraction in malignant non- Hodgkin's lymphomas. Lancet *2*, 448–449.

Geuting, V., Reul, C., and Löbrich, M. (2013). ATM Release at Resected Double-Strand Breaks Provides Heterochromatin Reconstitution to Facilitate Homologous Recombination. PLoS Genet. *9*, 1–14.

Gibcus, J. H., and Dekker, J. (2013). Connecting the genome: dynamics and stochasticity in a new hierarchy for chromosome conformation. Mol. Cell *49*, 773–782.

Gonzalo, S. *et al.* (2005). Role of the RB1 family in stabilizing histone methylation at constitutive heterochromatin. Nat. Cell Biol. *7*, 420–428.

Goto, H. *et al.* (1999). Identification of a Novel Phosphorylation Site on Histone H3 Coupled with Mitotic Chromosome Condensation. J. Biol. Chem. *274*, 25543–25549.

Grewal, S. I. S., and Elgin, S. C. R. (2002). Heterochromatin: New possibilities for the inheritance of structure. Curr. Opin. Genet. Dev. *12*, 178–187.

Guelen, L. *et al.* (2008). Domain organization of human chromosomes revealed by mapping of nuclear lamina interactions. Nature *453*, 948–951.

Guiley, K. Z., Liban, T. J., Felthousen, J. G., Ramanan, P., Litovchick, L., and Rubin, S. M. (2015). Structural mechanisms of DREAM complex assembly and regulation. Genes Dev. *29*, 961–974.

Guo, C., and Morris, S. A. (2017). Engineering cell identity: establishing new gene regulatory and chromatin landscapes. Curr. Opin. Genet. Dev. *46*, 50–57.

Gurpinar, E., and Vousden, K. H. (2015). Hitting cancers' weak spots: Vulnerabilities imposed by p53 mutation. Trends Cell Biol. *25*, 486–495.

Hacisuleyman, E. *et al.* (2014). Topological organization of multichromosomal regions by the long intergenic noncoding RNA Firre. Nat Struct Mol Biol *21*, 198–206.

Haeusler, R. a, and Engelke, D. R. (2006). Spatial organization of transcription by RNA polymerase III. Nucleic Acids Res. *34*, 4826–4836.

Harr, J. C., Luperchio, T. R., Wong, X., Cohen, E., Wheelan, S. J., and Reddy, K. L. (2015). Directed targeting of chromatin to the nuclear lamina is mediated by chromatin state and A-type lamins. J. Cell Biol. *208*, 33–52.

Hatanaka, Y., Inoue, K., Oikawa, M., Kamimura, S., Ogonuki, N., Kodama, E. N., Ohkawa, Y., Tsukada, Y., and Ogura, A. (2015). Histone chaperone CAF-1 mediates repressive histone modifications to protect preimplantation mouse embryos from endogenous retrotransposons. Proc. Natl. Acad. Sci. U. S. A. *112*, 14641–14646.

Hernandez-verdun, D., and Gautier, T. (1994). The Chromosome periphery during mitosis. Bioessays *16*, 179–185.

Hernandez, A. R., Klein, A. M., and Kirschner, M. W. (2012). Kinetic Responses of beta-catenin specify the sites of wnt control. Science (80-.). *338*, 1337–1340.

Heyer, W.-D., Ehmsen, K. T., and Liu, J. (2010). Regulation of homologous recombinatino in eukaryotes. Annu Rev Genet *44*, 113–139.

Hiragami-Hamada, K. *et al.* (2016). Dynamic and flexible H3K9me3 bridging via HP1β dimerization establishes a plastic state of condensed chromatin. Nat. Commun. *7*, 11310.

Van Hooser, A. A., Yuh, P., and Heald, R. (2005). The perichromosomal layer. Chromosoma *114*, 377–388.

Houlard, M., Berlivet, S., Probst, A. V., Quivy, J. P., Héry, P., Almouzni, G., and Gérard, M. (2006). CAF-1 is essential for heterochromatin organization in pluripotent embryonic cells. PLoS Genet. *2*, 1686–1696.

Hurford, R. K., Cobrinik, D., Lee, M., and Dyson, N. (1997). pRB and p107 / p130 are required for the regulated expression of different sets of E2F responsive genes. Genes Dev. *11*, 1447–1463.

Ianari, A., Natale, T., Calo, E., Ferretti, E., Alesse, E., Screpanti, I., Haigis, K., Gulino, A., and Lees, J. A. (2009). Pro-apoptotic functino of the retinoblastoma tumor suppressor protein. Cancer Cell *15*, 184–194.

Imai, T., Sakano, H., and Vosshall, L. B. (2010). Topographic Mapping — The Olfactory System. Cold Spring Harb Perspect Biol, 1–19.

Ishida, S., Huang, E., Zuzan, H., Spang, R., Leone, G., West, M., and Nevins, J. R.

(2001). Role for E2F in Control of Both DNA Replication and Mitotic Functions as Revealed from DNA Microarray Analysis. Mol. Cell. Biol. *21*, 4684–4699.

Ishiuchi, T., Enriquez-Gasca, R., Mizutani, E., Bošković, A., Ziegler-Birling, C., Rodriguez-Terrones, D., Wakayama, T., Vaquerizas, J. M., and Torres-Padilla, M.-E. (2015). Early embryonic-like cells are induced by downregulating replication-dependent chromatin assembly. Nat. Publ. Gr. *22*, 662–671.

Ishiuchi, T., and Torres-Padilla, M. E. (2013). Towards an understanding of the regulatory mechanisms of totipotency. Curr. Opin. Genet. Dev. *23*, 512–518.

Isola, J., Helin, H., and Kallioniemi, O. P. (1990). Immunoelectron-microscopic localization of a proliferation-associated antigen Ki-67 in MCF-7 cells. Histochem. J. *22*, 498–506.

Jacobs, S., and Sepideh, K. (2002). Structure of the HP1 chromodomain bound to histone H3 methylated at lysine 9. Nature *295*, 2080–2083.

Johansen, K. M., and Johansen, J. (2006). Regulation of chromatin structure by histone H3S10 phosphorylation. Chromosom. Res. *14*, 393–404.

Johnson, W. L., and Straight, A. F. (2017). RNA-mediated regulation of heterochromatin. Curr. Opin. Cell Biol. *46*, 102–109.

Junk, D. J., Vrba, L., Watts, G. S., Oshiro, M. M., Martinez, J. D., and Futscher, B. W. (2008). Different mutant/wild-type p53 combinations cause a spectrum of increased invasive potential in nonmalignant immortalized human mammary epithelial cells. Neoplasia *10*, 450–461.

Kakarougkas, A., Ismail, A., Klement, K., Goodarzi, A. A., Conrad, S., Freire, R., Shibata, A., Lobrich, M., and Jeggo, P. A. (2013). Opposing roles for 53BP1 during homologous recombination. Nucleic Acids Res. *41*, 9719–9731.

Kametaka, A., Takagi, M., Hayakawa, T., Haraguchi, T., Hiraoka, Y., and Yoneda, Y. (2002). Interaction of the chromatin compaction-inducing domain (LR domain) of Ki-67 antigen with HP1 proteins. Genes to Cells *7*, 1231–1242.

Kausch, I., Lingnau, A., Endl, E., Sellmann, K., Deinert, I., Ratliff, T. L., Jocham, D., Sczakiel, G., Gerdes, J., and Böhle, A. (2003). Antisense treatment against Ki-67 mRNA inhibits proliferation and tumor growth in vitro and in vivo. Int. J. Cancer *105*, 710–716.

Kelsey, A. D., Yang, C., Leung, D., Minks, J., Dixon-McDougall, T., Baldry, S. E. L., Bogutz, A. B., Lefebvre, L., and Brown, C. J. (2015). Impact of flanking chromosomal sequences on localization and silencing by the human non-coding RNA XIST. Genome Biol. *16*, 208.

Kill, I. R. (1996). Localisation of the Ki-67 antigen within the nucleolus. Evidence for a fibrillarin-deficient region of the dense fibrillar component. J. Cell Sci. *109 (Pt 6)*, 1253–1263.

Kim, D., Pertea, G., Trapnell, C., Pimentel, H., Kelley, R., and Salzberg, S. L. (2013). TopHat2: accurate alignment of transcriptomes in the presence of insertions, deletions and gene fusions. Genome Biol. *14*, R36.

Kind, J., Pagie, L., Ortabozkoyun, H., Boyle, S., De Vries, S. S., Janssen, H., Amendola, M., Nolen, L. D., Bickmore, W. A., and Van Steensel, B. (2013a). Single-cell dynamics of genome-nuclear lamina interactions. Cell *153*, 178–192.

Kind, J., Pagie, L., Ortabozkoyun, H., Boyle, S., De Vries, S. S., Janssen, H., Amendola, M., Nolen, L. D., Bickmore, W. A., and Van Steensel, B. (2013b). Single-cell

dynamics of genome-nuclear lamina interactions. Cell *153*, 178–192.

Kohlmaier, A., Savarese, F., Lachner, M., Martens, J., Jenuwein, T., and Wutz, A. (2004). A chromosomal memory triggered by Xist regulates histone methylation in X inactivation. PLoS Biol. *2*, E171.

Kolodner, R. D., Putnam, C. D., and Myung, K. (2002). Maintenance of genome stability in Saccharomyces cerevisiae. Science (80-.). *297*, 552–557.

Koningsbruggen, S. van, Gierlinski, M., Schofield, P., Martin, D., Barton, G. J., Ariyurek, Y., Dunnen, J. T. den, and Lamond, A. I. (2010). High-Resolution Whole-Genome Sequencing Reveals That Specific Chromatin Domains from Most Human Chromosomes Associate with Nucleoli. Mol. Biol. Cell *21*, 3735–3748.

Kreitz, S., Fackelmayer, F. O., Gerdes, J., and Knippers, R. (2000). The proliferation-specific human Ki-67 protein is a constituent of compact chromatin. Exp. Cell Res. *261*, 284–292.

Krude, T. (1995). Chromatin assembly factor 1 (CAF-1) colocalizes with replication foci in HeLa cell nuclei. Exp. Cell Res. *220*, 304–311.

Kumar, G. S., Gokhan, E., De Munter, S., Bollen, M., Vagnarelli, P., Peti, W., and Page, R. (2016). The Ki-67 and RepoMan mitotic phosphatases assemble via an identical, yet novel mechanism. Elife *5:e16539*.

Kumaran, R. I., and Spector, D. L. (2008). A genetic locus targeted to the nuclear periphery in living cells maintains its transcriptional competence. J. Cell Biol. *180*, 51–65.

Labaer, J., Garrett, M. D., Stevenson, L. F., Slingerland, J. M., Sandhu, C., Chou, H. S., Fattaey, A., and Harlow, E. (1997). New functional activities for the p21 family of CDK inhibitors. Genes Dev. *11*, 847–862.

Leger, I., Guillaud, M., Krief, B., and Brugal, G. (1994). Interactive computer-assisted analysis of chromosome 1 colocalization with nucleoli. Cytometry *16*, 313–323.

Leiber, M. R. (2010). The mechanism of double-stranded DNA break repair by the nonhomologous DNA end joining pathway. Annu Rev Biochem *79*, 181–211.

Lemaître, C., Grabarz, A., and Tsouroula, K. (2014). Nuclear position dictates DNA repair pathway choice Nuclear position dictates DNA repair pathway choice. 0–14.

Lewis, A., Mitsuya, K., Umlauf, D., Smith, P., Dean, W., Walter, J., Higgins, M., Feil, R., and Reik, W. (2004). Imprinting on distal chromosome 7 in the placenta involves repressive histone methylation independent of DNA methylation. Nat. Genet. *36*, 1291–1295.

Li, V. S. W. *et al.* (2012). Wnt Signaling through Inhibition of β-Catenin Degradation in an Intact Axin1 Complex. Cell *149*, 1245–1256.

Lin, T. C. *et al.* (2016). The nucleolar protein NIFK promotes cancer progression via ck1α/β-catenin in metastasis and ki-67-dependent cell proliferation. Elife *5*, 1–21.

Litovchick, L., Sadasivam, S., Florens, L., Zhu, X., Swanson, S. K., Velmurugan, S., Chen, R., Washburn, M. P., Liu, X. S., and DeCaprio, J. A. (2007). Evolutionarily Conserved Multisubunit RBL2/p130 and E2F4 Protein Complex Represses Human Cell Cycle-Dependent Genes in Quiescence. Mol. Cell *26*, 539–551.

Llères, D., James, J., Swift, S., Norman, D. G., and Lamond, A. I. (2009).

Quantitative analysis of chromatin compaction in living cells using FLIM-FRET. J. Cell Biol. *187*, 481–496.

Lopez, F., Belloc, F., Lacombe, F., Dumain, P., Reiffers, J., Bernard, P., and Boisseau, M. R. (1991). Modalities of synthesis of Ki67 antigen during the stimulation of lymphocytes. Cytometry *12*, 42–49.

Lucchesi, J. C., Kelly, W. G., and Panning, B. (2005). Chromatin Remodeling in Dosage Compensation. Annu. Rev. Genet. *39*, 615–651.

Lukas, C. *et al.* (2011a). 53BP1 nuclear bodies form around DNA lesions generated by mitotic transmission of chromosomes under replication stress. Nat. Cell Biol. *13*, 243–253.

Lukas, J., Lukas, C., and Bartek, J. (2011b). More than just a focus: The chromatin response to DNA damage and its role in genome integrity maintenance. Nat. Cell Biol. *13*, 1161–1169.

Luo, Y., Ren, F., Liu, Y., Shi, Z., Tan, Z., Xiong, H., Dang, Y., and Chen, G. (2015). Clinicopathological and prognostic significance of high Ki-67 labeling index in hepatocellular carcinoma patients: A meta-analysis. Int. J. Clin. Exp. Med. *8*, 10235–10247.

Ma, H., Naseri, A., Reyes-Gutierrez, P., Wolfe, S. A., Zhang, S., and Pederson, T. (2015). Multicolor CRISPR lableing of chromosomal loci in human cells. Proc. Natl. Acad. Sci. U. S. A. *112*, 3002–3007.

MacCallum, D. E., and Hall, P. A. (1999). Biochemical characterization of pKi67 with the identification of a mitotic-specific form associated with hyperphosphorylation and altered DNA binding. Exp. Cell Res. *252*, 186–198.

Macfarlan, T. S., Gifford, W. D., Driscoll, S., Lettieri, K., Rowe, H. M., Bonanomi, D., Firth, A., Singer, O., Trono, D., and Pfaff, S. L. (2012). Embryonic stem cell potency fluctuates with endogenous retrovirus activity. Nature *487*, 57–63.

Mangan, H., Gailín, M. O., and Mcstay, B. (2017). Integrating the genomic architecture of human nucleolar organizer regions with the biophysical properties of nucleoli. FEBS J., 1–9.

Manning, A. L., Longworth, M. S., and Dyson, N. J. (2010). Loss of pRB causes centromere dysfunction and chromosomal instability. Genes Dev. *24*, 1364–1376.

Manning, A. L., Yazinski, S. A., Nicolay, B., Bryll, A., Zou, L., and Dyson, N. J. (2014). Suppression of genome instability in prb-deficient cells by enhancement of chromosome cohesion. Mol. Cell *53*, 993–1004.

Marikawa, Y., and Alarcon, V. B. (2009). Establishment of trophectoderm and inner cell mass lineages in the mouse embryo. Mol Reprod Dev *76*, 1019–1032.

Matheson, T. D., and Kaufman, P. D. (2015). Grabbing the genome by the NADs. Chromosoma *1*, 1–11.

Matheson, T. D., and Kaufman, P. D. (2017a). The p150N domain of Chromatin Assembly Factor-1 regulates Ki-67 accumulation on the mitotic perichromosomal layer. Mol. Biol. Cell *28 (1)*, 21–29.

Matheson, T. D., and Kaufman, P. D. (2017b). The p150N domain of chromatin assembly factor-1 regulates Ki-67 accumulation on the mitotic perichromosomal layer. Mol. Biol. Cell *28*, 21–29.

Mattout, A., Cabianca, D. S., and Gasser, S. M. (2015). Chromatin states and nuclear organization in development--a view from the nuclear lamina. Genome Biol.

16, 174.

McStay, B. (2016). Nucleolar organizer regions: genomic "dark matter" requiring\nillumination. Genes Dev. *30*, 1598–1610.

Merkenschlager, M., and Nora, E. P. (2016). CTCF and Cohesin in Genome Folding and Transcriptional Gene Regulation. Annu. Rev. Genomics Hum. Genet. *17*, 17–43.

Meuleman, W., Peric-hupkes, D., Kind, J., Beaudry, J., Pagie, L., Kellis, M., Reinders, M., Wessels, L., and Steensel, B. Van (2013). Constitutive nuclear lamina – genome interactions are highly conserved and associated with A / T-rich sequence. Genome Res. *23*, 270–280.

Mohammad, F., Mondal, T., Guseva, N., Pandey, G. K., and Kanduri, C. (2010). Kcnq1ot1 noncoding RNA mediates transcriptional gene silencing by interacting with Dnmt1. Development *137*, 2493–2499.

Mohammad, F., Pandey, R. R., Nagano, T., Chakalova, L., Mondal, T., Fraser, P., and Kanduri, C. (2008). Kcnq1ot1/Lit1 Noncoding RNA Mediates Transcriptional Silencing by Targeting to the Perinucleolar Region. Mol. Cell. Biol. *28*, 3713–3728.

Mondal, T., Fraser, P., and Kanduri, C. (2008). Kcnq1ot1 / Lit1 Noncoding RNA Mediates Transcriptional Silencing by Targeting to the Perinucleolar Region †. *28*, 3713–3728.

Morris, E., and Dyson, N. (2001). Retinoblastoma Protein partners. Adv Cancer REs *82*, 54.

Murzina, N., Verreault, A., Laue, E., and Stillman, B. (1999). Heterochromatin dynamics in mouse cells: Interaction between chromatin assembly factor 1 and HP1 proteins. Mol. Cell *4*, 529–540.

Negi, S. S., and Olson, M. O. J. (2006). Effects of interphase and mitotic phosphorylation on the mobility and location of nucleolar protein B23. J. Cell Sci. *119*, 3676–3685.

Németh, A., Conesa, A., Santoyo-Lopez, J., Medina, I., Montaner, D., Péterfia, B., Solovei, I., Cremer, T., Dopazo, J., and Längst, G. (2010). Initial genomics of the human nucleolus. PLoS Genet. *6*, e1000889.

Nielsen, P. R., Nietlispach, D., Mott, H. R., Callaghan, J., Bannister, A., Kouzarides, T., Murzin, A. G., Murzina, N. V, and Laue, E. D. (2002). Structure of the HP1 chromodomain bound to histone H3 methylated at lysine 9. Nature *416*, 103–107.

Norton, J. T., Wang, C., Gjidoda, A., Henry, W. R., and Huang, S. (2009). The perinucleolar compartment is directly associated with DNA. J. Biol. Chem. *284*, 4090–4101.

Padeken, J., and Heun, P. (2014). Nucleolus and nuclear periphery: Velcro for heterochromatin. Curr. Opin. Cell Biol. *28*, 54–60.

Pan, W., Tsai, H., Wang, S., Hsiao, M., Wu, P., and Tsai, M. (2015). The RNA recognition motif of NIFK is required for rRNA maturation during cell cycle progression. RNA Biol. *12*, 255–267.

Pandey, R. R., Mondal, T., Mohammad, F., Enroth, S., Redrup, L., Komorowski, J., Nagano, T., Mancini-DiNardo, D., and Kanduri, C. (2008). Kcnq1ot1 Antisense Noncoding RNA Mediates Lineage-Specific Transcriptional Silencing through Chromatin-Level Regulation. Mol. Cell *32*, 232–246.

Pederson, T. (2011). The nucleolus. Cold Spring Harb. Perspect. Biol. *3*, 1–15.

Pederson, T., and Tsai, R. Y. L. (2009). In search of nonribosomal nucleolar protein function and regulation. J. Cell Biol. *184*, 771–776.

Peric-Hupkes, D. *et al.* (2010). Molecular Maps of the Reorganization of Genome-Nuclear Lamina Interactions during Differentiation. Mol. Cell *38*, 603–613.

Petitjean, a, Achatz, M. I. W., Borresen-dale, a L., Hainaut, P., Olivier, M., and Paolo, S. (2007). TP53 mutations in human cancers: functional selection and impact on cancer prognosis and outcomes. Oncogene *26*, 2157–2165.

Pezzilli, R., Partelli, S., Cannizzaro, R., Pagano, N., Crippa, S., Pagnanelli, M., and Falconi, M. (2016). Ki-67 prognostic and therapeutic decision driven marker for pancreatic neuroendocrine neoplasms (PNENs): A systematic review. Adv. Med. Sci. *61*, 147–153.

Pickersgill, H., Kalverda, B., de Wit, E., Talhout, W., Fornerod, M., and van Steensel, B. (2006). Characterization of the Drosophila melanogaster genome at the nuclear lamina. Nat Genet *38*, 1005–1014.

Politz, J. C. R., Scalzo, D., and Groudine, M. (2013). Something silent this way forms: the functional organization of the repressive nuclear compartment. Annu. Rev. Cell Dev. Biol. *29*, 241–270.

Politz, J. C. R., Scalzo, D., and Groudine, M. (2016). The redundancy of the mammalian heterochromatic compartment. Curr. Opin. Genet. Dev. *37*, 1–8.

Pontvianne, F. *et al.* (2016). Identification of Nucleolus-Associated Chromatin Domains Reveals a Role for the Nucleolus in 3D Organization of the A.thaliana Genome. Cell Rep. *16*, 1574–1587.

Probst, A. V., Santos, F., Reik, W., Almouzni, G., and Dean, W. (2007). Structural differences in centromeric heterochromatin are spatially reconciled on fertilisation in the mouse zygote. Chromosoma *116*, 403–415.

Pyo, J. S., Kang, G., and Sohn, J. H. (2015). Ki-67 labeling index can be used as a prognostic marker in gastrointestinal stromal tumor: a systematic review and meta-analysis. Int J Biol Markers *31*, 0.

Quivy, J.-P., Gérard, A., Cook, A. J. L., Roche, D., and Almouzni, G. (2008). The HP1-p150/CAF-1 interaction is required for pericentric heterochromatin replication and S-phase progression in mouse cells. Nat. Struct. Mol. Biol. *15*, 972–979.

Quivy, J.-P., Le Roche, D., Kirschner, D., Tagami, H., Nakatani, Y., and Ve Almouzni, G. (2004). A CAF-1 dependent pool of HP1 during heterochromatin duplication. EMBO J. *23*, 3516–3526.

Ragoczy, T., Telling, A., Scalzo, D., Kooperberg, C., and Groudine, M. (2014). Functional redundancy in the nuclear compartmentalization of the late-replicating genome. Nucleus *5*, 626–635.

Rahmanzadeh, R., Hüttmann, G., Gerdes, J., and Scholzen, T. (2007). Chromophore-assisted light inactivation of pKi-67 leads to inhibition of ribosomal RNA synthesis. Cell Prolif. *40*, 422–430.

Rayman, J. B., Takahashi, Y., Indjeian, V. B., Dannenberg, J. H., Catchpole, S., Watson, R. J., Riele, H., and Dynlacht, B. D. (2002). E2F mediates cell cycle-dependent transcriptional repression in vivo by recruitment of an HDAC1/mSin3B corepressor complex. Genes Dev. *16*, 933–947.

Rebelo, S., Santos, M., Martins, F., da Cruz e Silva, E. F., and da Cruz e Silva, O.

A. B. (2015). Protein phosphatase 1 is a key player in nuclear events. Cell. Signal. *27*, 2589–2598.

Reddy, K. L., Zullo, J. M., Bertolino, E., and Singh, H. (2008). Transcriptional repression mediated by repositioning of genes to the nuclear lamina. Nature *452*, 243–247.

Reichow, S. L., Hamma, T., FerreD'Amare, A. R., and Varani, G. (2007). The structure and function of small nucleolar ribonucleoproteins. Nucleic Acids Res. *35*, 1452–1464.

Reinhardt, H. C., Aslanian, A. S., Lees, J. A., and Yaffe, M. B. (2007). p53-Deficient Cells Rely on ATM- and ATR-Mediated Checkpoint Signaling through the p38MAPK/MK2 Pathway for Survival after DNA Damage. Cancer Cell *11*, 175–189.

Reinhardt, H. C., Jiang, H., Hemann, Mi. T., and Yaffe, M. (2009). Exploiting synthetic lethal interactions for targeted cancer therapy. Cell Cycle *8*, 3112–3119.

Richards-Taylor, S., Ewings, S. M., Jaynes, E., Tilley, C., Ellis, S. G., Armstrong, T., Pearce, N., and Cave, J. (2015). The assessment of Ki-67 as a prognostic marker in neuroendocrine tumours: a systematic review and meta-analysis. J. Clin. Pathol., jclinpath-2015-203340.

S. Pedersen, R. *et al.* (2016). Profiling DNA damage response following mitotic perturbations. Nat. Commun. *7*, 13887.

Sadasivam, S., and DeCaprio, J. A. (2013). The DREAM complex: master coordinator of cell cycle-dependent gene expression. Nat. Rev. Cancer *13*, 585–595.

Saiwaki, T., Kotera, I., Sasaki, M., Takagi, M., and Yoneda, Y. (2005). In vivo dynamics and kinetics of pKi-67: Transition from a mobile to an immobile form at the onset of anaphase. Exp. Cell Res. *308*, 123–134.

Saksouk, N., Simboeck, E., and Déjardin, J. (2015). Constitutive heterochromatin formation and transcription in mammals. Epigenetics Chromatin *8*, 3.

Sarraf, S. A., and Stancheva, I. (2004). Methyl-CpG binding protein MBD1 couples histone H3 methylation at lysine 9 by SETDB1 to DNA replication and chromatin assembly. Mol. Cell *15*, 595–605.

Schluter, C., Duchrow, M., Wohlenberg, C., Becker, M. H. G., Key, G., Flad -, H. D., and Gerdes, J. (1993). The cell proliferation-associated antigen of antibody Ki-67: A very large, ubiquitous nuclear protein with numerous repeated elements, representing a new kind of cell cycle-maintaining proteins. J. Cell Biol. *123*, 513–522.

Schmit, F., Korenjak, M., Mannefeld, M., Schmitt, K., Franke, C., Von Eyss, B., Gagrica, S., Hänel, F., Brehm, A., and Gaubatz, S. (2007). LINC, a human complex that is related to pRB-containing complexes in invertebrates regulates the expression of G2/M genes. Cell Cycle *6*, 1903–1913.

Scholzen, T., Endl, E., Wohlenberg, C., van der Sar, S., Cowell, I. G., Gerdes, J., and Singh, P. B. (2002). The Ki-67 protein interacts with members of the heterochromatin protein 1 (HP1) family: a potential role in the regulation of higher-order chromatin structure. J. Pathol. *196*, 135–144.

Shachar, S., Voss, T. C., Pegoraro, G., Sciascia, N., and Misteli, T. (2016). systematic identification of gene positioning factors. *162*, 911–923.

Shibahara, K., and Stillman, B. (1999). Replication-dependent marking of DNA by PCNA facilitates CAF-1-coupled inheritance of chromatin. Cell *96*, 575–585.

Shimi, T., Kittisopikul, M., Tran, J., Goldman, A. E., Adam, S. A., Zheng, Y., Jaqaman, K., and Goldman, R. D. (2015). Structural organization of nuclear lamins A, C, B1, and B2 revealed by superresolution microscopy. Mol. Biol. Cell *26*, 4075–4086.

Simon, J. A., and Kingston, R. E. (2013). Occupying chromatin: Polycomb mechanisms for getting to genomic targets, stopping transcriptional traffic, and staying put. Mol. Cell *49*, 808–824.

Sirri, V., Urcuqui-Inchima, S., Roussel, P., and Hernandez-Verdun, D. (2008). Nucleolus: The fascinating nuclear body. Histochem. Cell Biol. *129*, 13–31.

Smith, C. L., Matheson, T. D., Trombly, D. J., Sun, X., Campeau, E., Han, X., Yates, J. R., and Kaufman, P. D. (2014). A separable domain of the p150 subunit of human chromatin assembly factor-1 promotes protein and chromosome associations with nucleoli. Mol. Biol. Cell *25*, 2866–2881.

Smith, S., and Stillman, B. (1989). Purification and characterization of CAF-I, a human cell factor required for chromatin assembly during DNA replication in vitro. Cell *58*, 15–25.

Smith, S., and Stillman, B. (1991). Immunological characterization of chromatin assembly factor I, a human cell factor required for chromatin assembly during DNA replication in vitro. J. Biol. Chem. *266*, 12041–12047.

Sobecki, M. *et al.* (2016). The cell proliferation antigen Ki-67 organises heterochromatin. Elife *5:e13722*.

Sobecki, M., Mrouj, K., Colinge, J., Gerbe, F., Jay, P., Krasinska, L., Dulic, V., and Fisher, D. (2017). Cell cycle regulation accounts for variability in Ki-67 expression levels. Cancer Res., canres.0707.2016.

Somech, R., Shaklai, S., Geller, O., Amariglio, N., Simon, A. J., Rechavi, G., and Gal-Yam, E. N. (2005). The nuclear-envelope protein and transcriptional repressor LAP2β interacts with HDAC3 at the nuclear periphery, and induces histone H4 deacetylation. J. Cell Sci. *118*, 403–410.

Starborg, M., Gell, K., Brundell, E., and Höög, C. (1996). The murine Ki-67 cell proliferation antigen accumulates in the nucleolar and heterochromatic regions of interphase cells and at the periphery of the mitotic chromosomes in a process essential for cell cycle progression. J. Cell Sci. *109 (Pt 1*, 143–153.

Steensel, B., and Henikoff, S. (2000). Identification of in vivo DNA targets of chromatin proteins using tethered dam methyltransferase. Nat. Biotechnol. *18*, 424–428.

van Steensel, B., and Belmont, A. S. (2017). Lamina-Associated Domains: Links with Chromosome Architecture, Heterochromatin, and Gene Repression. Cell *169*, 780–791.

van Steensel, B., Delrow, J., and Henikoff, S. (200AD). Chromatin profiling using targeted DNA adenine methyltransferase. Nat. Genet. *27*, 304–308.

Strom, A. R., and Alexander, V. (2017). Phase separation drives heterochromatin domain formation. Nature *547*, 241–245.

Sueishi, M., Takagi, M., and Yoneda, Y. (2000). The forkhead-associated domain of Ki-67 antigen interacts with the novel kinesin-like protein Hklp2. J. Biol. Chem. *275*, 28888–28892.

Surendranath, V., Theis, M., Habermann, B. H., and Buchholz, F. (2013). Designing efficient and specific endoribonuclease-prepared siRNAs. Methods Mol.

Biol. *942*, 193–204.

Taddei, A., Hediger, F., Neumann, F. R., and Gasser, S. M. (2004). The function of nuclear architecture: a genetic approach. Annu Rev Genet *38*, 305–345.

Takagi, M., Matsuoka, Y., Kurihara, T., and Yoneda, Y. (1999). Chmadrin: a novel Ki-67 antigen-related perichromosomal protein possibly implicated in higher order chromatin structure. J. Cell Sci. *112 (Pt 1*, 2463–2472.

Takagi, M., Nishiyama, Y., Taguchi, A., and Imamoto, N. (2014). Ki67 antigen contributes to the timely accumulation of protein phosphatase 1γ on anaphase chromosomes. J. Biol. Chem. *289*, 22877–22887.

Takagi, M., Sueishi, M., Saiwaki, T., Kametaka, A., and Yoneda, Y. (2001). A Novel Nucleolar Protein, NIFK, Interacts with the Forkhead Associated Domain of Ki-67 Antigen in Mitosis. J. Biol. Chem. *276*, 25386–25391.

Talluri, S., and Dick, F. A. (2012). Regulation of transcription and chromatin structure by pRB Here , there and everywhere Bioscience . Cell Cycle *11*, 3189–3198.

Thomson, I., Gilchrist, S., Bickmore, W. A., and Chubb, J. R. (2004). The Radial Positioning of Chromatin Is Not Inherited through Mitosis but Is Established de Novo in Early G1. Curr. Biol. *14*, 166–172.

Towbin, B. D., González-Aguilera, C., Sack, R., Gaidatzis, D., Kalck, V., Meister, P., Askjaer, P., and Gasser, S. M. (2012). Step-wise methylation of histone H3K9 positions heterochromatin at the nuclear periphery. Cell *150*, 934–947.

Trapnell, C., Pachter, L., and Salzberg, S. L. (2009). TopHat: Discovering splice junctions with RNA-Seq. Bioinformatics *25*, 1105–1111.

Trapnell, C., Williams, B. a, Pertea, G., Mortazavi, A., Kwan, G., van Baren, M. J., Salzberg, S. L., Wold, B. J., and Pachter, L. (2010). Transcript assembly and abundance estimation from RNA-Seq reveals thousands of new transcripts and switching among isoforms. Nat. Biotechnol. *28*, 511–515.

Traut, W., Endl, E., Scholzen, T., Gerdes, J., and Winking, H. (2002). The temporal and spatial distribution of the proliferation associated Ki-67 protein during female and male meiosis. Chromosoma *111*, 156–164.

Trinkle-Mulcahy, L., Andersen, J., Yun, W. L., Moorhead, G., Mann, M., and Lamond, A. I. (2006). Repo-Man recruits PP1 to chromatin and is essential for cell viability. J. Cell Biol. *172*, 679–692.

Uchimura, Y., Ichimura, T., Uwada, J., Tachibana, T., Sugahara, S., Nakao, M., and Saitoh, H. (2006). Involvement of SUMO modification in MBD1- and MCAF1- mediated heterochromatin formation. J. Biol. Chem. *281*, 23180–23190.

Untergasser, A., Cutcutache, I., Koressaar, T., Ye, J., Faircloth, B. C., Remm, M., and Rozen, S. G. (2012). Primer3-new capabilities and interfaces. Nucleic Acids Res. *40*, 1–12.

Vanneste, D., Takagi, M., Imamoto, N., and Vernos, I. (2009). The Role of Hklp2 in the Stabilization and Maintenance of Spindle Bipolarity. Curr. Biol. *19*, 1712–1717.

Verheijen, R., Kuijpers, H. J., van Driel, R., Beck, J. L., van Dierendonck, J. H., Brakenhoff, G. J., and Ramaekers, F. C. (1989a). Ki-67 detects a nuclear matrix-associated proliferation-related antigen. II. Localization in mitotic cells and association with chromosomes. J. Cell Sci. *92 (Pt 4)*, 531–540.

Verheijen, R., Kuijpers, H. J., Schlingemann, R. O., Boehmer, A. L., van Driel, R.,

Brakenhoff, G. J., and Ramaekers, F. C. (1989b). Ki-67 detects a nuclear matrix-associated proliferation-related antigen. I. Intracellular localization during interphase. J. Cell Sci. *92 (Pt 1)*, 123–130.

Waga, S., and Stillman, B. (1998). Cyclin-dependent kinase inhibitor p21 modulates the DNA primer-template recognition complex. Mol. Cell. Biol. *18*, 4177–4187.

Wen, B., Wu, H., Shinkai, Y., Irizarry, R. A., and Feinberg, A. P. (2009). Large histone H3 lysine 9 dimethylated chromatin blocks distinguish differentiated from embryonic stem cells. Nat. Genet. *41*, 246–250.

Xiong, Y., Hannon, G. J., Zhang, H., Casso, D., Kobayashi, R., and Beach, D. (1993). p21 is a universal inhibitor of cyclin kinases. Nature *363*, 210–211.

Yang, F. *et al.* (2015). The lncRNA Firre anchors the inactive X chromosome to the nucleolus by binding CTCF and maintains H3K27me3 methylation. Genome Biol. *16:52*.

Yeo, C. Q. X., Alexander, I., Lin, Z., Lim, S., Aning, O. A., Kumar, R., Sangthongpitag, K., Pendharkar, V., Ho, V. H. B., and Cheok, C. F. (2016). P53 Maintains Genomic Stability by Preventing Interference between Transcription and Replication. Cell Rep. *15*, 132–146.

Yusufzai, T. M., Tagami, H., Nakatani, Y., and Felsenfeld, G. (2004). CTCF Tethers an Insulator to Subnuclear Sites, Suggesting Shared Insulator Mechanisms across Species. Mol. Cell *13*, 291–298.

Zhang, L. F., Huynh, K. D., and Lee, J. T. (2007). Perinucleolar Targeting of the Inactive X during S Phase: Evidence for a Role in the Maintenance of Silencing. Cell *129*, 693–706.

Zheng, J., Ma, T., Cao, J., Sun, X., Chen, J., Li, W., Wen, R., Sun, Y., and Pei, D. (2006). Knockdown of Ki-67 by small interfering RNA leads to inhibition of proliferation and induction of apoptosis in human renal carcinoma cells. Life Sci. *78*, 724–729.

Zhu, L. J., Gazin, C., Lawson, N. D., Pagès, H., Lin, S. M., Lapointe, D. S., and Green, M. R. (2010). ChIPpeakAnno: a Bioconductor package to annotate ChIP-seq and ChIP-chip data. BMC Bioinformatics *11*, 237.